THE UNIVERSITY OF CHICAGO

EXPLORING DPR-DIP FUNCTION IN THE DEVELOPMENT OF THE *DROSOPHILA* NEUROMUSCULAR JUNCTION

A DISSERTATION SUBMITTED TO

THE FACULTY OF THE DIVISION OF THE BIOLOGICAL SCIENCES

AND THE PRITZKER SCHOOL OF MEDICINE

IN CANDIDACY FOR THE DEGREE OF

DOCTOR OF PHILOSOPHY

GRADUATE PROGRAM IN CELL AND MOLECULAR BIOLOGY

BY

MEIKE LOBB-RABE

CHICAGO, ILLINOIS

DECEMBER 2023

Copyright © 2023 Meike Lobb-Rabe

All Rights Reserved

TABLE OF CONTENTS

LIST OF FIGURES vi

LIST OF TABLES viii

ACKNOWLEDGMENTS ix

ABSTRACT xii

1. INTRODUCTION
    - 1.1 The *Drosophila* larval neuromuscular junction is an excellent model to examine neural circuit assembly 2
        - 1.1.1 Overview of the *Drosophila* nervous system 3
            - 1.1.1.1 The Ventral Nerve Cord 4
            - 1.1.1.2 Motor neurons 6
            - 1.1.1.3 Muscles 8
            - 1.1.1.4 Glia 9
        - 1.1.2 Development of the neuromuscular circuit 10
            - 1.1.2.1 Pathfinding 11
            - 1.1.2.2 Synaptic partner recognition 14
            - 1.1.2.3 Synaptic growth and maintenance 15
    - 1.2 Dprs and DIPs function in circuit assembly 17
        - 1.2.1 Structural and biochemical understanding of Dprs and DIPs 18
            - 1.2.1.1 Structure and biochemical properties 18
            - 1.2.1.2 Binding affinity 19
            - 1.2.1.3 IgLONs 20
            - 1.2.1.4 Direct vs indirect signaling of cell surface proteins 21
        - 1.2.2 Dprs and DIPs have multiple roles during nervous system development 22
            - 1.2.2.1 Dprs and DIPs instruct synaptic partner preferences 22
            - 1.2.2.2 Dpr10 is involved in axon pathfinding 23
            - 1.2.2.3 Dprs and DIPs impact cell survival 24
            - 1.2.2.4 Dprs and DIPs pair stochastic and deterministic wiring mechanisms 25
        - 1.2.3 Open Questions 26
            - 1.2.3.1 Signaling 26
            - 1.2.3.2 Function of additional domains 27
            - 1.2.3.3 Trafficking and regulation 27
2. NEURONAL WIRING RECEPTORS DPRS AND DIPS ARE GPI ANCHORED AND THIS MODIFICATION CONTRIBUTES TO THEIR CELL SURFACE ORGANIZATION
    - 2.1 Introduction 29

2.2 Some Dprs and DIPs are predicted to be GPI anchored 32
2.3 Dprs and DIPs are anchored to the membrane via glycophosphatidyl linkages .. 39
2.4 GPI anchor cleavage eliminates Dpr-DIP mediated cell aggregation 43
2.5 Dpr and DIP proteins are GPI anchored in vivo 46
2.6 GPI anchors alter localization in neurons and muscle cells 50
2.7 Discussion 53
2.7.1 Predicting GPI anchors 53
2.7.2 Dpr and DIP clustering is aided by their GPI anchors 54
2.7.3 Dpr-DIP-mediated cell adhesion depends on their GPI anchors . 55
2.7.4 GPI anchors in neural circuit assembly 56
2.8 Materials and Methods 58
2.8.1 Sequence selection and molecular cloning 58
2.8.2 Predictions of GPI anchors and transmembrane helices 58
2.8.3 *Drosophila* reagents, dissections, and immunohistochemistry 58
2.8.4 PLC cleavage assay with S2 cells 59
2.8.5 Flow cytometry 60
2.8.6 Cell aggregation assay with Sf9 cells 61
2.8.7 Tissue PLC experiment 62
2.8.8 Tissue Localization experiment 62
2.8.9 Statistical Analysis 63
2.8.10 Tissue and cell imaging protocol 63
3. DPR10 AND NOCTE ARE REQUIRED FOR *DROSOPHILA* MOTOR AXON PATHFINDING
3.1 Introduction 66
3.2 Dpr10 is required for ISNb pathfinding and innervation 69
3.3 Dpr10 interacts with Nocte and cDIP in vivo 73
3.4 Nocte is required for motor neuron pathfinding 76
3.5 *nocte* mutant embryos exhibit delayed nerve innervation 80
3.6 *nocte* is expressed in subsets of neurons, muscles, and glia 82
3.7 Nocte localizes to the cytoplasm and nucleus 86
3.8 Nocte is required in neurons to instruct axon pathfinding 89
3.9 Nocte and Dpr10 genetically interact 92
3.10 Discussion 95
3.10.1 Examining Dpr-DIP mediated mechanisms 95
3.10.2 ISNb pathfinding is mediated by multiple pathways 97
3.10.3 Putative function of Nocte in axon pathfinding 98
3.11 Methods 101
3.11.1 *Drosophila* melanogaster stocks and reagents 101
3.11.2 Scoring misrouting defects 101
3.11.3 Larval dissections 101
3.11.4 Biochemistry 102
3.11.5 Embryos 102
3.11.6 Immunohistochemistry 103
3.11.7 Imaging protocols 104
3.11.8 Analysis 104

4. DIP-α AND DPR10 SUPPRESS SYNAPTIC ARBOR GROWTH THROUGH DRAPER AND LAR AT THE *DROSOPHILA* NMJ
4.1 Introduction 106
4.2 DIP-α inhibits growth of the motor neuron terminal 109
4.3 Dpr10 inhibits growth of the motor neuron terminal 111
4.4 Dpr10 is required in muscles to inhibit synaptic growth 113
4.5 DIP-α—Dpr10 binding affinity influences growth and innervation differently 115
4.6 Dpr10 is required for normal active zone number 118
4.7 *draper* genetically interacts with *DIP-α* and *Dpr10* to regulate synaptic growth 120
4.8 *LAR* genetically interacts with *DIP-α* and *Dpr10* to regulate synaptic growth . 122
4.9 Discussion 125
4.9.1 Dprs and DIPs are reused for sequential steps of neural development 125
4.9.2 Dprs and DIPs require co-receptors 126
4.9.3 CSPs are integrating different pathways with similar functions 127
4.10 Methods 128
4.10.1 Drosophila husbandry, reagents, and dissections 128
4.10.2 Imaging Protocol 128
4.10.3 Analysis 129
5. DISCUSSION AND FUTURE DIRECTIONS
5.1 Summary 132
5.2 Dprs and DIPs in neural circuit assembly 132
5.2.1 Expression patterns of Dprs and DIPs 133
5.2.2 Dprs and DIPs are utilized in sequential neural developmental steps 134
5.2.3 Structure of Dprs and DIPs informs their function 135
5.3 Insights from GPI anchor status of Dprs and DIPs 136
5.3.1 GPI-anchored proteins require co-receptors for signaling 136
5.3.2 Localization 137
5.3.3 Missing insights into GPI anchored protein QC/trafficking/regulation 138
5.4 Conclusions 139
6. APPENDICES
6.1 Appendix A: Characterizing DIP-α-GAL4 141
6.2 Appendix B: In vivo evidence for C-terminal retention of would-be GPI-anchored DIP-α 145
6.3 Appendix C: Developmental timing of bouton addition in *Drosophila* larvae . 148
7. REFERENCES 151

LIST OF FIGURES

1.1 The larval *Drosophila* nervous system 4
1.2 Motor neurons of the larval *Drosophila* NMJ 6
1.3 Synaptic growth at the NMJ 16
1.4 The Dpr-ome, binding between Dprs and DIPs 18
2.1 GPI anchoring predictions for the Dpr and DIP families of CSPs 34
S2.1 Transmembrane region predictions by Phobius and DeepTMHMM 37
S2.2 Summary of GPI anchor and TM helix predictions 37
S2.3 Expression of V5-agged Dprs and DIPs in Sf9 ells used in cell aggregation assays 38
2.2 PLC treatment cleaves Dprs and DIPs from S2 cells, as observed by western blotting 41
2.3 Surface display of Dprs and DIPs is reduced by PLC treatment, as observed by flow cytometry 42
2.4 PLC cleavage eliminates Dpr-DIP mediated cell aggregation 45
2.5 Dpr and DIP proteins are GPI anchored in vivo 48
S2.4 DIP-ζ aggregates in response to PLC treatment 49
2.6 GPI anchor alters localization of DIP-α in neurons and Dpr10 in muscles 51
S2.5 Example particle counting used to examine pre- and postsynaptic localization of Dpr10 and DIP-α 52
3.1 Dpr10 is required for ISNb pathfinding 71
S3.1 Muscle patterning defects in dpr10 mutants 72
3.2 Immunoprecipitation followed by Mass Spectrometry of Dpr10 uncovers in vivo interactors 75
3.3 *nocte* mutants exhibit ISNb pathfinding errors 78
S3.3 *nocte* mutants exhibit normal innervation of m4 but display muscle defects 79
3.4 Loss of *nocte* causes stalling of ISNb before reaching terminal muscle targets 81
3.5 *nocte* is broadly expressed in larvae 84
S3.5 Nocte peripheral expression 85
3.6 Sub-cellular localization of Nocte 87
S3.6 AlphaFold structural predictions of Nocte 88
3.7 Tissue specific knockdown of *nocte* using RNAi 90
S3.7 Muscle patterning defects caused by knockdown of *nocte* in muscles 91
3.8 $nocte^{P}$ and $dpr10^{CR}$ double mutants are indistinguishable from $dpr10^{CR}$ single mutants 93
S3.8 Muscle defects in nocte.dpr10 double mutants 94
4.1 DIP-α inhibits growth of motorneuron terminal size 110
4.2 Dpr10 inhibits growth of motorneuron terminal size 112
4.3 Dpr10 is required in muscles to inhibit synaptic growth 114
4.4 DIP-α—Dpr10 binding affinity influences growth and innervation differently 116
4.5 Dpr10—DIP-α binding affinity influences growth and innervation differently 117
4.6 Dpr10 is required for normal active zone number 119
4.7 Draper genetically interacts with DIP-α and Dpr10 to regulate synaptic growth 121
4.8 Lar genetically interacts with DIP-α and Dpr10 to regulate synaptic growth 123
S4.1 Neither Ena nor Lirprin-α interact with Dpr10 and DIP-α 124
A1. Quantification of Is boutons on m12 and m13 in controls versus DIP-α-GAL4 heterozygous and homozygous animals 142
A2. Larval VNC staining of DIP-α antibody 143

A3. Western gel of UAS-DIP-α constructs expressed in S2 cells 144
B1. In vivo evidence for C-terminal retention of GPI-anchored DIP-α 147
C1. Quantification of boutons on m12 on different segments at 24 and 96 hours after embryos are laid 149
C2. Quantification of Is bouton number on m12 and m13 throughout development 150

LIST OF TABLES

1.1 Selection of sequences used in our analysis 35
1.2 GPI site predictions by PredGPI and NetGPI 36
1.3 The antibodies used for this study 64
1.4 The fly lines used for this study 65
2.1 The fly lines used for this study 105
3.1 The fly lines for this study 130
3.2 The antibodies used for this study 131

ACKNOWLEDGEMNTS

These past six years have been incredibly fulfilling and fun, filled with growth and learning. It would not have been possible without my incredible family, friends, and community. Words cannot express my gratitude for the support and love I've received.

To my family, thank you and I love you. The Lobbs are a matriarchy, led by strong women who break barriers and lead with kindness and compassion. To my mom, thank you for teaching me to follow my dreams and believe in myself. I couldn't have done any of this without your love and support—good job AliLobb. Papa, vielen, vielen Dank für all Deine Liebe und Unterstützung. Deine Besuche waren immer ein Highlight der letzten Jahren. To my grandma, Sally, I'm honored and blessed to have gotten to play penuckle with you and grandpa, and receive the articles that made you think of me while I was in college. Cailin and Henrik, I couldn't be more thankful for the unconditional love and support you've given me always—our success is always shared and the product of our joint efforts and this is no exception. Ken, Terri, Howie, and Amy, thank you for everything. To the Trapps, Andy, Kasey, Lana, Toño, and Ryan, thank you. Knecht Familie, Anne, Jule, Caro, Tilman, und Steffen, Ihr seid die Besten, und Ich bin so dankbar, dass ihr ein Teil meines Lebens seid. Julianna, thank you for being such an amazing, thoughtful, and supportive partner; I can't express the gratitude I feel at getting to share my life with you.

I would like to thank Dr. Robert Carrillo with my whole heart. I joined your lab, not only because the research is fascinating, but because of the exceptional mentor and person you are. You've shaped me as a scientist and your impact on my life cannot be overstated. You are everything that academia needs. Additionally, Yupu Wang, had immense influence on the direction my research and story-telling took. I admire your intellect, work-ethic, and humor, and

consider myself lucky to have gotten to work with and know you. Katie DeLong, you were the perfect undergad, thank you for helping me become a better mentor and keeping me young. I have been so immensely blessed to have worked with everyone in the Carrillo Lab. James, Veera, Violet, Stephanie, Rio, Renee, Parisa, and Darian, all of you impacted my science and made my life richer. In addition, I would like to thank the 9th floor fly community, especially Sherzod, I could not have imagined a better environment to do my research.

Thank you to my committee: Ilaria Rebay, Engin Özkan, and Xioxi Zhuang. I always looked forward to our meeting and am grateful for the guidance you provided me.

Viola Nawrocka was integral in teaching me about biochemistry and our collaborations was one of the most fun projects I've worked on.

To my graduate school friends: this journey would have been nothing without you and I am thankful beyond words. Emily our years of domestic partnership were so fun and fulfilling. Devin, Devin, Kourtney, Steven, Evan, Vaughn, Cat, Jimmy, Fernando, Liz, Matt, Jordan, Sammy, Jake, Simon, I love you. I could not have made it through shutdown or grad school without our friendship.

My CMSA pals, life got brighter when I met you all. Izzy, cut from the same cloth, I'm so happy to know you. Tia, Kris, Indi, Sondj, Kate, Abby, Nora, Sel, Elizabeth, Cal sharing courts, dance floors, and meals together brought me joy beyond words. Isaac, you opened up my world and filled it with so much light, I love you.

I would like to close by thanking the friends that have been with me since before grad school. There is such immense comfort in being known and having had a world outside of Chicago. Allie, Shannon, Rachel, Jaclyn, Mel, Lyss growing up together and now watching everyone's kids do the same has been the privilege of a lifetime. Thank you for always keeping

me grounded. Shannon and Cy, you are angels and I love you. Lilah, Camille, Esa you bring so much laughter and joy into my life.

Thank you, thank you, thank you.

ABSTRACT

How neural circuits form and function has been an area of scientific research for over a century. In my doctoral thesis, I aim to add to our understanding of these processes at a fundamental level. The common fruit fly, *Drosophila melanogaster,* is an excellent model to examine the basic principles and molecules that govern neural development. Here, I utilize the cell surface protein families, the Dprs and DIPs, to study specific steps of neural circuit assembly: axonal pathfinding and synaptic growth. Specifically, I show that Dpr10 functions in axonal guidance in the embryonic peripheral nervous system. In addition, Dpr10 and its binding partner DIP-α inhibit synaptic growth, thereby contributing to the specification of synaptic arbor size in a motor neuron and target dependent manner. To understand how these processes occur at the molecular level, I collaborated with Viola Nawrocka to examine the biochemical properties of the Dprs and DIPs and demonstrated that most are tethered to the outer leaflet of the cell membrane through GPI anchors; this modification has implications for their subcellular localization and potential signaling mechanisms. Together, this body of work examines how cell surface proteins contribute to neural circuit assembly and development.

CHAPTER 1

INTRODUCTION

All organisms must be able to perceive stimuli and respond to them. More complex organisms utilize a nervous system—with cells that can sense different stimuli and transmit information into electrical or molecular signals. Some nervous systems contain millions and even billions of neurons yet their organization is highly stereotyped. Neurons form connections, called synapses, with other cells, and the number of synapses is orders of magnitude greater than the number of neurons. Despite these exuberant numbers, there is also stereotypy in the organization of the synapses. One of the fundamental questions in developmental neurobiology is how these complex networks of cells know where to go and which cells to connect with. One hypothesis is that neurons use cell surface molecular barcodes that identify one cell from another, and only when the correct barcodes match do neurons form stable synapses (Sperry, 1963). The barcode is comprised of cell surface proteins (CSPs).

The common fruit fly, *Drosophila melanogaster*, is an excellent model to examine CSPs and the molecular mechanisms underlying their functions. With around 150,000 neurons in an adult fly brain, it is a fraction of the size of the 100 billion neurons that make up the human brain. Although relatively 'simple', the fly brain faces similar challenges as a human brain—it must organize circuits and neurons must find their correct synaptic partners in a very dense tissue. The complex, crowded environment in the brain hinders easy access to each synaptic connection. Here, I will leverage the larval *Drosophila* neuromuscular system, where peripheral muscles are stereotypically innervated by 1-4 motor neurons, to examine the molecular determinants that instruct different steps of neural circuit assembly.

Specifically, I studied the Dprs and DIPs, two related families of immunoglobulin superfamily CSPs that interact hetero- and homophilically. Since the discovery of their interactions in 2013, Dprs and DIPs have been intensively studied for their roles including synaptic partner matching, axon guidance, and cell survival. In a fruitful collaboration with a fellow graduate student, Viola Nawrocka, I investigated how the Dprs and DIPs are attached to the cell membrane to better understand how these CSPs function. With an incredibly talented and hard-working former undergraduate, Katherine DeLong, I described a novel function for one family member, Dpr10, in axon pathfinding. Lastly, I demonstrated that DIP-α and Dpr10 inhibit neuromuscular junction (NMJ) elaboration, highlighting the multifaceted roles of Dprs and DIPs in multiple steps of nervous system development: axon guidance, synaptic partner matching, and synaptic growth.

1.1 The *Drosophila* larval neuromuscular junction is an excellent model to examine neural circuit assembly

Drosophila melanogaster, or the common fruit fly, is one of the most well-established model systems used to study the basic biological principles of genetics, behavior, and disease. Fruit flies were first used to establish and demonstrate chromosome theory—that chromosomes are the genetic vehicles of inheritance (Morgan, 1910). In addition, Notch and its signaling pathway were first identified in flies (reviewed in (Artavanis-Tsakonas et al., 1999)). Like many other discoveries in Drosophila, these fundamental mechanisms are conserved and represent a minute fraction of the discoveries made in fruit flies (Bellen et al., 2010). For over 100 years, fruit flies have continued to thrive as a model organism with a plethora of genetic tools to study

the function of genes and proteins. My work will focus on the nervous system of *Drosophila* embryo and larva.

After a male and female fly mate and the female lays a fertilized embryo, the life cycle of a fly begins. During embryonic development, axon guidance, synaptic partner matching, and synaptogenesis occur. At 25°C, the embryo will hatch into a first instar larvae after one day, at which point its larval body plan is finalized and the neuronal connectivity pattern has been established. Once hatched, the animal begins to search for food. Over the next 4-5 days, the larvae will rapidly grow. During this period, the connectivity map will remain, but pre- and postsynaptic arbors will expand to keep pace with the rapidly growing tissues. Toward the end of the third instar larval stage, the larva will crawl away from its food source, begin to form a hard outer casing, and cease to move as it transitions into the pupal stage—a time of morphogenesis lasting 4 days in which the body plan is completely altered, and the fly takes on its adult form. During the pupal stage, the nervous system is wholly remodeled from neuroblasts that were generated during the larval stage, and the adult nervous system is assembled. Once complete, the adult fly hatches from its pupal casing, its wings unfurl and the cycle beings anew.

The life cycle of the fly has two stages of neural development, first after the embryo is laid and again during the pupal stages when the adult nervous system is assembled (Truman, 1990; Yoshihara et al., 1997). My work will focus on the earlier development, from embryo to late larva.

1.1.1 Overview of the larval *Drosophila* nervous system

The fly nervous system shares many of the central components of the vertebrate nervous system. Like vertebrates, flies have a central and peripheral nervous system, the CNS and PNS

respectively. The CNS is composed of the central brain and the ventral nerve cord (VNC), a structure akin to the vertebrate spinal cord. The VNC houses the motor neuron (MN) cell bodies which extend axons that exit the VNC in nerve bundles to innervate the muscles of the body. In the periphery, sensory neurons collect external and proprioceptive information and relay it to the brain via the same nerves as the MN axons. In addition to structural similarities with vertebrates, flies also have many conserved genes, making this model a powerful system to study the basic biology underlying complex human diseases.

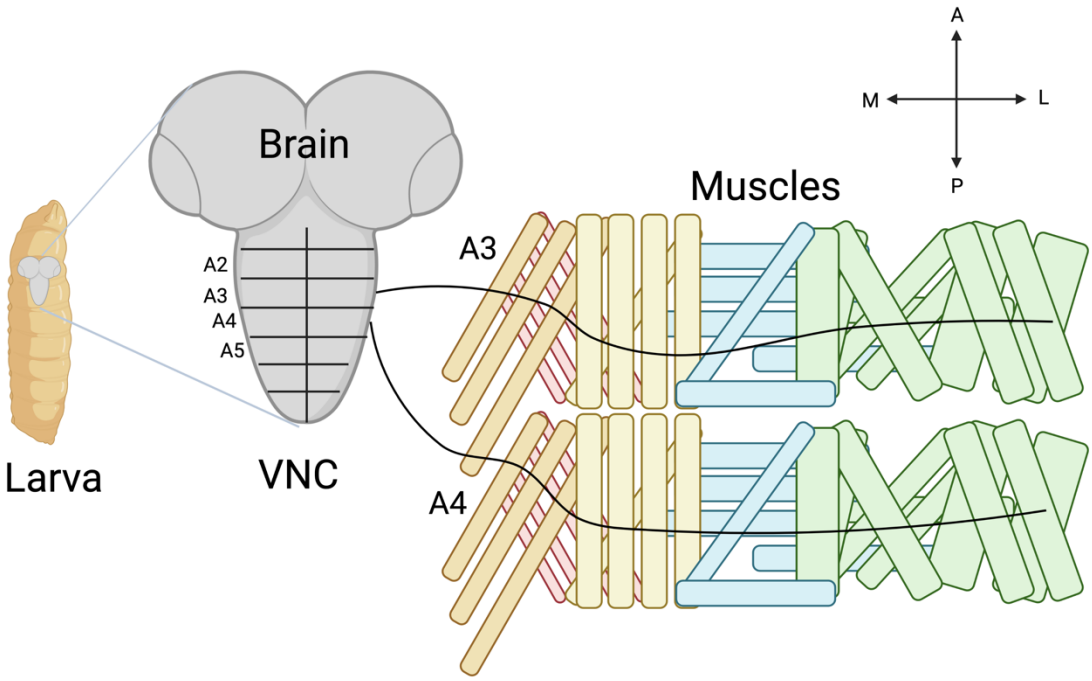

Figure 1.1 The larval *Drosophila* nervous system.
The Drosophila larva, with an enlarged central nervous system shown in gray, comprised of the brain and the ventral nerve cord (VNC). Nerves exiting the hemineuromeres and traversing the corresponding hemisegments of the peripheral body wall muscles in segments A3 and A4.

1.1.1.1 The Ventral Nerve Cord

The VNC is a dense, neural tissue extending from the posterior of the central brain (Figure 1.1). The VNC has an outer layer comprised of the neuronal cell bodies and a dense

neuropil in the center where synaptic connections are made. Surrounding the cell bodies are layers of glia, which act as the blood brain barrier, insulating the nervous system from the surrounding hemolymph that bathes the larval organs.

Like the larval body wall, the VNC is also segmented, and the layout mirrors that of the body; each segment is bilaterally symmetrical, and each hemisegment is referred to as a hemineuromere (Meng and Heckscher, 2020). Thus, each hemineuromere of the VNC matches up anatomically with a hemisegment of the body. In early embryonic stages, each VNC hemineuromere houses neuroblasts which give rise to mature neurons, including the MNs that will innervate the corresponding hemisegment in the periphery (Landgraf et al., 2003; Mark et al., 2021; Menon et al., 2013). The neuroblasts are mapped, named for the column and row they occupy within their hemineuromere, and for most, their progeny is known (Skeath, 1999; Truman and Bate, 1988). In addition, the wiring map of the VNC neurons has been elucidated based on serial electron microscopy of a male larval brain (Ohyama et al., 2015; Winding et al., 2023).

1.1.1.2 Motor neurons

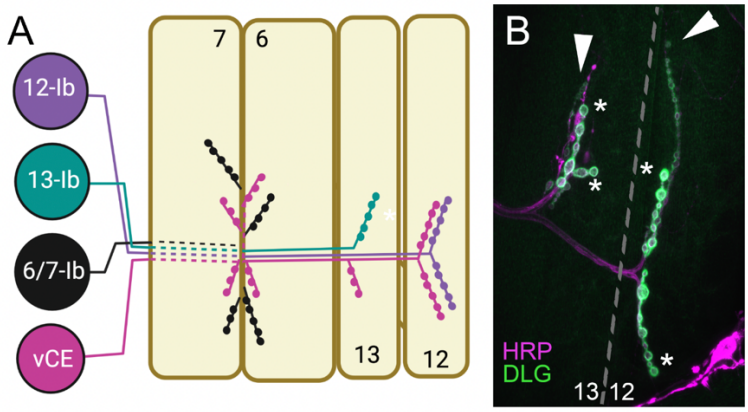

Figure 1.2 Motor neurons of the larval *Drosophila* neuromuscular system.
(A) Schematic of the MNs that innervate the ventral muscle field via the ISNb nerve. MN cell bodies (circles) and axons traveling below (dotted lines) or above (solid lines) muscles (yellow). Boutons depicted as beads-on-a-string covering the muscle circle. (B) Confocal image of the NMJs at m12 and m13, with neuronal membrane shown in magenta (horseradish peroxidase, HRP) and the postsynapse labeled for Discs Large (DLG, green). Arrowheads mark the ends of Is arbors and asterisks the ends of Ib arbors.

Motor neurons synapse with muscles and, when excited, elicit contractions from their muscle targets. Their cell bodies sit in the VNC, and they can innervate muscles at the animal's posterior, making them some of the longest cells in the body. Flies have three types of MNs, type I are glutamatergic, type II are octopaminergic, and type III are peptidergic (Menon et al., 2013; Stocker et al., 2018). Of the ~33 MNs that innervate each segment, ~30 are Type I, 1-3 are Type II, and one is Type III (Anderson et al., 1988; Koon et al., 2011; Landgraf et al., 1997; Wang et al., 2022). Type I MNs are further divided into Ib (big) and Is (small), and they are easily distinguished by the amount of Discs-Large (DLG) staining surrounding their boutons—Ibs are surrounded by a thicker layer of DLG staining compared to Is neurons (Guan et al., 1996). Almost all Ib MNs innervate single muscle targets (e.g. muscle 12 is innervated by MN12-Ib) (Figure 1.3). On the other hand, Is MNs innervate multiple muscles and are thought to assist in

coordinating muscle movement. Each hemisegment has two Is MNs, one that innervates the dorsal muscle field and one that innervates the ventral muscle field. Because they innervate multiple muscles, they are also called common exciters: the dorsal common exciter and ventral common exciter (dCE and vCE, respectively) (Figure 1.3). Is and Ib are the most commonly studied MNs and are responsible for muscle contractions.

The developmental MNs has been extensively studied, providing a detailed atlas of their birth and anatomy. MNs are born from at least ten neuroblasts (Landgraf et al., 1997). For example, NB7-1 (the neuroblast found in row 7 and column 1 of each hemineuromere) produces the Ib MNs that innervate the dorsal muscles, m9, m10, m2, m3, m4 (Meng et al., 2019). Another example is NB3-1, which produces the vCE and Ib MNs that innervate some of the dorsal muscles, m12, m13, m30, m6, m7 (Meng et al., 2020). These NBs also give rise to interneurons, and their identity is thought to be determined by the expression profile of transcription factors that is maintained in the NB after birth (Meng and Heckscher, 2020). Unlike vertebrate NMJss, which are cholinergic, the excitatory MNs of the fly are glutamatergic, and therefore more akin to vertebrate excitatory central synapses (Menon et al., 2013).

Ib and Is neurons have distinct firing behaviors – Ib neurons are tonic, while Is neurons are phasic. A tonic response occurs when a neuron has sustained firing activity that activates during the stimulus, while a phasic response is transient with only a few action potentials at the onset of the stimulus (Wang et al., 2014). In addition, Ib MNs have a lower threshold to elicit action potentials than Is MNs (Aponte-Santiago et al., 2020; Jan and Jan, 1976; Lnenicka and Keshishian, 2000; Wang et al., 2021). Due to the physical and genetic access, the *Drosophila* neuromuscular system has been an excellent model to study how synaptic perturbations induce homeostatic plasticity in neurotransmission. Also, recent single-cell RNA-seq experiments

probing the transcriptional landscapes of Is and Ib MNs will provide molecular insights and guide future work aimed at understanding the differences between these MNs types (Jetti et al., 2023).

1.1.1.3 Muscles

Each abdominal hemisegment of the larval *Drosophila* body has ~30 muscles that are highly stereotyped; each muscle cell is a large syncytium formed by the fusion of founder cells and fusion competent myoblasts (Bate, 1990). Each founder cell carries the information of its future muscle identity before fusion begins, and this information is at least partially specified by Hox genes (Enriquez et al., 2010; Rushton et al., 1995). For a comprehensive review on muscle development please see (Poovathumkadavil and Jagla, 2020).

Although some genes are more highly expressed in some muscles than others, muscles have largely eluded molecular identification at an individual level and are therefore usually treated as a roughly homogenous tissue. Early work to molecularly distinguish muscles used micropipettes to suction the cytosol of m12 and m13 in third instar larvae and then compared the RNAs isolated from each muscle (Inaki et al., 2007). Although differentially expressed factors were identified, none were expressed in just one muscle. More recent work using single cell RNA-seq methods in embryos has yielded data sets with distinguishable muscle clusters; however, to my knowledge, none have resulted in identification of specific muscles (Calderon et al., 2022; Jetti et al., 2023; Seroka et al., 2022).

Due to the lack of a molecular muscle atlas, tools targeting individual muscles or subsets of muscles are limited. To my knowledge the only tools available to target a subset of the muscles in larvae are H94-GAL4 which has higher expression in m6 than m7 and also higher

expression in m12 than m13 (Davis and Goodman, 1998). In addition, there is a m12 specific GAL4 (M12-GAL4, also known as 5053A-GAL4), but it is unclear to what extent it is expressed in other cells and tissues (Ljaschenko et al., 2013; Ritzenthaler et al., 2000). Lastly, Dpr10 is expressed in almost all ventral and dorsal muscles while absent in all but one lateral muscle (Wang et al., 2022).

It is unclear if mature larval muscles have not been molecularly identified because limitations in techniques or because, at this stage, they are molecularly roughly homogenous. Given the molecular classification at embryonic stages and evidence that individual muscles display different phenotypes in whole animal mutants of developmental factors, it seems likely that with higher resolution and larger datasets, muscle identity classification will become possible.

1.1.1.4 Glia

Both the central and peripheral nervous systems have glial cells that perform critical roles for development and neural function. The central nervous system has six types of glia: astrocytes, ensheathing glia, cell body glia, perineural glia, subperineural glia, and wrapping glia while the peripheral nervous system has three types: wrapping glia, subperineural glia, and perineural glia (Freeman, 2015; Hartenstein, 2011; Yildirim et al., 2019). Glial cells function as the support and immune cells of the brain performing critical functions for healthy nervous system function, and in *Drosophila*, formation of both glial and immune cells are governed by the transcription factor glial cells missing (GCM) (Freeman et al., 2003). GCM acts as a binary switch that specifies glial cell fate in neuronal progenitors; when GCM is removed glial cells are

lost, however when GCM is overexpressed virtually all CNS cells become glia (Hosoya et al., 1995).

Glia have important functions in injury response, development, and maintenance of neural circuits. Glia clear axonal debris after injury or cell death (Kato et al., 2018; MacDonald et al., 2006; Purice et al., 2017). In addition, glia shape neural development, guiding neural differentiation and contributing to neural arbor growth (Fernandes et al., 2017; Fuentes-Medel et al., 2009; Sepp et al., 2000). Moreover, glia are important for regulating neural homeostasis and trigger homeostasis in bystander neurons (Otto et al., 2018; Wang et al., 2023).

Although glia are fascinating, my work will only briefly touch on glia; for more detailed reviews, please see (Freeman, 2015; Yildirim et al., 2019) and the thesis of Dr. Yupu Wang.

1.1.2 Development of the neuromuscular circuit

Although synapses are typically thought of as occurring between two neurons, synapses can also occur between neurons and other cells types, including muscles. These MN-muscle synapses, termed neuromuscular junctions (NMJs), allow organisms to control their bodies and move through their environments in targeted ways. Although these synapses exist at long distances away from the central nervous system, the neuromuscular system shares many of the same molecules and developmental steps as central neural circuits. The *Drosophila* larval NMJ is a relatively simple circuit which can be used as a model to study fundamental processes that are required to build a nervous system. This assembly can be broken down into several steps: (1) Pathfinding—MNs send their axons into the periphery where they follow a defined path, (2) Synaptic partner recognition—the axon terminal contacts different potential targets, rejecting incorrect ones and forming a connection with the correct partner(s), (3) Synaptogenesis—pre-

and postsynaptic organizers recruit neurotransmitter machinery and receptors, respectively, to create functional connection, (4) Synaptic growth and maintenance—once the connection has been made, the axon terminal grows to a functionally appropriate size. Each of these steps is governed by molecular cues from the environment and anterograde and retrograde signaling between the synaptic partners through ligand/receptor interactions.

1.1.2.1 Pathfinding

As motor axons extend into the periphery, their growth cones—specialized structures with filopodia at the tips of extending axons—sense the surrounding environment. CSPs on the growth cone receive information via binding to ligands and contacting surrounding cells. In the *Drosophila* embryo, there are two primary systems used to study pathfinding: axons crossing the midline in the VNC and MN axons exiting the VNC to innervate muscles in the periphery. Here, I will focus on the latter.

There are three nerves that enter each hemisegment from the ventral midline: the intersegmental nerve (ISN), segmental nerve (SN) and transverse nerve (TN). These are further subdivided into ISN, SNa, ISNb, SNc, and ISNd, each of which carry multiple axons that innervate groups of muscles anatomically near one another (Hoang and Chiba, 2001; Kohsaka et al., 2012). Most axon pathfinding studies have focused on the ISNb during embryonic development as it travels across and innervates the ventral muscles: m12, m13, m6, m7, m14, and m30. Below, I will review a few of the well-known axon guidance cues.

Netrin-1 is one of the most well studied, conserved axon guidance cues. In vertebrates, Netrin-1 is required for commissural axon guidance, and it was long believed that Netrin-1 was released from floor plate cells (Serafini et al., 1996). However, more recent work altered the

existing model in mammals, demonstrating that Netrin-1 is produced by neural progenitors and not floor plate cells for crossing of commissural axons (Varadarajan et al., 2017). In flies, the soluble factor Netrin has two receptors, UNC5 and frazzled/DCC (Hiramoto et al., 2000; Keleman and Dickson, 2001). Netrin can act either as a repulsive or attractive cue depending on which receptor and in which configuration it is binding; homodimers of DCC:DCC are attractive while heterodimer pairing of UNC5:DCC and UNC5:DSCAM lead to repulson (Boyer and Gupton, 2018; Serafini et al., 1996; Torre et al., 1997). Additionally, the concentration of Netrin is believed to act as a switch that can change the response from attractive to repulsive by altering the types of receptor dimers that form, biasing the attractive pairing of DCC:DCC over the repulsive pairing of UNC5:DCC (Boyer and Gupton, 2018). In *Drosophila*, Netrin has been characterized in embryonic midline crossing in the VNC and peripheral axon guidance (Hiramoto et al., 2000; Keleman and Dickson, 2001; Mitchell et al., 1996).

Another well established and conserved axon guidance cue is Slit, which was first identified in the original Nüsslein-Vollhard screen describing embryonic patterning defects (Nüsslein-Volhard et al., 1984). Slit is a secreted protein that binds its receptor Robo to drive axon repulsion (Blockus and Chédotal, 2016; Brose et al., 1999). In the adult *Drosophila* visual system, Robo-3 guides R8 growth cones to their layer in the medulla (Pappu et al., 2011). In the embryonic VNC, Robo-Slit signaling is critical for ventral midline crossing (Dickson and Gilestro, 2006; Gilestro, 2008; Kidd et al., 1998).

The Beats and Sides are two families of Ig proteins that selectively interact; there are 14 Beats and 8 Sides (Li et al., 2017; Özkan et al., 2013; Siebert et al., 2009). Early work in *Drosophila* embryos showed that multiple members of the Beat family are important for both commissure crossing in the VNC and ISNb guidance in the periphery (Kinold et al., 2018; Pipes

et al., 2001; Siebert et al., 2009). To date, seven of the 22 Beats and Sides are orphaned receptors with no known binding partners, providing an interesting area of future research (Li et al., 2017; Özkan et al., 2013).

A screen of CSPs containing leucine rich repeat (LRR) domains examined axon pathfinding in the peripheral nervous system of the *Drosophila* larva (Kurusu et al., 2008). Specifically, they focused on axon pathfinding of the ISNb at m6, m7, m13 and m12. Characterization of two candidates, *capricious* and *tartan*, found that loss of these CSPs caused mistargeting in 5% and 40% of hemisegments examined, respectively (Kurusu et al., 2008). Although many of the candidates have not been characterized further, this screen provides a model for utilizing the NMJ to examine molecules involved in axon pathfinding in a medium-throughput manner.

This brief overview touches on only a few examples of molecules that have been implicated in axon guidance in *Drosophila*. Moreover, loss of most of these axon guidance molecules have relatively mild phenotypes of 30% or less, suggesting redundancy between various axon guidance pathways. Indeed, the presence of redundancy is somewhat perplexing, for if two genes are truly redundant, there would be no evolutionary pressure against mutations in one of the redundant copies (Nowak et al., 1997). However, genetic redundancy exists is many crucial biological processes, including neural development, immunology, and the cell cycle. One hypothesis is that feedback between redundant genes facilitates signal transduction and the control of gene expression levels (Kafri et al., 2009). All steps of neural circuit assembly, to my knowledge, display functional redundancy and this is also observed in the work I will present in this thesis.

1.1.2.2. Synaptic partner recognition

After completion of axon guidance, the neuron faces a new challenge—synaptic partner recognition: differentiating incorrect and correct synaptic targets. At this stage, the motor axon growth cone has reached the correct vicinity and has made contacts with nearby cells with the finger-like filopodial projections of the growth cone (Nose, 2012). In the neuromuscular system, the filipodia form contacts with projections from the muscles called myopodia (Nose, 2012). Most interactions are brief unless stabilized by CSP interactions between apposing membranes. It should be noted that perturbation of many of the axon guidance cues described in the above section would also ultimately result in loss of synaptic connectivity so caution must be taken when dissecting axon guidance and synaptic connectivity molecules and mechanisms. I will focus this section on factors that are implicated in synaptic partner recognition.

Teneurins are large CSPs containing EGF repeats that localize to the larval *Drosophila* NMJ (Baumgartner et al., 1994; Baumgartner and Chiquet-Ehrismann, 1993; Tucker, 2018). In the adult, Ten-m and Ten-a coordinate correct matching of olfactory receptor neurons and their downstream targets, the projection neurons, which form synapses in distinct neuropil compartments in the olfactory bulb called glomeruli (Hong et al., 2012). Similarly, at the larval NMJ, presynaptic Ten-a binds muscle Ten-m to affect cytoskeletal organization and Ten-m is also required for innervation of m3 (Mosca et al., 2012).

The Dprs and DIPs are two related families of Ig-CSPs (Carrillo et al., 2015; Cosmanescu et al., 2018; Özkan et al., 2013). Many of the family members have been implicated in synaptic partner matching, and although I will discuss these CSPs in more detail later, here I will illustrate their function using an example at the larval NMJ. Dpr10 is expressed in muscles and one of its interactors, DIP-α, is expressed in multiple MNs, including the Is MNs, vCE and dCE (Ashley et

al., 2019; Wang et al., 2022). In *dpr10* or *DIP-α* mutants, the dCE fails to innervate m4 100% of the time. Other dCE connections are only partially lost, suggesting additional molecules are required (Ashley et al., 2019). Similar to axon pathfinding, loss of most genes implicated in connectivity leads to relatively low penetrance phenotypes (except for the Dpr10-DIP-α example above), indicating that redundant mechanisms are prevalent.

1.1.2.3 Synaptic growth and maintenance

MN-muscle partner matching occurs in the embryo, and the connectivity map is maintained during larval development. After the two membranes of opposing cells come together and the cue that correct partners have matched is relayed, proteins that form the synaptic machinery accumulate at the contact site and bead like structures called boutons form. Boutons house the presynaptic neurotransmitter release sites where information is passed from the neuron to the muscle. Each muscle is covered in synaptic arbors—branches of beads of boutons. After hatching, the larva undergoes rapid size expansion with muscle surface area increasing ~100 fold (Menon et al., 2013). With this rapid growth, NMJs must also expand to maintain synaptic efficacy; this is achieved through the addition of boutons (Figure 1.3). Here, I will focus only on subset of CSPs implicated in NMJ growth (reviewed in (Menon et al., 2013)).

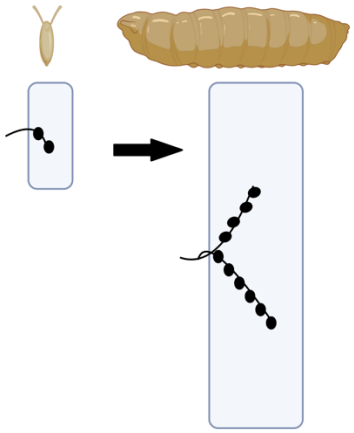

Figure 1.3 Synaptic growth at the NMJ.
As the animal grows from embryo (left) to larva (right), muscles increase in size and there is a concomitant expansion of the synaptic arbor on the muscle. Boutons are depicted as black circles on the muscle surface.

Leukocyte antigen-like receptor (LAR) is a receptor protein tyrosine phosphatase with extracellular Ig and Fibronectin type III domains (Kawakami et al., 2022). In vertebrates, there are three LAR receptors, all of which are associated with neurological diseases when they become mutated or dysregulated (Cornejo et al., 2021). At the *Drosophila* NMJ, *LAR* mutants exhibit fewer boutons on m6/m7 (Bali et al., 2022; Berke et al., 2013). *LAR* is expressed in MNs and is activated by the ligand Syndecan to promote bouton growth; while the receptor dally-like protein inhibits LAR leading to decreased active zone stabilization and fewer boutons (Johnson et al., 2006). *LAR* is expressed in both Ib and Is type MNs and acts in cis with its ligand Stick and Stones to regulate NMJ morphology in larvae (Bali et al., 2022). Intracellularly, LAR binds Liprin-α and Liprin-γ, adaptor proteins that interact with active zone components. Loss of *liprin-α* and *liprin-γ* results in undergrown NMJs on m6/m7 (Astigarraga et al., 2010).

The engulfment receptor Draper is expressed in glia and muscles, and *draper* mutants exhibit fewer Ib boutons on m6/m7, more ghost boutons (boutons that contain presynaptic signal but lack postsynaptic DLG), and more synaptic debris (neuronal staining not associated with a

nerve) (Fuentes-Medel et al., 2009). The decreased number of boutons is evident when Draper or its downstream signaling component CED-6 are knocked down in either muscles or glia (Fuentes-Medel et al., 2009). Like in axon guidance, these examples are only a fraction of what is known about synaptic arbor growth.

1.2 Dprs and DIPs function in circuit assembly

Dprs and DIPs are two related subfamilies of the immunoglobulin (Ig) superfamily that selectively bind one another hetero- and homophilically (Carrillo et al., 2015; Özkan et al., 2013) (Figure 1.4). In addition, the common DIP, cDIP, an unrelated LRR protein binds many of the Dprs and DIPs (Özkan et al., 2013). Defective proboscis response protein 1 (Dpr1) was first described in a study examining the gustatory response to salt and the additional 20 Dprs were discovered based on sequence similarity (Nakamura et al., 2002; Özkan et al., 2013). Dpr-Interacting Proteins (DIPs) were discovered in an in vitro binding assay and named for their interactions with the Dprs (Carrillo et al., 2015).

Initial in vivo work demonstrated that Dpr-DIP binding partners were selectively expressed in pre- and postsynaptic neurons in the adult *Drosophila* visual system, and loss of a *dpr11* and *DIP-γ* resulted in synaptic mistargeting (Carrillo et al., 2015; Tan et al., 2015). Since their initial characterization, many labs have described additional functions in various facets of nervous system development, which I will discuss later in this introduction.

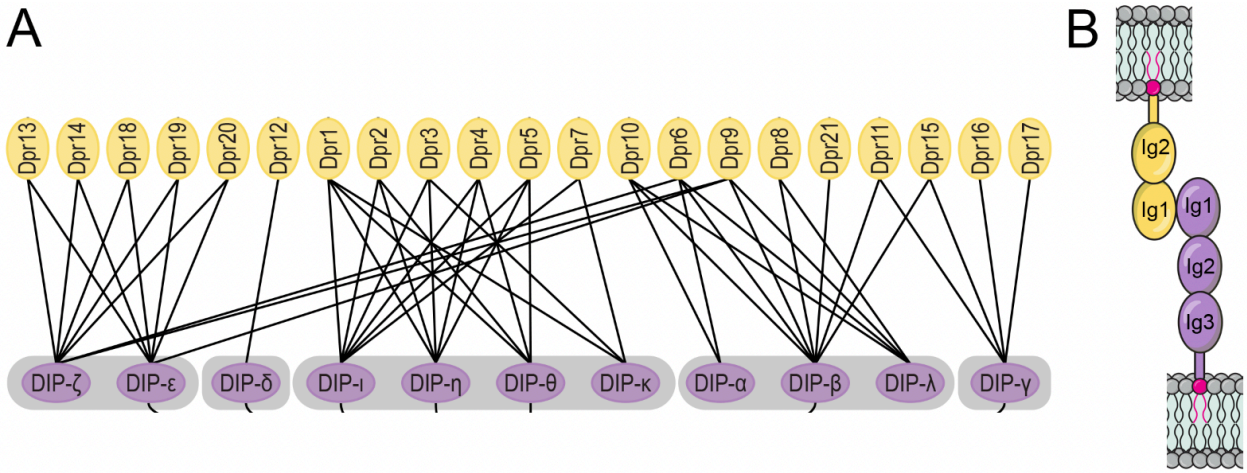

Figure 1.4 The Dpr-ome, binding between Dprs and DIPs.
Hetero- and homophilic binding of Dprs (gold) and DIPs (purple) depicted as black lines. Common DIP, cDIP (blue), binds many family members. (B) Schematics of Dpr-DIP binding at their D1 domains.

1.2.1 Structural and biochemical understanding of Dprs and DIPs

Many studies have characterized the function of Dprs and DIPs for their roles in neural development, but substantial work has also focused on characterizing and studying their biochemical and structural properties. These characteristics have made them an excellent model for protein biochemists to examine binding selectivity.

1.2.1.1 Structure and biochemical properties

Dprs and DIPs have two and three Ig domains, respectively (Carrillo et al., 2015; Cosmanescu et al., 2018; Özkan et al., 2013). They bind through an interface on their first Ig domains (most distal from the membrane), and to date it is unclear what function the other Ig domains serve (Figure 1.4). Although the binding specificity was originally thought to be coded by different landscapes of hydrophobic faces matching shapes like the palms of a hand, later studies demonstrated that charged residues at the edges of the binding interface were important

and could be altered to change binding partner preferences (Carrillo et al., 2015; Cheng et al., 2019a; Cosmanescu et al., 2018; Sergeeva et al., 2020). Most models of Dpr-DIP function are based on binding partners being expressed on opposing membranes and binding in trans although evidence exists that they can also bind in cis on the same membrane (Ashley et al., 2019; Cheng et al., 2019a).

1.2.1.2 Binding affinity

The binding affinity between most Dprs and DIPs is in the low micromolar range. However, binding affinities within the family vary up to 100-fold, with some lower affinity interactions like Dpr5 and DIP-ι with ~115μM K_D and some higher affinity interactions like DIP-α and Dpr10 with ~2μM K_D (Cosmanescu et al., 2018). It is perhaps no coincidence that most of the research has focused on the higher affinity interactions, as their phenotypes are likely more penetrant and easier to observe.

Recent work from Kai Zinn's lab utilized the structural details of Dprs and DIPs coupled with their role in synaptic partner matching in the adult eye to examine how binding affinity underlies their function (Xu et al., 2022). In the medulla, Dm12 neurons synapse with laminar L3 neurons and this interaction is mediated by DIP-α and Dpr10. Xu and colleagues made endogenous CRISPR mutations that alter the binding affinity of DIP-α and Dpr10 and examined innervation of the Dm12 neuron in the pupal optic lobe. Using this system, they demonstrated that binding affinity scales with innervation accuracy, and further, that the neurons that mistargeted died via apoptosis. During pupal development, an excess of Dm12 neurons are born, presumably to provide buffer for cells that mistarget or otherwise die. When DIP-α–Dpr10 binding affinity was strengthened, an increased number of correctly innervating Dm12 neurons

were observed (Xu et al., 2022). Although these animals were not behaviorally or functionally examined, it would be interesting to examine what the consequences of these additional neurons and synapses are. Additionally, increased protein expression can compensate for decreased binding affinity, demonstrating that the system responds to is the total amount of binding—avidity—between the two membranes. The Dprs and DIPs display a variety of binding affinities and promiscuities, so the functional significance of avidity may help us understand redundancy in these families. For example, does reducing expression of DIP-α in one neuron lead to increased expression of DIP-β, a family member that also binds Dpr10 and Dpr6? If the important output of Dprs and DIPs is overall binding, then redundancy could be used to maintain binding strength in the face of different biological perturbations.

1.2.1.3. IgLONs

The vertebrate orthologs of the Dprs and DIPs are the IgLONs, a family of proteins containing five members: LSAMP (limbic system-associated membrane protein), NTM (neurotrimin), OPCML (opioid-binding cell adhesion molecule), NEGR1 (neuronal growth regulator 1), and IgLON5 (Cheng et al., 2019b; Zinn and Özkan, 2017). Like Dprs and DIPs, IgLONs are CSPs that form homo- and heterophilic dimeric complexes and have been implicated in numerous processes related to neural circuit formation including neurite outgrowth and dendritic arborization (Gil et al., 2002; Pischedda and Piccoli, 2016; Reed et al., 2004; Sanz et al., 2015). In addition, some family members are affiliated with human diseases including IgLON5 disease and schizophrenia (Heidbreder and Philipp, 2018; Karis et al., 2018).

IgLONs are tethered to the membrane through glycophosphoinositol (GPI) anchors, and thus they require a coreceptor to transmit information into the cells (Hachisuka et al., 1996; Itoh

et al., 2008). To date, only one such coreceptor has been identified—FGFR2. The FGF pathway receptor binds Negr1 to promote neuronal arborization (Pischedda and Piccoli, 2016). Moreover, IgLONs can be cleaved by the surface metalloprotease ADAM10 and cleavage is thought to be a part of its function in promoting neuronal growth (Sanz et al., 2015). Although implicated in human health, this family of proteins is severely understudied, and we lack insights about how they are regulated and the downstream signaling pathways.

1.2.1.4 Direct vs Indirect signaling of cell surface proteins

Receptors typically function by interacting with the extracellular environment, responding to a cue, and then transmitting that information into the cell, where downstream effectors result in a response to the initial cue in a process termed signal transduction. Most CSPs have a dedicated transmembrane domain, an extracellular portion, and an intracellular region. These transmembrane proteins can respond to extracellular cues—mechanical pressure, binding of a ligand, cleavage—and transduce this signal through the transmembrane domain to the inside of the cell, where secondary messengers respond to the signaling event. On the other hand, CSPs that are tethered to the outside of the cell and lack a transmembrane domain, including IgLONs, require a coreceptor because they themselves cannot transduce information across the lipid bilayer. When the transmembrane domain is present the signaling is direct and when CSP lacks the transmembrane domain it is indirect. Although indirect signaling requires additional factors, it allows for additional regulation and presents interesting avenues of future research.

1.2.2 Dprs and DIPs have multiple roles in nervous system development

The Dprs and DIPs are two related families of CSPs that belong to the immunoglobulin (Ig) super family and are expressed widely throughout the *Drosophila* nervous system. Due to their selective binding within the family, and their specific expression within subclasses of neurons, it was hypothesized that Dprs and DIPs could instruct synaptic partner matching (Carrillo et al., 2015; Özkan et al., 2013; Tan et al., 2015). Since their initial description, Dprs and DIPs have been shown to indeed instruct circuit wiring, but they are also required for several additional steps of nervous system development.

1.2.2.1 Dprs and DIPs instruct synaptic partner preferences

In several larval and adult *Drosophila* circuits, Dprs and DIPs instruct synaptic partner matching. Here, I will first describe the roles of Dprs and DIPs in synaptic connectivity in pupal and adult circuits before summarizing what is known in larval circuits.

In pupae, Dpr12 and DIP-δ specify innervation of mushroom body compartments by dopaminergic neurons (Bornstein et al., 2021). In the olfactory system, DIP-η is important for correct sorting of olfactory receptor neurons into glomerulus Or47b, as mutants display aberrant innervation of the neighboring Or88a glomerulus (Barish et al., 2018). In the visual system, DIP-γ and Dpr11 are required for yR7 targeting into the medulla (Carrillo et al., 2015; Courgeon and Desplan, 2019). In addition, DIP-α and Dpr6/Dpr10 are required for correct layer innervation of Dm4 and Dm12 neurons, with mutants overshooting their targets (Xu et al., 2018a). In the lamina, L4 neurons mistarget and have ectopic synapse formation and dendritic arbor morphology in the absence of *DIP-β* (Xu et al., 2019) In the adult leg, MN axon branching is lost

from proximal portions of the femur and tibia when *DIP-α* or *dpr10* are removed (Venkatasubramanian et al., 2019).

In larvae, Dpr10 and DIP-α instruct m4-Is innervation; Dpr10 is expressed in muscles and DIP-α is expressed in Is MNs. Removing either *dpr10* and *DIP-α* eliminates this synapse completely (Ashley et al., 2019). Although other NMJs share these two molecules, only m4-Is is completely lost. Thus, Dprs and DIPs are used in various compartments of the brain and peripheral circuits to instruct synaptic partner matching. However, very little is known about if Dpr/DIP function in these varying contexts is the same. For instance, is signaling required after Dpr-DIP binding, and if so, are the signaling components the same at different synapses? It seems likely that the mechanism for Dpr10 and DIP-α mediated MN-motor wiring would be similar in embryos and adults given that the same cell types and family members are at play. However, it is less clear whether Dpr-DIP function in the central nervous system and the peripheral nervous system would utilize the same signaling pathways, given the variety of cell types, complexity of the tissue, and differences in developmental stages.

1.2.2.2 Dpr10 is involved in axon pathfinding

In pupal and adult flies, olfactory receptor neurons synapse with their downstream projection neurons in discrete neuropil structures called glomeruli. These structures are highly stereotyped and serve as an excellent model for synaptic partner matching. In the pupal olfactory lobe, Dpr10 plays a role in glomerular organization. Although *dpr10* mutant phenotypes of two glomeruli, innervated by Gr21a and Or47b neurons were relatively mild, with a slight shift or elongation of the glomerulus, glomeruli innervated by Or10a and Or47a were more pronounced with an apparent shift in the path the axons took once they reach the olfactory bulb (Barish et al.,

2018). Given the many studies that implicate Dprs and DIPs in synaptic partner matching and the few (2) that demonstrate a function in pathfinding implicate only Dpr10, it seems possible that this is not a widespread function in the Dpr/DIP families.

1.2.2.3 Dprs and DIPs impact cell survival

When a neuron cannot find its correct synaptic partner, the partnerless cell can initiate programmed cell death. The initiation of cell death is likely due to the lack of trophic support that comes from forming synapses with the correct partners. This phenomenon has been observed in Dpr-DIP mediated synaptic partner matching as well. For example, in *dpr11* and *DIP-γ* mutant pupal eyes, yR7s overshoot their targets and miss the Dm8 layer, and the number of Dm8 neurons decreases to about 50% relative to controls (Carrillo et al., 2015; Courgeon and Desplan, 2019). Also, loss of *DIP-α* resulted in ~50% reduction in medullar Dm4 neurons and loss of *dpr6/dpr10* resulted in a more modest but still significant reduction of ~20% Dm4s (Xu et al., 2018a). In mutants that alter the binding affinity between Dpr10 and DIP-α, in addition to mistargeting in the pupal eye, there was a loss of Dm12 cells (Xu et al., 2022). The loss of Dm12 cells was affinity dependent: as binding affinity decreased, the number of Dm12 cells that died increased.

Notably, apoptosis has not been reported in the peripheral nervous system, suggesting that innervation of correct targets may not be as critical in the periphery as it is in the central nervous system (Ashley et al., 2019; Venkatasubramanian et al., 2019). In the periphery, rather than initiating apoptosis, Ib MNs innervate alternative partners as is seen when the target muscle is ablated and the MN innervates a nearby muscle instead (Cash et al., 1992). In another instance, MN identity was altered by overexpression of temporal transcription factors leading to ectopic

innervation in the vicinity of the muscle target (Meng et al., 2019). Thus, Dprs and DIPs impact cell survival only at central synapses, suggesting different signaling cascades and/or redundant pathways compared with peripheral synapses.

In these examples, when neurons fail to form synapses with their correct partners, they either form synapses with nearby neurons and survive or make no connection and die. The underlying mechanism is unknown; how does Dpr-DIP binding at the cell surface inhibit apoptosis? One possibility is that Dprs and DIPs bring the two opposing cells together long enough for other important trophic factors to bind and stabilize the cell. Once the membranes are stability opposed, the synapse forms and the cell functions normally. However, when the membranes aren't initially stabilized through the Dpr-DIP interaction, other trophic factors do not bind, synapses do not form, and the cell initiates apoptosis. In this way, the Dpr-DIP binding facilitates the proximity of the membranes allowing time and opportunity for the other CSPs or trophic factors to come together. In the case where Dpr-DIP binding does not occur but cells form synapses, perhaps the other CSPs and trophic factors were still able to bind and function at high enough concentrations for the cell to survive. However, this is speculation and ongoing research is exploring these possibilities.

1.2.2.4 Dprs and DIPs pair stochastic and deterministic wiring mechanisms

In the pupal eye, stochastic specification determines the type of rhodopsin a photoreceptor will express with a 70/30 split between yellow photoreceptors (yR7) and pale photoreceptors (pR7), respectively (Wernet et al., 2006). yR7s express Dpr11 and their target yDm8s in the medulla express DIP-γ (Carrillo et al., 2015; Courgeon and Desplan, 2019; Menon et al., 2019). Only when the correct pairing is present, do the cells survive. If either *dpr11* or

DIP-γ are lost, yDm8s undergo apoptosis. yDm8s express DIP-γ early in their development, long before they contact yR7s (Courgeon and Desplan, 2019). This allows for the correct pairing of a stochastically generated cell type (yR7s) with their obligate downstream binding partners (yDm8s) (Courgeon and Desplan, 2019; Menon et al., 2019).

1.2.3 Open Questions

Many important questions remain about how the Dpr/DIP family performs its multifaceted functions and by extension how biological systems have evolved to build complex neural circuits. Dprs and DIPs have been an ongoing model to study these questions in many labs leading to a rapid increase in our understanding of them.

1.2.3.1 Signaling

The question that fascinated me most when I started my PhD was how do Dprs and DIPs perform their many functions? Our understanding has significantly expanded in the years I have worked on them. Most notably, we now know that they are GPI anchored rather than transmembrane domain containing proteins, suggesting that Dprs and DIPs cannot signal directly. These findings have contributed to our models for how these CSPs perform their multifaceted functions. For example, do Dprs and DIPs interact with other CSPs that contain transmembrane and intracellular domains? And if so, how are these interactions regulated? To answer these, and other questions, a multitude of approaches are being applied including single cell RNA-seq, proximity ligation, and mass spectroscopy.

1.2.3.2 Function of additional domains

Almost all understanding of Dprs and DIPs hinges on one interface of one domain – the first Ig domain. In the adult visual system, loss of Dm4 neurons in *DIP-α* and *dpr10* mutants is rescued with constructs where the first Ig domain was replaced with Nec1 and Nec3, suggesting that the primary function of the first Ig is adhesion (Xu et al., 2018a). However, these constructs retained the remaining Ig domains from DIP-α and Dpr10 leading to a critical question: what, if any function, do the other one/two Ig domains have?

1.2.3.3 Trafficking and regulation

Although we know that the exquisite expression patterns of Dprs and DIPs are restricted in cell subtype specific ways in the adult olfactory lobe (Barish et al., 2018), in the adult optic lobe (Carrillo et al., 2015; Cosmanescu et al., 2018; Tan et al., 2015), the larval VNC (Carrillo et al., 2015), and the larval periphery (Wang et al., 2022), we know very little about how these expression patterns are established. Work from Chris Doe, Ellie Heckscher, Claude Desplan, and others has demonstrated that from very early on, newborn neurons "know" what they will become and who they will synapse with, likely carrying the molecular information from birth (Meng et al., 2019). Therefore, it stands to reason that the Dprs and DIPs, located all over the *Drosophila* genome, are regulated by transcription factors that can discern their promoters. However, not all Dprs and DIPs are far apart. For example, Dpr6 and Dpr10 are within a few kilobases on chromosome III, and yet only Dpr10 is expressed in muscles (Ashley et al., 2019; Wang et al., 2022). Understanding how this is regulated will be greatly beneficial to our understanding of cell type specificity.

To perform their functions, Dprs and DIPs must localize to specific regions of the cell such as the tips of filopodia on growth cones. However, we lack any insight into how Dprs and DIPs are trafficked. Later, my work in collaboration with Viola Nawrocka will show that they are GPI anchored, a feature that influences how Dprs and DIPs are trafficked. Here, I will aim to address the following questions: How are Dprs and DIPs attached to cells? Is their expression maintained throughout development because they have additional functions beyond synaptic partner matching? What interactions do Dprs and DIPs have outside of their families?

CHAPTER 2

NEURONAL WIRING RECEPTORS DPRS AND DIPS ARE GPI ANCHORED AND THIS MODIFICATION CONTRIBUTES TO THEIR CELL SURFACE ORGANIZATION

Viola Nawrocka performed the GPI anchor predictions, FACS experiments, cell aggregation assays, and cloning. This chapter is currently under revision and can be found on BioRxiv.

2.1 Introduction

Cell Surface Proteins (CSPs) allow a cell to interact with neighboring cells and the extracellular matrix and interpret chemical cues from its environment. CSPs can be attached to cells through hydrophobic transmembrane domains that traverse the lipid bilayer or via post-translational modifications that anchor the protein in the plasma membrane. One such modification is the addition of a glycosylphosphatidylinositol (GPI) anchor, which is covalently linked to the C-terminus of the protein and embeds its hydrophobic acyl chains into the outer leaflet of the cell membrane (Ferguson and Williams, 1988; Finean, 1977; Ikezawa and Nakajima, 1976). GPI anchors are attached at the ω site, typically a small amino acid, flanked upstream by an unstructured region and downstream by a stretch of hydrophobic residues (Eisenhaber et al., 1999). The GPI anchor is added in the ER lumen during protein synthesis, and the mature protein is trafficked to the cell membrane through the secretory pathway (Orlean and Menon, 2007). GPI-anchored proteins cannot signal into the cells directly, as the anchors do not physically reach into the cell interior. Thus, the interaction of GPI linked proteins with intracellular signaling pathways likely requires engagement of transmembrane co-receptors able to transduce the signal inside the cell.

The human genome is predicted to encode at least 129 GPI-anchored proteins

(Consortium, 2015). These include molecules implicated in a variety of functions in the nervous system including axon guidance and synaptic adhesion (reviewed in (Um and Ko, 2017)). Abrogation of GPI anchoring and defects in biosynthesis of GPI anchors have been implicated in various diseases including central nervous system disorders (Lukacs et al., 2019).

Computational tools to predict GPI-anchored proteins have been unreliable due, in part, to small training sets and similarity of features associated with GPI anchors and transmembrane domains. Compounding issues with predictions, the membrane-anchoring status of a particular protein cannot simply be deduced from its homology with other proteins; protein families may include members that can be transmembrane, GPI anchored and secreted. For example, the Semaphorin family of key axon guidance cues includes members that are secreted (classes 2 and 3), transmembrane (classes 1, 4, 5, 6) and GPI anchored (class 7) (Kruger et al., 2005). Sema7A is GPI anchored and involved in axonal outgrowth (Pasterkamp et al., 2003), synaptic pruning (Uesaka et al., 2014), and integrin-dependent stimulation of immune cells (Suzuki et al., 2008). Ephrins, the membrane-tethered ligands for the receptor tyrosine kinases, Ephs, are divided into GPI anchored ephrin-A and single-pass transmembrane ephrin-B classes and act by binding their cognate EphA and EphB receptors, respectively (Committee, 1997; Gale et al., 1996). Interestingly, GPI-anchored Ephrin-A5 has been shown to transmit an intracellular signal despite the lack of intracellular region; it partitions into caveolae-like microdomains and engages Fyn protein tyrosine kinase signaling upon interaction with an externally applied soluble form of EphA5 receptor (Davy et al., 1999).

The IgLONs, a five-member family of conserved mammalian CSPs, are GPI anchored and function in neurite outgrowth and synaptogenesis (Hachisuka et al., 1996; Itoh et al., 2008; Sanz et al., 2015; Struyk et al., 1995). IgLON-mediated signaling remains poorly understood although one member, Negr1, is cleaved by an ADAM-family protease and binds to an FGF

receptor to stimulate dendritic arbor growth (Pischedda and Piccoli, 2016). The *Drosophila melanogaster* orthologs of the IgLONs, the Dpr–DIP family of CSPs (Cheng et al., 2019b), have been implicated in a variety of functions, including synapse specificity (Ashley et al., 2019; Carrillo et al., 2015; Courgeon and Desplan, 2019; Menon et al., 2019; Venkatasubramanian et al., 2019; Xu et al., 2018a, 2022), axonal pathfinding and fasciculation (Barish et al., 2018; Bornstein et al., 2021; Lobb-Rabe et al., 2022), cell fate determination (Courgeon and Desplan, 2019), cell survival (Carrillo et al., 2015; Xu et al., 2019, 2022), and behavior (Brovero et al., 2021). Structurally, the ectodomains of Dprs and DIPs consist of two and three immunoglobulin (Ig) domains, respectively (Carrillo et al., 2015; Courgeon and Desplan, 2019), similar to IgLONs which have three Ig domains and interact in a structurally similar manner to Dprs and DIPs (Cheng et al., 2019b; Courgeon and Desplan, 2019). However, how these proteins are linked to the cell membrane has not been determined.

Here, we tested whether members of the *Drosophila* Dpr/DIP family are GPI anchored. We observed that most, if not all, Dprs and DIPs have a GPI anchor; this was not expected as only a few family members are predicted to have GPI anchors. To bolster our hypothesis that these proteins are GPI anchored, we examined a subset of Dprs and DIPs in insect cells and live fly tissues. Treatment with GPI-specific phospholipase-C (PLC) causes shedding of Dprs and DIPs from the cell and tissue surface; this cleavage is GPI anchor-dependent, as it is lost when the GPI anchor site is replaced with a transmembrane domain of a CD4 glycoprotein. Additionally, cleavage of GPI anchors also abolishes Dpr–DIP-mediated cell aggregation. Finally, replacing the GPI anchor with a transmembrane domain perturbs presynaptic and postsynaptic localization of these CSPs. Together these findings suggest that GPI anchors of Dpr/DIP contribute to their localization and function.

2.2 Some Dprs and DIPs are predicted to be GPI anchored

The Dprs and DIPs bind selectively with one another via their ectodomains, forming an elaborate network of homo- and heterophilic interactions (Figure 2.1A). Their multifunctional roles in neural circuit development partially relies on their abilities to act as cell adhesion molecules. However, whether and how Dprs and DIPs signal intracellularly has not been examined. Determining if they are transmembrane (TM) or GPI anchored proteins would shed light on their potential signaling mechanisms.

To gain insight into how Dprs and DIPs associate with the cell membrane we used two transmembrane region prediction tools, Phobius (Käll et al., 2004) and DeepTMHMM (Hallgren et al., 2022). We first removed N-terminal signal peptides recognized by SignalP-6.0 (Teufel et al., 2022) to avoid their classification as TM domains, which is an inherent challenge for prediction tools due to the hydrophobic nature of both types of sequences. Phobius predicted 15 of the Dprs and DIPs and Klingon to have C-terminal TM regions while DeepTMHMM indicated only Dpr9 as a TM protein (Figure S2.1).

Next, we hypothesized that those Dprs and DIPs that were not transmembrane proteins may be anchored to the membrane via GPI modification (Figure 2.1B). We used two GPI signal prediction tools, PredGPI (Pierleoni et al., 2008) and NetGPI (Gíslason et al., 2021). PredGPI is built using a Hidden Markov Model (HMM) and a Support Vector Machine (SVM), trained on experimentally validated GPI anchored proteins, and produces minimal false positives while correctly identifying 89% of known GPI-containing proteins. The output of the PredGPI prediction is the most likely position of the ω site – the residue to which the lipid anchor is attached, and the "specificity" index expressing the probability of the protein to be GPI-anchored. The recently released NetGPI uses recurrent neural networks to predict GPI anchoring, the most likely position of the ω site, and the likelihood of the selected position being correct.

NetGPI was reported to slightly outperform PredGPI (Gíslason et al., 2021).

We examined all 32 members of the Dpr/DIP family and Klingon, a *Drosophila* immunoglobulin superfamily (IgSF) protein previously demonstrated to be GPI anchored (Butler et al., 1997), with PredGPI and NetGPI, and the majority of these CSPs were predicted to lack GPI anchors (Figure 2.1C and Table S2.2). PredGPI indicated 8 Dprs and DIPs (25%) as likely GPI linked (specificity above 99%) and Klingon as not GPI anchored as it fell under the threshold for positivity with its specificity value of 98.5%. NetGPI predicted 11 Dprs and DIPs (34%) to be GPI anchored and correctly classified Klingon. Among the proteins predicted to have a GPI modification by NetGPI, 67% were also predicted by PredGPI. Dpr3, Dpr5, and DIP-η were classified by NetGPI as likely GPI anchored, but obtained very low specificity index values of 37.3%, 16.0%, and 1.0%, respectively with PredGPI.

Overall, 12 Dprs and DIPs were predicted to be GPI anchored by either PredGPI or NetGPI (Figure S2.2). 15 Dprs and DIPs were predicted to have TM helices, and five of these CSPs were also predicted to have a GPI anchor (Dpr5, Dpr11, DIP-γ, DIP-ζ, and DIP-η). Ten Dprs and DIPs were not predicted to be GPI linked nor to contain a TM helix (Dpr4, Dpr6, Dpr10, Dpr13, Dpr15, Dpr16, Dpr17, DIP-θ, DIP-ι). Thus, using prediction tools alone did not unequivocally classify how these CSPs are anchored to the cell.

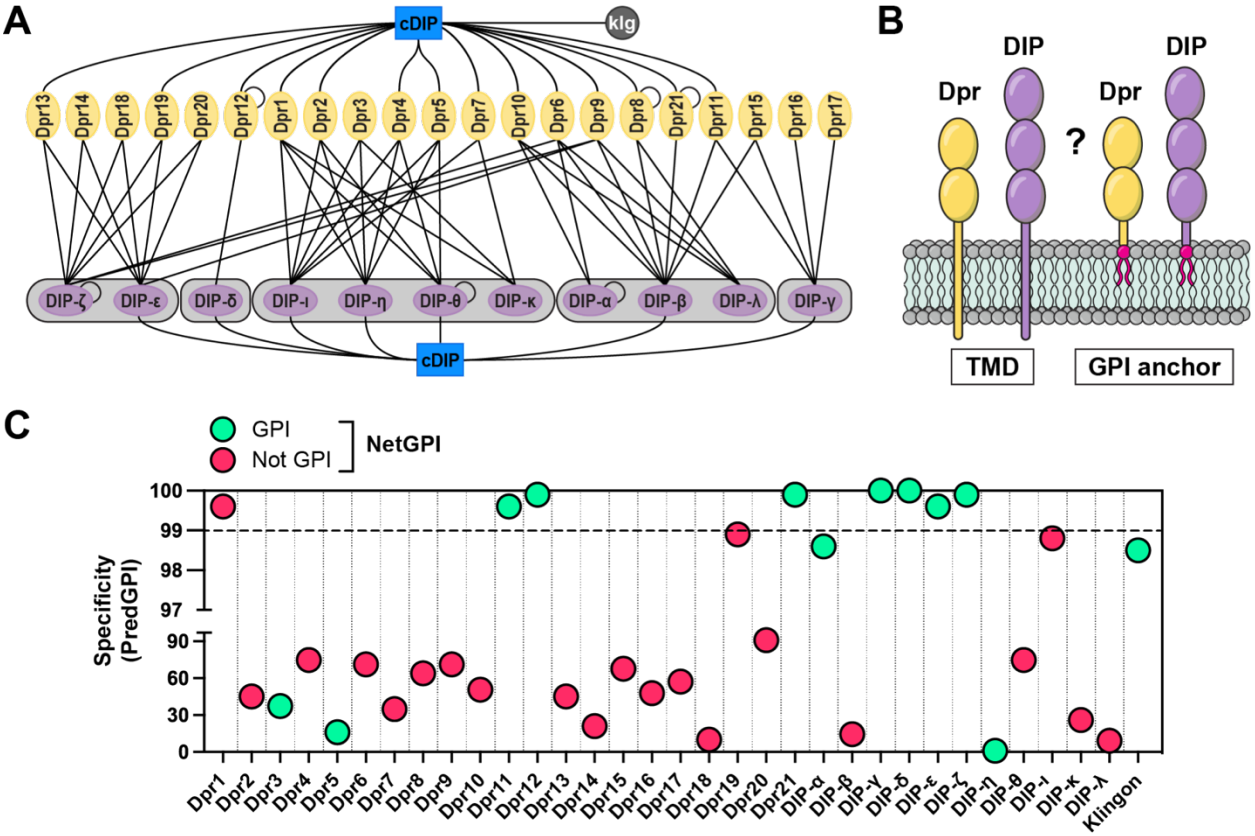

Figure 2.1 GPI anchoring predictions for the Dpr and DIP families of CSPs.
(A) Dpr-DIP interactome. Lines indicate interactions determined in previously published *in vitro* studies. cDIP, common DIP- interacting protein; Klg, Klingon. (B) Two potential membrane-anchoring modes of Dprs and DIPs. TMD, transmembrane domain; GPI, glycosylphosphatidylinositol. (C) GPI anchor predictions using PredGPI and NetGPI. Specificity values as calculated by PredGPI were plotted for each protein. Proteins with specificity values above 99% are considered GPI-anchored. For NetGPI, positive predictions are shown as green and negative are shown as red.

Protein	Isoform	FlyBase ID	Source	DGRC cDNA clone
Dpr1	A	FBcl0481435	DGRC	IP20514
Dpr2	F	FBtr0340553	Extended ECD	-
Dpr3	B	FBtr0300671	Extended ECD	-
Dpr4	B	FBcl0702669	DGRC	FI04761
Dpr5	B	FBcl0135155	DGRC	GH08163
Dpr6	C	FBtr0331536	Extended ECD	-
Dpr7	F	FBtr0334408	Extended ECD	-
Dpr8	A	FBcl0120305	DGRC	GH05565
Dpr9	X	FBcl0129707	DGRC	GH01517
Dpr10	D	FBtr0331552	Extended ECD	-
Dpr11	B	FBcl0127201	DGRC	GH22307
Dpr12	C	FBcl0317539	DGRC	IP17045
Dpr13	B	FBcl0345923	DGRC	IP04317
Dpr14	A	FBcl0119149	DGRC	GH19181
Dpr15	X	FBcl0474633	DGRC	FI05813
Dpr16	B	FBtr0110950	Extended ECD	-
Dpr17	A	FBcl0743266	DGRC	FI20195
Dpr18	A	FBcl0212563	DGRC	RE24718
Dpr19	A	FBcl0191639	DGRC	LP09705
Dpr20	A	FBcl0124577	DGRC	GH16485
Dpr21	C	FBtr0334939	Extended ECD	-
DIP-α	A	FBcl0222778	DGRC	RE16159
DIP-β	G	FBtr0343091	Extended ECD	-
DIP-γ	A	FBcl0116341	DGRC	GH08175
DIP-δ	D	FBcl0303889	DGRC	IP08460
DIP-ε	A	FBtr0299967	Extended ECD	-
DIP-ζ	A	FBcl0474748	DGRC	FI03417
DIP-η	B	FBtr0302933	Extended ECD	-
DIP-θ	A	FBtr0079114	Extended ECD	-
DIP-ι	B	FBcl0293758	DGRC	IP10422
DIP-κ	A	FBcl0202207	DGRC	RE42927
DIP-λ	A	FBtr0346766	Extended ECD	-
Klingon	-	FBcl0158367	DGRC	LD10776

Table 1.1 Selection of sequences used in our analysis.
X under isoform indicates the exact sequence used in our analysis.

Protein	PredGPI prediction	Specificity	NetGPI prediction	Likelihood
Dpr1	GPI	99.60%	Not-GPI	0.975
Dpr2	Not-GPI	45.20%	Not-GPI	0.978
Dpr3	Not-GPI	37.30%	GPI	0.565
Dpr4	Not-GPI	74.80%	Not-GPI	0.813
Dpr5	Not-GPI	16.00%	GPI	0.407
Dpr6	Not-GPI	71.20%	Not-GPI	0.994
Dpr7	Not-GPI	34.80%	Not-GPI	0.508
Dpr8	Not-GPI	64.00%	Not-GPI	0.885
Dpr9	Not-GPI	71.20%	Not-GPI	0.995
Dpr10	Not-GPI	50.70%	Not-GPI	0.989
Dpr11	GPI	99.60%	GPI	0.341
Dpr12	GPI	99.90%	GPI	0.542
Dpr13	Not-GPI	45.20%	Not-GPI	0.922
Dpr14	Not-GPI	21.10%	Not-GPI	0.831
Dpr15	Not-GPI	67.70%	Not-GPI	0.992
Dpr16	Not-GPI	47.80%	Not-GPI	0.305
Dpr17	Not-GPI	57.20%	Not-GPI	0.793
Dpr18	Not-GPI	10.10%	Not-GPI	0.612
Dpr19	Not-GPI	98.90%	Not-GPI	0.352
Dpr20	Not-GPI	90.90%	Not-GPI	0.338
Dpr21	GPI	99.90%	GPI	0.283
DIP-α	Not-GPI	98.60%	GPI	0.301
DIP-β	Not-GPI	14.50%	Not-GPI	0.941
DIP-γ	GPI	100.00%	GPI	0.686
DIP-δ	GPI	100.00%	GPI	0.432
DIP-ε	GPI	99.60%	GPI	0.45
DIP-ζ	GPI	99.90%	GPI	0.643
DIP-η	Not-GPI	1.00%	GPI	0.422
DIP-θ	Not-GPI	74.80%	Not-GPI	0.606
DIP-ι	Not-GPI	98.80%	Not-GPI	0.501
DIP-κ	Not-GPI	25.90%	Not-GPI	0.992
DIP-λ	Not-GPI	9.10%	Not-GPI	0.802
Klingon	Not-GPI	98.50%	GPI	0.486

Table 1.2 GPI site predictions by PredGPI and NetGPI.
Results of GPI-anchor site predictions with PredGPI and NetGPI. Values of specificity index calculated by PredGPI indicate the probability of the presence of a GPI-anchor. Likelihood values for the positive calls from NetGPI pertain to the prediction of the ω site position.

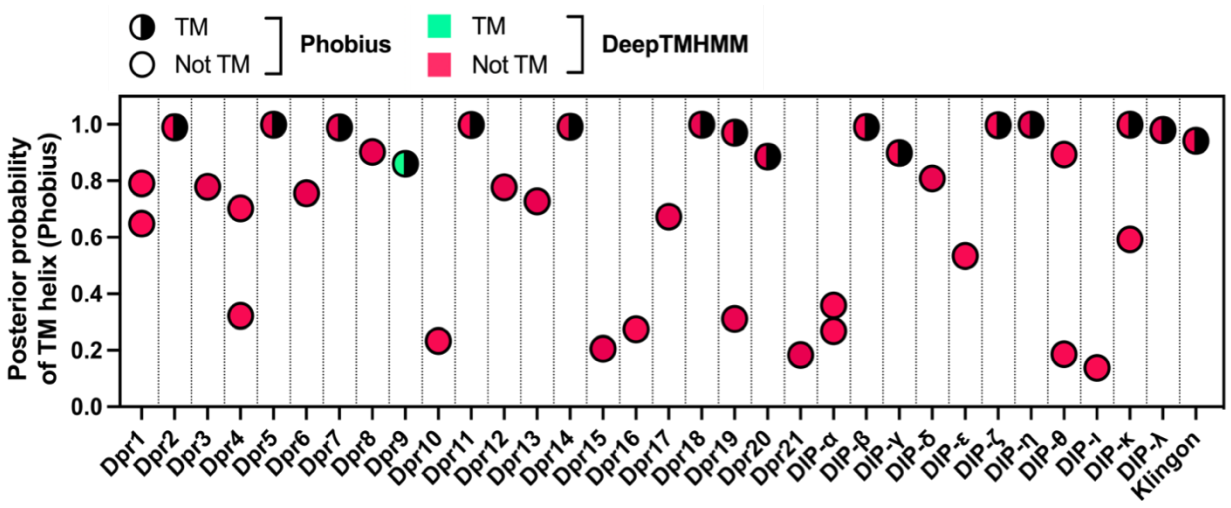

Figure S2.1 Transmembrane region prediction by Phobius and DeepTMHMM.
Plotted are the highest values of posterior probability of a TM helix reported from Phobius. In cases where there were two regions with posterior probability of TM helix above 0.1, the highest values for both were plotted. TM, transmembrane. The highest values of posterior probability in Phobius do not always correlate with positive prediction for a given protein (Käll et al., 2007; for example, posterior probabilities of TM helix for Dpr8 or DIP-θ are higher than the one for Dpr9, but the former two were not predicted by Phobius to have a TM helix).

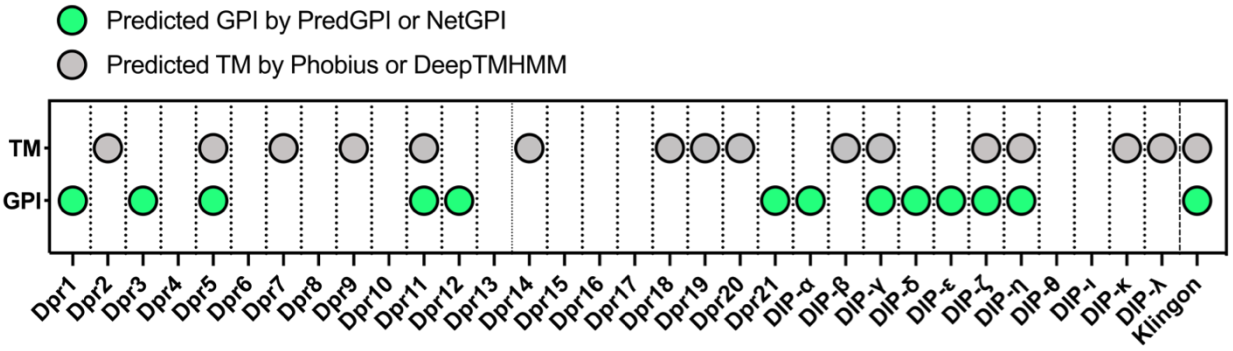

Figure S2.2 Summary of GPI anchor and TM helix predictions.

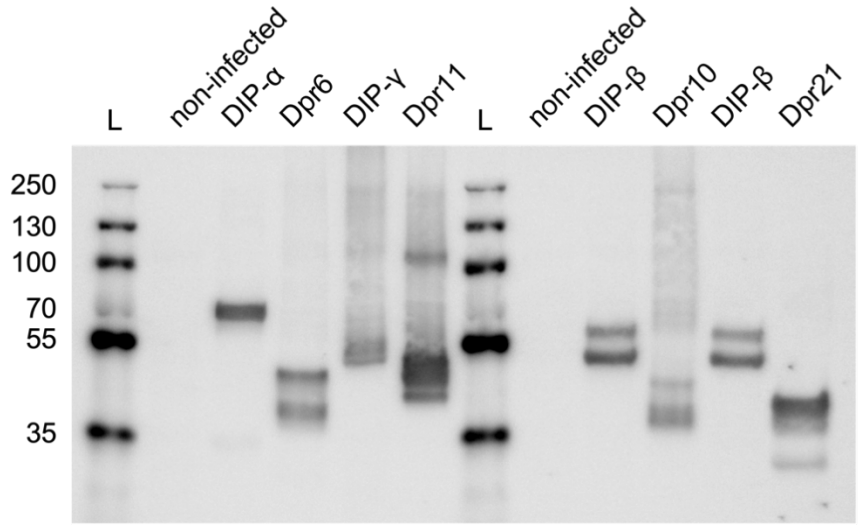

Figure S2.3 Expression of V5-tagged Dprs and DIPs in Sf9 cells used in cell aggregation assays.
Sf9 cell pellets were solubilized and used in western blot with anti-V5-Alexa Fluor 647 antibody. L, molecular weight ladder. Expected molecular weights of proteins before N-linked glycosylation: DIP-α: 58.7 kDa; Dpr6: 41.9 kDa; DIP-γ: 45.7 kDa; Dpr11: 36.2 kDa; DIP-β: 53.1 kDa; Dpr10: 40.7 kDa; Dpr21: 31.7 kDa.

2.3 Dprs and DIPs are anchored to the membrane via glycophosphatidyl linkages

Because of limitations in GPI predictions, such as the lack of a consensus GPI motif, we hypothesized that the predictors underestimated the number of Dprs and DIPs that are GPI modified. To complement the prediction tools and examine the membrane anchoring mechanism(s) of all Dprs and DIPs, we setup an S2 cell culture pipeline with V5-tagged, full-length proteins (see Table S2.1 and the methods section for details). Duplicate S2 cultures were established for each CSP, and one culture was treated with the GPI-cleaving enzyme Phospholipase C (PLC). Supernatant and cell fractions were collected and used for western blot analyses to determine if the CSP was cleaved by PLC. The GPI-anchored protein Klingon was used as the positive control and the secreted cDIP and transmembrane IgSF proteins Roughest (Rst) and Kirre served as negative controls (Butler et al., 1997; Carrillo et al., 2015; Ramos et al., 1993; Ruiz-Gómez et al., 2000). If the CSPs are GPI anchored, we expect an increase of protein in the supernatant and a concomitant decrease in the cell fraction after PLC treatment (Figure 2.2A). Remarkably, all Dprs and DIPs displayed these trends, suggesting that Dprs and DIPs are GPI anchored (Figure 2.2B). We observed differences between samples with some CSPs cleaved more readily than others (i.e. more CSP in the supernatant or less CSP in the cell lysate after PLC treatment). However, even our positive control, Klingon, was not completely cleaved (Figure 2.2B), as observed before (Butler et al., 1997). These observations may be due to incomplete GPI processing and trafficking, incomplete access of the PLC to a subset of CSPs, chemical heterogeneities in GPI anchors, insufficient amounts of PLC used in the assay, or variations in CSP expression levels. Some of the CSPs appear as doublets in "–PLC" cell lysates. PLC treatment releases the lower band into media, as observed before in other GPI-anchored proteins (e.g., see (Moran et al., 1991)), where the upper band was shown to represent full-length protein, not processed to add a GPI anchor and not yet transported to cell surface.

We next used flow cytometry as an orthogonal method to demonstrate the GPI anchoring of Dprs and DIPs. We expressed the same, N-terminally V5-tagged constructs of three Dprs and three DIPs in Sf9 cells using baculoviral infection. The cultures expressing individual Dprs and DIPs, as well as the negative control, Rst, were split into two samples: one was treated with PLC, and the other served as an untreated control. Both samples were stained with fluorescent antibodies against V5 tag and the relative levels of proteins on the surface of PLC-treated and untreated cells were assessed using a flow cytometer. All DIPs tested, DIP-α, DIP-β, and DIP-γ, showed a significant decrease in protein levels on the surface of Sf9 cells after PLC treatment (Figure 2.3A-C). Similarly, all Dprs tested, Dpr10, Dpr11, and Dpr21, were mostly cleaved off the cell surface by PLC (Figure 2.3D-F). In contrast, the level of Rst on the cell surface remained unaffected by PLC cleavage (Figure 2.3G-H), as expected for a transmembrane protein. The differential extent of cleavage between all tested Dprs and DIPs may be explained by the potentially different accessibility of the GPI cleavage site for each of the proteins. The results obtained using flow cytometry corroborate the observations made using western blot analyses. Together, these findings demonstrate that Dprs and DIPs are GPI anchored.

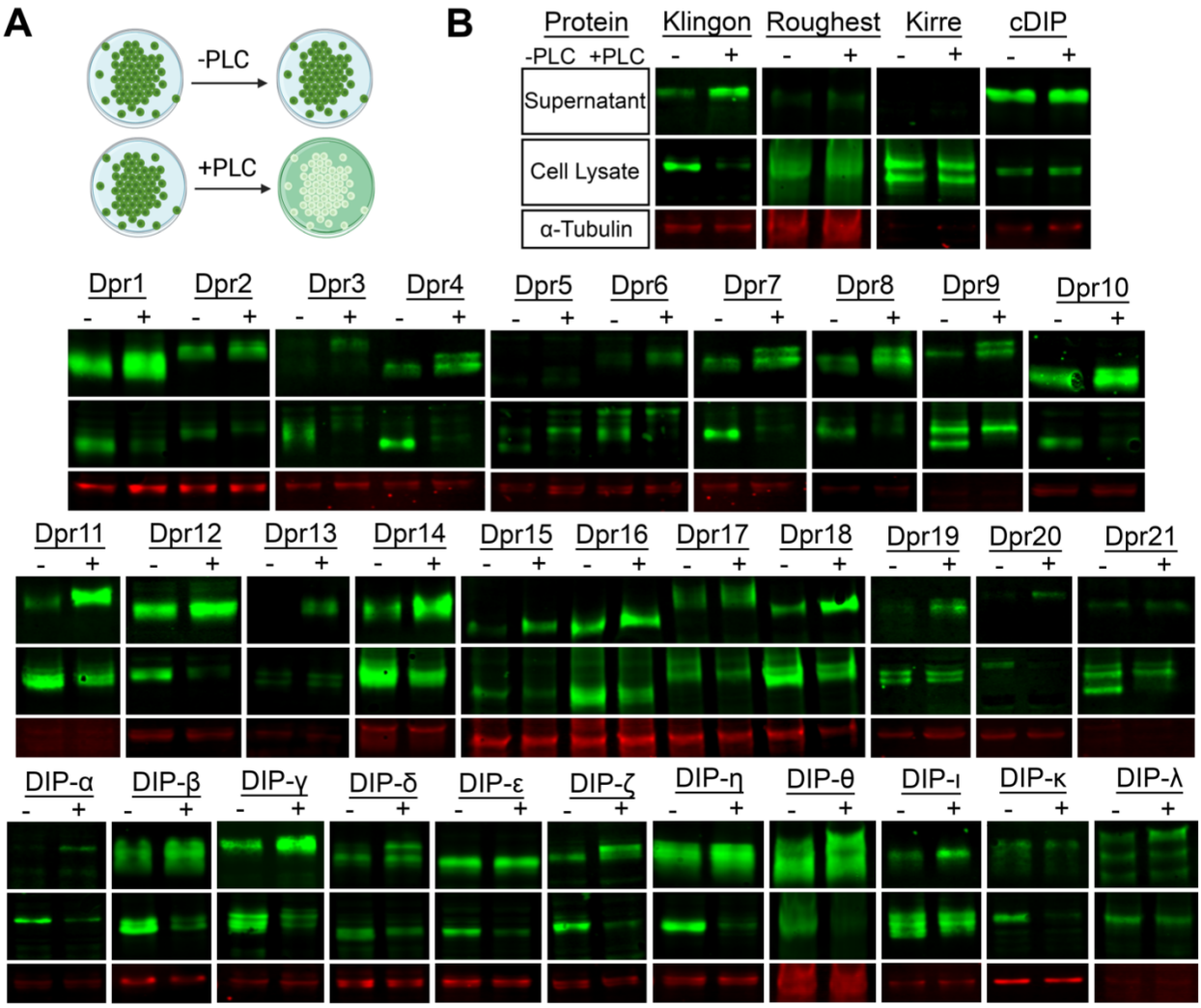

Figure 2.2 PLC treatment cleaves Dprs and DIPs from S2 cells, as observed by western blotting.

(A) Schematic for PLC cleavage assay on S2 cells, when a CSP is GPI anchored. Green color indicates where the GPI-anchored protein is (on cells or in culture media). (B) Western blots of the supernatant fraction, cell lysate, and Tubulin-α loading control for with (+) and without (–) PLC treatment for all members of Dpr/DIP subfamilies. See key in the top row for B.

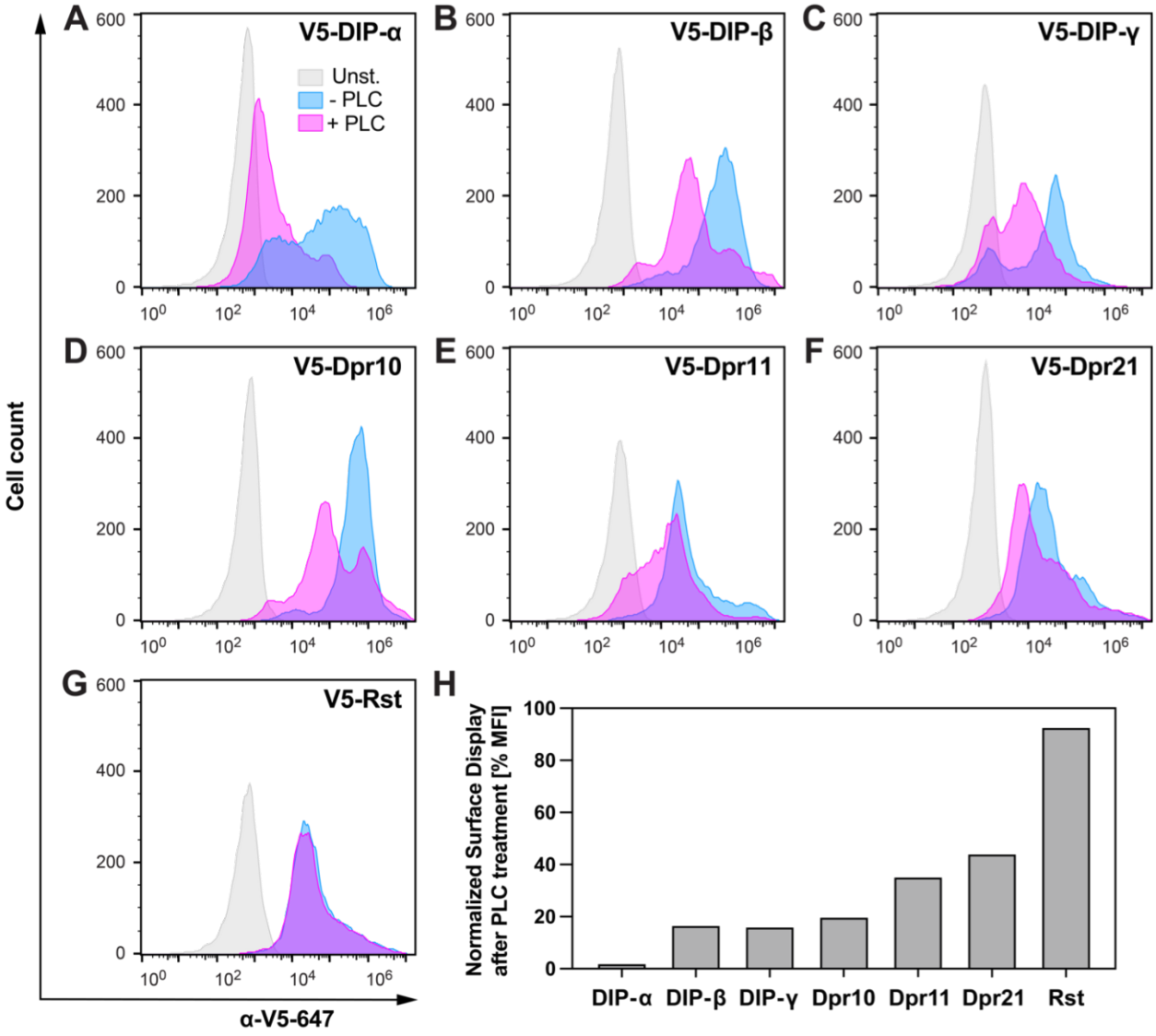

Figure 2.3 Surface display of Dprs and DIPs is reduced by PLC treatment, as observed by flow cytometry.
(A-G) Histograms showing fluorescence levels of baculovirus-infected, unstained Sf9 cells (gray), cells infected and stained with anti-V5-Alexa Fluor 647 antibody (blue), and cells infected, treated with PLC and stained with anti-V5-Alexa Fluor 647 antibody (magenta). (H) Remaining Dpr and DIP levels on Sf9 cell surface following PLC treatment, normalized as the ratio of median fluorescence intensity (MFI) for PLC-treated and not treated cells after subtraction of the background MFI value of unstained cells.

2.4 GPI anchor cleavage eliminates Dpr–DIP-mediated cell aggregation

Dprs and DIPs are thought to mediate cell adhesive interactions to accomplish many of their roles in the nervous system (Xu et al., 2022). A powerful in vitro approach to study cell adhesion interactions is the cell aggregation assay (Honig and Shapiro, 2020; Kumari and Varadaraj, 2009). Here, we combined cell aggregation and PLC assays to test whether cleavage of GPI anchors abrogates cell adhesion mediated by Dprs and DIPs.

For our combined aggregation/PLC assay, we used Sf9 cells infected with baculoviruses encoding mScarlet or EGFP followed by V5-tagged, full-length Dpr or DIP, respectively, separated by a P2A peptide. We confirmed the expression of Dprs and DIPs using western blots with an anti-V5 antibody (Figure S2.3). Cultures expressing individual Dprs with mScarlet were mixed with cultures expressing cognate DIP partners and EGFP. We predicted that, if Dprs and DIPs are GPI-anchored cell adhesion molecules, Dpr–DIP interactions would lead to aggregation between the respective cells, and application of PLC would break up the aggregates.

Levels of clustering observed in cell aggregation assays are a function of (i) expression levels, (ii) CSPs' affinities and dissociation kinetics, (iii) competing *cis* interactions, and (iv) experimental conditions, such as mixing speeds, incubation and washing times. While we can control (iv), the others are different for every CSP pair, and therefore cell cluster size and extent of aggregation are different across different pairs of CSPs (Foty and Steinberg, 2005; Katsamba et al., 2009). However, since –PLC and +PLC samples for a given Dpr-DIP pair are split from the same population of transfected cells, our assay comparing Dpr-DIP-mediated aggregation with and without PLC treatment do not suffer from any of the variations in aggregation mentioned above.

Among the four pairs of cognate Dprs and DIPs tested, DIP-α and Dpr6, DIP-β and Dpr10, and DIP-γ and Dpr11 induced robust aggregation of Sf9 cells (Figure 2.4A-E). DIP-β and

Dpr21-expressing cells aggregated significantly less, which was unexpected considering their relatively high affinity compared to other Dpr–DIP pairs (Cosmanescu et al., 2018), and that the expression levels of DIP-β and Dpr21 were comparable to other proteins tested here. One reason for the reduced aggregation may be weak homophilic Dpr21 interactions (K_D ~ 50 μM) on the same cell that may prevent efficient heterophilic interactions with DIP-β between cells, as homophilic and heterophilic complexes use the same interfaces and cannot co-exist (Cheng et al., 2019a; Cosmanescu et al., 2018). Nonetheless, the addition of PLC either significantly reduced or abolished cell aggregation for all four pairs of Dprs and DIPs (Figure 2.4E). These results demonstrate that Dpr–DIP interactions instruct cell adhesion and suggest that Dprs and DIPs are anchored to the cell surface membrane via GPI modifications.

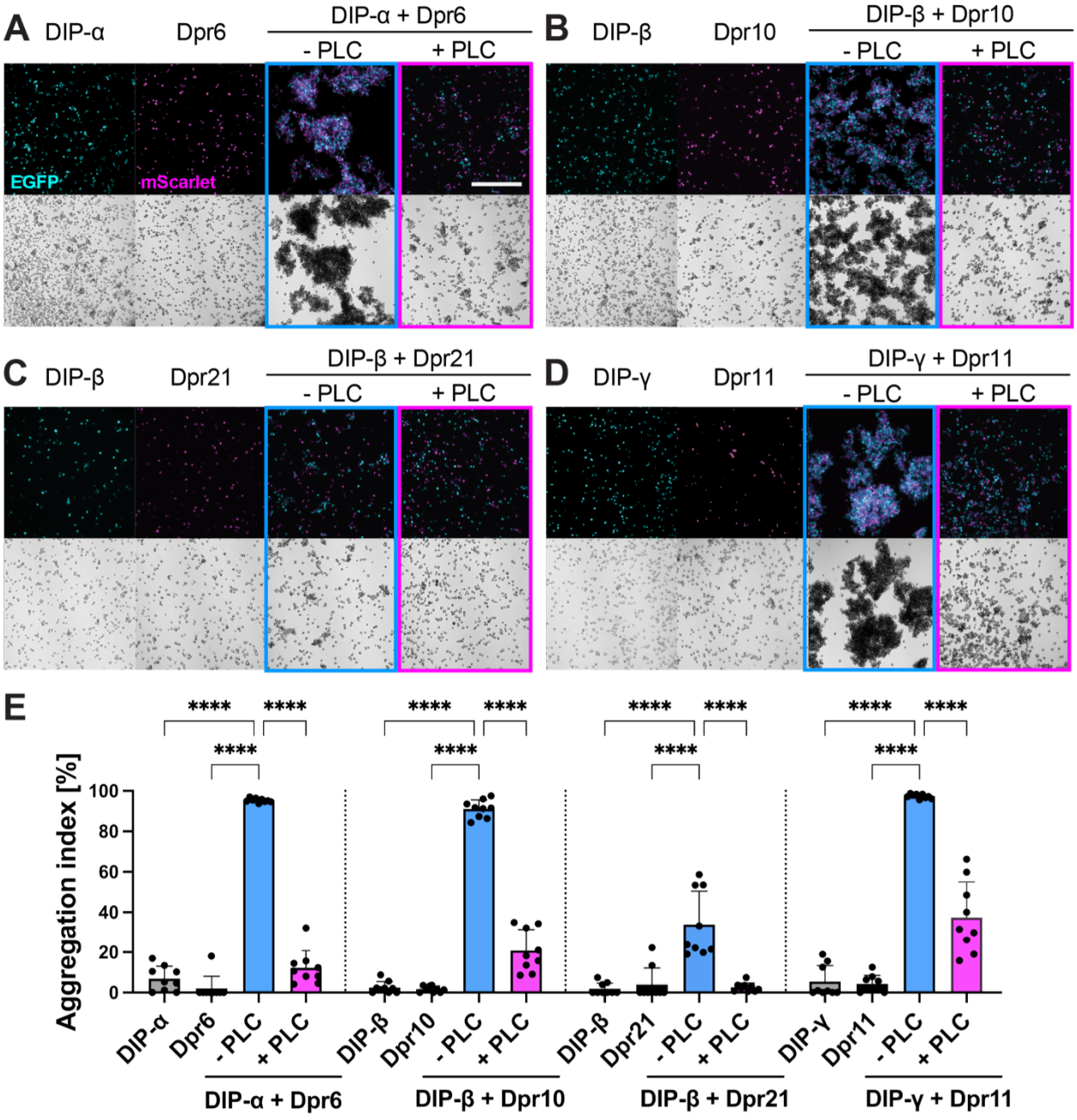

Figure 2.4 PLC cleavage eliminates Dpr–DIP-mediated cell aggregation. (A-D) Cell aggregation experiments with Sf9 cells. Controls included cultures expressing either DIP or Dpr (first two panels from the left) and cultures expressing DIP or Dpr mixed together but not treated with PLC (-PLC). Cell aggregation was abolished when PLC was added to the mixed cultures 30 minutes after aggregation (+PLC). Scale bar = 500 μm. (E) Cell aggregation index for the samples shown in A-D; ****$p < 0.0001$; one-way ANOVA.

2.5 Dpr and DIP proteins are GPI anchored in vivo

Having demonstrated that most, if not all, Dprs and DIPs are GPI anchored in vitro, we hypothesized that the same modification occurs in fly tissue. To test this, we expressed tagged forms of a subset of Dprs and DIPs in the neuromuscular circuit using the GAL4-UAS system. The larval *Drosophila* neuromuscular junction (NMJ) is an excellent system to examine cell surface proteins, as the circuit is well characterized and easily imaged. Moreover, Dprs and DIPs are endogenously expressed at the larval NMJ (Wang et al., 2022), and several Dprs and DIPs are implicated in NMJ development. DIP-α and Dpr10 are known to function in motor axon pathfinding and innervation (Ashley et al., 2019; Lobb-Rabe et al., 2022), and DIP-γ and Dpr11 regulate synaptic growth through the BMP pathway (Carrillo et al., 2015).

To achieve high protein levels in a cell type that would allow for easy visualization of Dprs and DIPs on the cell surface, we expressed proteins in muscles using *Mef2-GAL4* and omitted detergents in the initial steps of our staining protocol. Muscles are highly stereotyped, multinucleated cells that are easily imaged. In third instar larvae, V5-Dpr19 localized to the subsynaptic reticulum (SSR), a network of postsynaptic membrane folds surrounding the innervating presynaptic boutons (Figure 2.5A-B). After incubation with PLC, nearly all surface V5 signal was lost, indicating that Dpr19 is GPI anchored in vivo (Figure 2.5M). Similarly, V5-Dpr10 was localized to the SSR and PLC treatment significantly decreased the V5 signal (Figure 2.5C-D,N). However, unlike Dpr19, significant Dpr10 remained on the muscle surface in puncta surrounding boutons (Figure 2.5D,D'), suggesting that a population of Dpr10 was inaccessible to PLC or prevented from diffusing away by interacting with other CSPs at these sites. This observation matches the S2 and Sf9 insect cell data showing incomplete cleavage (Figures 2.2, 2.3, 2.4). To confirm that loss of the cell surface signal was due to cleavage of the GPI anchor, we generated chimeric transmembrane tethered Dpr10 proteins by replacing the second Ig

domain and C-terminus of Dpr10 with the fourth Ig and transmembrane domains of CD4 (a transmembrane protein not endogenously found in flies). As expected, the cell surface abundance of this chimeric Dpr10-CD4 was unaffected after PLC treatment, suggesting that Dpr10 is anchored at the NMJ via GPI modification (Figure 2.5E-F',O). Conversely, when we replaced Ig1 of Dpr10 with the first Ig domain of CD4 but retained the second Ig and C-terminus, this chimeric CD4-Dpr10 was efficiently released from the muscle surface by PLC (Figure 2.5G-H',P), indicating that some PLC-released Dpr10 was likely retained on the cell surface through its adhesion domain, Ig1, via interactions with endogenous Dprs and DIPs. These results demonstrate that Dpr10 and Dpr19 are GPI anchored in their endogenous tissue.

Next, we examined two DIPs, DIP-α and DIP-ζ. Although neither is endogenously expressed in muscles (Wang et al., 2022), an ectopically expressed DIP-α variant localized to the SSR (Figure 2.5I). Like Dpr10 and Dpr19, DIP-α was released from the muscle surface after PLC treatment (Figure 2.5I-J',Q). However, cleavage was less efficient, and DIP-α puncta formed on the muscle surface and around boutons after treatment. Similar to Dpr10, replacing Ig2-Ig3 and the C-terminus of DIP-α with CD4 blocked the PLC-mediated release from the muscle surface (Figure 2.5K-L',R). Strikingly, DIP-ζ did not localize to the SSR, and PLC treatment resulted in increased DIP-ζ puncta across the muscle surface (Figure S2.4A-C). Overall, these data show that PLC treatment affects Dpr10, DIP-α and -ζ attachment and localization in vivo and support our model that Dprs and DIPs are GPI anchored CSPs.

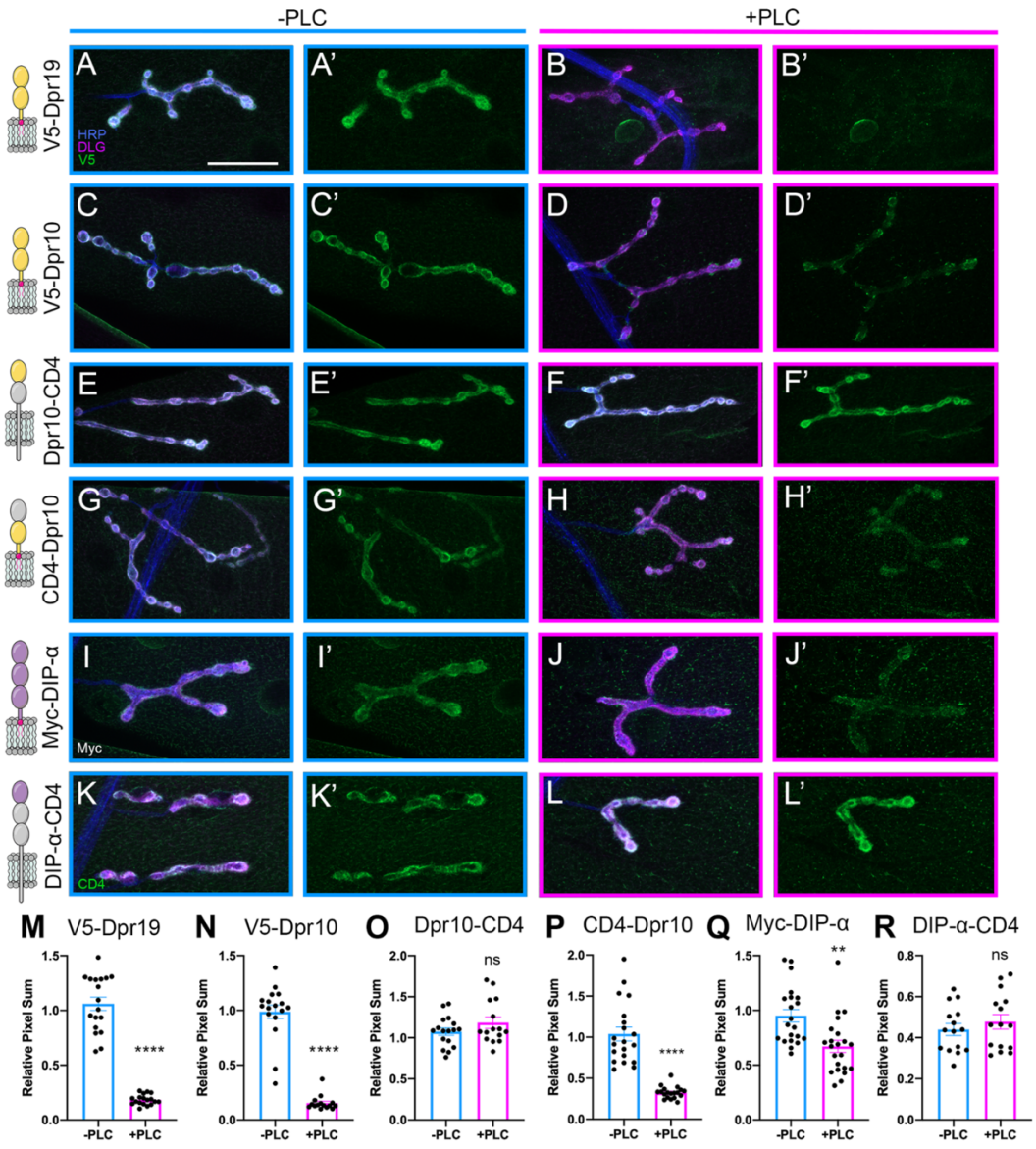

Figure 2.5 Dpr and DIP proteins are GPI anchored in vivo. (A-L') Tagged Dprs and DIPs were expressed in muscles, and dissected larvae were treated with PLC and compared to non-treated controls. Cartoon presentations of tagged Dprs and DIPs and their domains are depicted in left column. Surface localized proteins are shown in green, neuronal tissue in blue (HRP), and postsynaptic membrane in magenta (DLG). (A-B) PLC efficiently reduced surface labeling of V5 on muscles expressing V5-Dpr19 (n = 18/6 vs n = 18/6). (C-D) PLC efficiently reduced surface labeling of V5 on muscles expressing V5-Dpr10 (n = 12/6 vs n = 10/6). (E-F) PLC failed to reduce labeling of V5 in muscles expressing Dpr10-CD4 chimeras (n = 17/6 vs n = 15/6). (G-H) PLC efficiently reduced surface labeling of V5 in muscles expressing CD4-Dpr10 chimeras (n = 20/9 vs n = 19/9). (I-J) PLC reduced surface labeling of Myc on muscles expressing Myc-DIP-α (n = 21/9 vs n = 22/9). (K-L) PLC failed to reduce muscle labeling of CD4 on muscles expressing DIP-α-CD4 chimeras (n = 15/6 vs n = 15/6) (M- R) Quantification of experiments shown in A-L'. Number of n reported as $n = a/b$ where a = segments and b = animals for -PLC vs +PLC treatment. Scale bar = 50 μm. $^{**}p = 0.0097$, $^{****}p < 0.0001$; t-test.

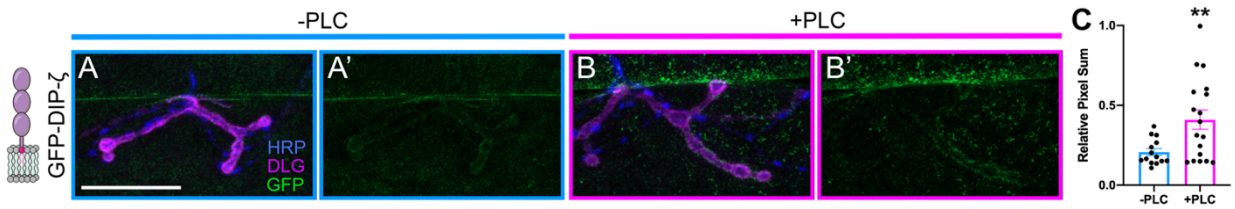

Figure S2.4. DIP-ζ aggregates in response to PLC treatment. (A-B') Tagged DIP-ζ was expressed in muscles and dissected larvae were treated with PLC and compared to non-treated controls. Cartoon of tagged DIP-ζ is shown in left column. Surface localized DIP-ζ is shown in green, neuronal tissue in blue (HRP), and postsynaptic membrane in magenta (DLG). (A-B) PLC efficiently increased surface labeling of V5 on muscles expressing EGFP-DIP-ζ. Scale bar = 50 μm. (C) Quantification of experiments shown in A-B'.

2.6 GPI anchor alters localization in neurons and muscle cells

GPI modifications have been shown to contribute to the subcellular localization of CSPs (Arumugam et al., 2021; Sharma et al., 2004). Thus, we examined localization of ectopically expressed wild type and chimeric Dpr10 and DIP-α in their endogenous tissues. DIP-α is expressed in a subset of motor neurons called the Is type and localizes to the axon terminals (Ashley et al., 2019; Carrillo et al., 2015; Wang et al., 2022). Using a Is motor neuron-specific driver, *A8-GAL4* (Venkatasubramanian et al., 2019; Wang et al., 2021), we confirmed that Myc-DIP-α localizes to puncta in the motor axon terminal (Figure 2.6A-B'). However, when the GPI anchor was replaced with a TM domain, DIP-α was redistributed and fewer puncta formed, suggesting that clustered presynaptic localization is partially due to the GPI anchor (Figure 2.6C-D'). These changes were confirmed by quantifying DIP-α puncta in the terminal three boutons in each condition: In order to determine the nature of this localization difference, samples were thresholded and collapsed to a binary representation (Figure 2.6B,D), and then the number of particles in and around the three terminal boutons of each arbor were quantified. Control and treatment larvae were pooled and stained together before images were collected using identical settings, and all samples were thresholded using the same parameters. Myc-DIP-α formed more and smaller puncta compared to DIP-α-CD4 (Figure 2.6I-J; Figure S2.5A-B), suggesting that the GPI anchor contributes to the subcellular localization of DIP-α in vivo.

As described above, expressing Dpr10 in muscles results in Dpr10 localization at the SSR, the membrane folds that form around in presynaptic boutons. However, additional puncta are observable away from boutons on the muscle surface (Figure 2.6E-H'). When quantifying the muscle field, these puncta were significantly reduced when compared to the localization of the chimeric DIP-α containing a transmembrane helix (Figure 2.6K-L; Figure S2.5C-D). Taken together, GPI anchors of DIP-α and Dpr10 contribute to both their pre- and postsynaptic

localization.

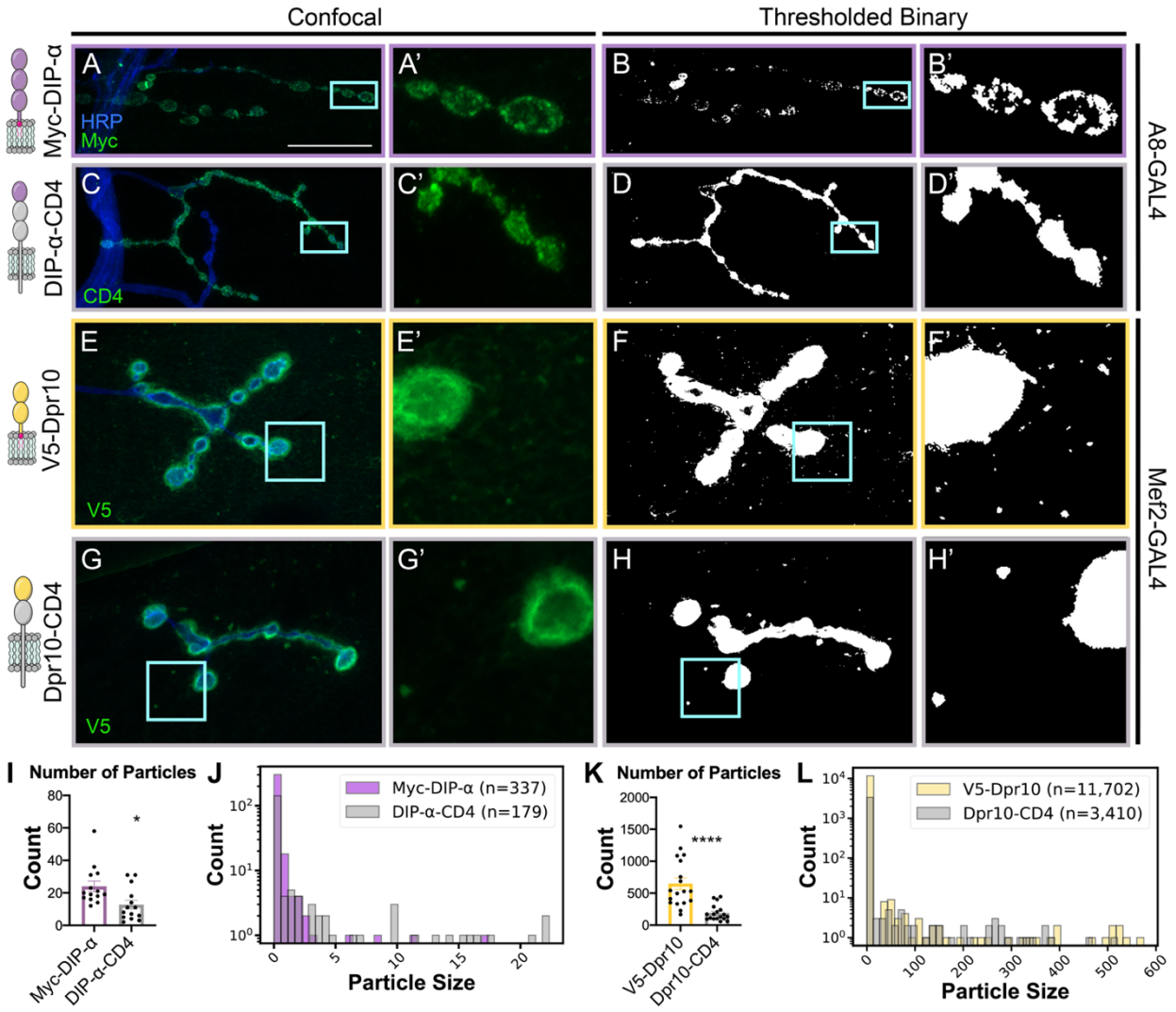

Figure 2.6 GPI anchor alters localization of DIP-α in neurons and Dpr10 in muscles. (A-H') Cartoon depictions of constructs are shown in left column. Surface localized proteins are shown in green, neuronal tissue in blue (HRP). Scale bar = 50 µm. (A-B) Tagged DIP-α and DIP-α-CD4 were expressed in Is motor neurons. (A-A') *A8-GAL4* driving Myc-DIP-α leads to punctate surface localization inside the boutons. (B-B') Binary thresholded image of A. (C-C') *A8-GAL4* driving DIP-α-CD4 leads to localization of DIP-α throughout the Is motor neuron terminal. (D-D') Binary thresholded image of C. (E-E') *Mef2- GAL4* driving V5-Dpr10 leads to punctate surface localization. (F-F') Binary thresholded image of E. (G- G') *Mef2-GAL4* driving Dpr10-CD4 leads to loss of Dpr10 throughout the muscle surface. (H-H') Binary thresholded image of G. (I,K) Particles counted for experiments depicted in A-D and E-H, respectively. (J, L) Histogram showing counts for particle size distribution, x-axis in pixels squared. *$p = 0.0129$, ****$p < 0.0001$; *t*-test.

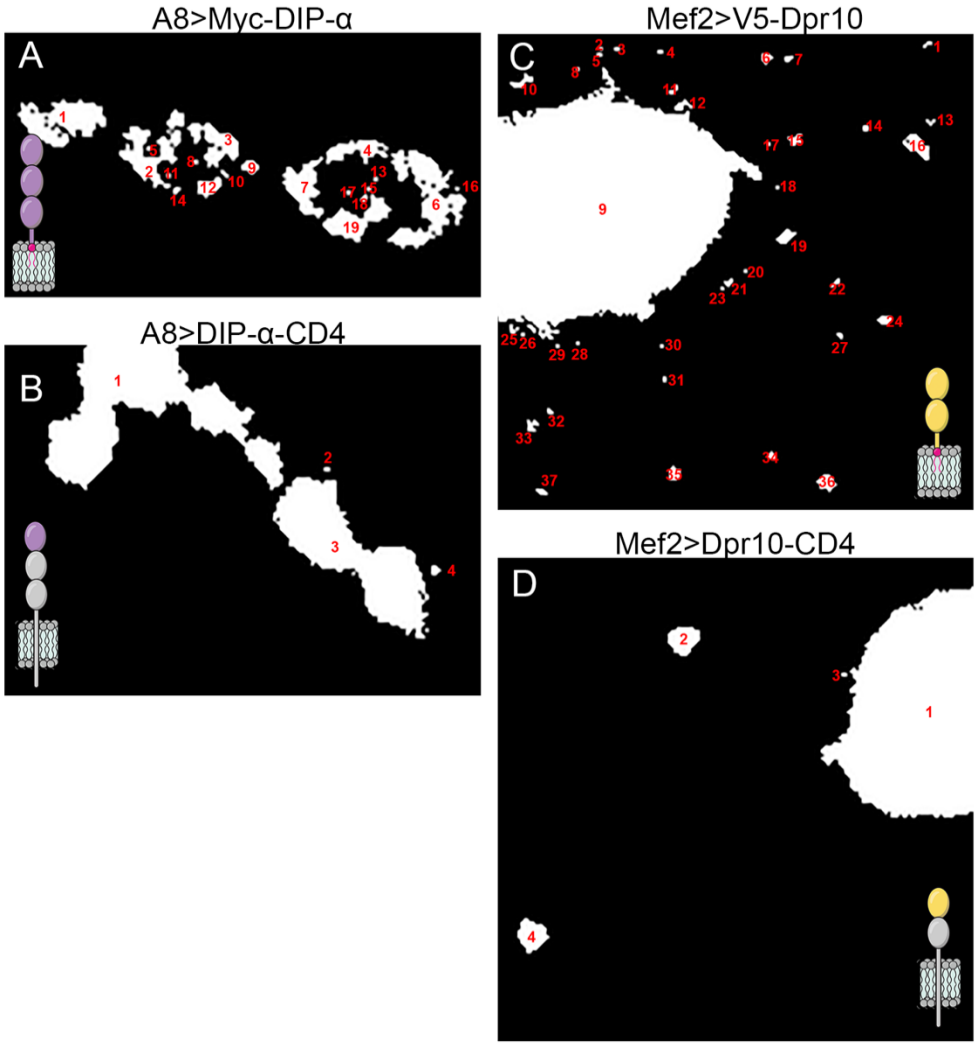

Figure S2.5. Example particle counting used to examine pre- and postsynaptic localization of Dpr10 and DIP-α. (A-D) Binary thresholded images of insets from Figure 6; white represents signal above the threshold, black fell below the threshold. Particle count assignment by ImageJ FIJI written in red text above white particles. Cartoons of protein being expressed in lower corner. (A) *A8-GAL4* driving Myc-DIP-α leads to punctate surface localization inside the boutons. (B) *A8-GAL4* driving transmembrane DIP-α-CD4 leads to even surface labeling of Is arbor. (C) *Mef2-GAL4* driving V5-Dpr10 leads to punctate localization on the muscle surface. (D) *Mef2-GAL4* driving transmembrane Dpr10-CD4 leads to few puncta on the muscle surface.

2.7 Discussion

Dprs and DIPs have been implicated in many aspects of neural circuit development. However, we lack a systematic analysis of how these CSPs are anchored to the cell membrane to provide insights into their signaling mechanisms. Here, we utilize several in vitro and in vivo approaches to demonstrate that most, if not all, Dprs and DIPs are attached to the cell membrane through GPI anchors. In tissue, we show that GPI anchors contribute to subcellular clustering on the presynaptic neuronal membrane. Our findings, that Dpr and DIPs are GPI anchored, suggest that Dpr/DIP-mediated functions must be achieved either by merely tethering two cells together and/or by signaling through a co-receptor.

2.7.1 Predicting GPI anchors

Predicting GPI anchors is intrinsically challenging for multiple reasons. There are no identified consensus sequence motifs for GPI anchor attachment signals. GPI signals are composites of features, including a stretch of hydrophobic amino acids C-terminal to the ω residue, chemically resembling transmembrane regions. This results in only ambiguous similarities that can be detected between different GPI anchored proteins at the sequence level. Therefore, identifying GPI anchor signals from sequence alignments of known GPI-linked proteins is not feasible. In line with this, C-termini of Dprs and DIPs are not conserved and cannot be aligned. The GPI prediction software must rely on models that include sequence properties beyond the simple profile searches (Eisenhaber et al., 1999, 1998), and that can be accomplished with methods based on machine-learning algorithms like PredGPI (HMM and SVM, (Pierleoni et al., 2008)) or NetGPI (neural networks, (Gíslason et al., 2021)). However, the success of these algorithms may depend on the availability of large experimentally validated datasets of GPI anchored proteins, which is known to be lacking (Gíslason et al., 2021). The

most recent NetGPI program used here could only use 161 sequences with experimental evidence as its training set. Our data containing 32 new sequences significantly expands this set.

In our predictions, a high number of false negatives was observed, as only one-third of Dprs and DIPs were predicted to be GPI anchored by PredGPI and NetGPI. Conversely, the TM prediction tool Phobius predicted 15 out of 32 Dprs and DIPs and Klingon as TM proteins, suggesting this software may not be robust at discriminating between the two membrane targeting motifs. The newest version of TMHMM, DeepTMHMM, based on a deep learning algorithm, performed significantly better than Phobius, classifying only Dpr9 as a TM protein. Unexpectedly, one-third of Dprs and DIPs were neither predicted to be GPI anchored nor to have a TM helix. Together our findings demonstrate that currently available GPI signal prediction tools can provide useful preliminary insights, especially in combination with TM prediction software. It is likely that significant improvements to predictions will come from larger high-quality training datasets of experimentally determined GPI signal sequences. However, experimental validation may for now be the primary way of assessing GPI anchor presence until better prediction tools are developed.

2.7.2 Dpr and DIP clustering is aided by their GPI anchors

CSP localization is often critical for their function. Here, we demonstrate that DIP-α, Dpr10, and Dpr19 localized to the postsynaptic membrane when expressed in muscles. Moreover, punctate Dpr10 localization on the muscle surface was diminished when we replaced the GPI anchor with a TM helix suggesting that this modification contributes to its localization. Similar results were observed for punctate DIP-α in presynaptic Is arbors. GPI-anchored proteins have been reported to localize to lipid rafts—domains in the lipid bilayer that have increased levels of sterols and are therefore slightly thicker and less mobile than the surrounding

membrane (Levental et al., 2020). Although still somewhat controversial, these domains are thought to scaffold proteins by increasing the local concentration of proteins that preferentially localize to lipid rafts such as GPI-anchored proteins, possibly including Dprs and DIPs within these rafts.

The PLC cleavage of Dpr10 and DIP-α from muscles was incomplete, leaving residual punctate signal around the boutons and on the muscle surface unlike Dpr19 that was almost completely lost. These differences in PLC cleavage efficiencies may be due to different local interactions of Dprs and DIPs with various proteins or lipids in the membrane. Alternatively, residual surface labeling could arise following complete cleavage where the cleaved CSPs remain as a result of binding nearby CSPs, preventing release from the tissue.

2.7.3 Dpr–DIP-mediated cell adhesion depends on their GPI anchors

Trans- and *cis*-interactions between Dprs and DIPs drive their roles in the nervous system. Dprs and DIPs may act similar to other cell adhesion molecules (e.g., integrins or cadherins) by clustering to generate avidity and strengthen cell-cell contacts during axonal fasciculation or synapse formation. We examined four Dpr–DIP pairs and all showed robust aggregation that was susceptible to PLC treatment, suggesting that the GPI anchors in Dprs and DIPs are accessible by PLC at the cell-cell contact sites. This phenomenon could have profound consequences in vivo for modulating cell adhesion, provided that specific lipases and proteases are present under physiological conditions at sufficient concentrations and exhibit high enough substrate turnover to cause structural changes to cell-cell contacts.

Shedding of cell surface molecules by hydrolytic enzymes like proteases and lipases has been implicated in various signaling mechanisms. Examples include activation of fibroblast growth factor 2 (FGF-2) via the release of soluble syndecan-1 (Kato et al., 1998) potentiation of

β-catenin signaling upon cleavage of neuronal cadherin (N-cadherin) (Reiss et al., 2005) modulation of Nodal signaling via GPI cleavage of CRIPTO (Lee et al., 2016), and bi-directional regulation of the Notch pathway through proteolysis of Notch or its ligands (Dyczynska et al., 2007; Mishra-Gorur et al., 2002; Ponio et al., 2007; Steinbuck and Winandy, 2018). GPI-anchored proteins are unable to directly signal intracellularly so acting as soluble factors for other receptors, either in *cis* or *trans*, could be a conceivable mode of action. A subset of Dprs (Droujinine et al., 2021) and DIPs were identified in a secretome screen as soluble factors in the hemolymph of larvae (Personal Communication, Norbert Perrimon and Justin Bosch), but the roles of these soluble variants are unknown. In addition to potential functions of soluble forms of these CSPs in the extracellular space, it would be interesting to explore if their shedding in vivo could affect Dpr–DIP-mediated cell adhesion, and have consequences for the structure and function of synapses or other specialized sites of cell-cell contact, as shown for some CAMs (Peixoto et al., 2012; Reiss et al., 2005; Rodríguez-Manzaneque et al., 2009; Stahl et al., 2014; Suzuki et al., 2012; Toth et al., 2013).

2.7.4 GPI anchors in neural circuit assembly

GPI-anchored proteins are critical for many physiological processes, including neural circuit formation. These proteins can be cleaved by lipases or proteases as part of their signaling mechanism. For example, the GPI-anchored protein RECK regulates motor neuron differentiation in mammals by inhibiting Notch signaling; only when RECK is cleaved and released from the membrane can the ADAM10 metalloprotease access and cleave the Notch ligand thereby promoting differentiation (Corda et al., 2014). In addition, IgLONs, the vertebrate orthologs of Dprs and DIPs, are shed from neurons via ADAM10 to promote neuronal growth of nearby neurons (Pischedda and Piccoli, 2016; Sanz et al., 2015). The presence of GPI anchors in

Dprs and DIPs suggests that their biology and signaling may be conserved with IgLONs. Finally, if the GPI-anchored protein is not cleaved, it can still signal through a co-receptor that traverses the cell membrane. To our knowledge, no Dpr or DIP co-receptors have been published and this provides an intriguing future avenue of research.

2.8 Materials and Methods

2.8.1 Sequence selection and molecular cloning

cDNAs of most of the full-length Dprs and DIPs used in the study were obtained from Drosophila Genomics Research Center (DGRC). The remaining full-length sequences were generated through the extension of existing ectodomain constructs subcloned by our groups (Özkan et al., 2013). Among the DGRC clones, the sequence of Dpr15 required modification to remove the insertion within the Ig2 domain to preserve its structural integrity. The source, isoform, and identification number of each used sequence can be found in Table S1. Sequences of full-length Dprs and DIPs with an N-terminal V5 tag were cloned into the pMT/BiP/V5-His A vector (Invitrogen) for expression in S2 *Drosophila* cells for PLC cleavage assay or into the pAcGP67 baculovirus transfer vector (BD Biosciences) for expression in Sf9 cells for cell flow cytometry and cell aggregation experiments. For cell aggregation, the constructs additionally included EGFP or mScarlet separated from V5-tagged Dprs or DIPs by the P2A sequence.

2.8.2 Predictions of GPI anchors and transmembrane helices

Predictions of GPI-linkage were carried out using PredGPI (Pierleoni et al., 2008) and NetGPI (Gíslason et al., 2021) tools available online. For predictions using PredGPI the general model was used. Predictions of transmembrane regions were performed using Phobius (Käll et al., 2004) and DeepTMHMM (Hallgren et al., 2022). Before analysis in Phobius and DeepTMHMM, the sequences of signal peptides predicted with SignalP-6.0 (Teufel et al., 2022) were removed.

2.8.3 *Drosophila* reagents, dissections, and immunohistochemistry

All flies were kept at 25°C except when otherwise noted. Crosses were set at medium density and crawling third instar larvae were dissected as before (Wang et al., 2022) in Phosphate

Buffered Saline (PBS, pH 7.4) on Sylgard dishes. Briefly, after fixing for 30 minutes in 4% paraformaldehyde, fillets were washed 3 times for 10 minutes in PBST (PBS + 0.05% Triton X-100, pH 7.4). Larval fillets were then blocked in 5% Normal Goat Serum in PBST. Samples were incubated in primary antibodies diluted in block and overnight at 4°C, extensively washed in PBST, and incubated with secondary antibodies for 2 hours at room temperature before the final washes in PBST. All washes and incubations occurred on nutators. Samples were then mounted in Vectashield (Vector Laboratories) and representative images were collected. HRP was used as a marker for neuronal membranes and DLG was used as a marker for postsynaptic membranes.

2.8.4 PLC cleavage assay with S2 cells

S2 cells were obtained from the Drosophila Genomics Research Center and maintained in Schneider's Medium (Sigma S0146), supplemented with Insect Media Supplement (Sigma I7267), and 90 U/ml Penicillin plus 90 µg/ml Streptomycin. Cells were maintained at room temperature. For experiments, confluent cells were split 1:2 into 6-well plates and transfected the following day. Complete Schneider's Media was mixed 2:1 with 250 µg/ml dimethyldioctadecyl-ammonium bromide (DDAB), allowed to mix, and then 500 µl DNA was added for each well to be transfected. Approximately 24 hours after transfection, protein expression was induced by adding 1 mM copper sulfate ($CuSO_4$). Three days later, 2 µl of 100 U/ml phosphatidylinositol-specific phospholipase C (PI-PLC, Life Technologies P-6466) was added to the treatment well, and cells were incubated for 4 hours.

To harvest cells, 2 ml from each well was collected and spun down at 500 x g for 5 minutes. The supernatant was collected and mixed with 6x Loading Buffer (375 mM Tris-Cl, pH 6.8, 9% SDS, 50% glycerol, 0.03% bromophenol blue, 9% β-mercaptoethanol) and boiled for 10 minutes. The

cell pellet was washed in PBS and spun down as before. Next, cells were lysed used using a buffer adapted from Bumgarner et al., 2005 (Bumgarner et al., 2005), consisting of 50 mM Tris-HCl pH 8.0, 150 mM NaCl, 1% Triton X-100, 5 mM EDTA, and protease inhibitors (one tablet per 50 ml; Pierce A32955). Tubes were incubated on a nutator at 4°C for 30 minutes and then at 37°C for 30 minutes. Tubes were centrifuged at 17,000 x g at room temperature for 15 minutes and mixed with 6x Loading Buffer.

Samples were then run on 12% SDS-polyacrylamide gels using the TGX FastCast system (BioRad 1610175). The samples were transferred overnight onto a nitrocellulose membrane (BioRad 1620115) at a constant current of 40 mA and blocked for one hour in 1% (w/v) Casein Block. Staining with primary and secondary antibodies was performed for 2 hours at room temperature with slight agitation and included washes in PBST after each incubation. Westerns were imaged on a LI-COR Odyssey imager.

2.8.5 Flow cytometry

Sf9 cell cultures at the density of 2×10^6 cells/ml were placed in 6-well plates, 3 ml per well. The cells were infected with baculoviruses encoding full-length Dprs and DIPs with an N-terminal V5 tag. Infected cultures were incubated for 48 hours on an orbital shaker at 125 rpm (Thermo MaxQ 430), at 28°C. 0.6 ml of each culture was transferred to a 24-well plate. 4 µl of PI-PLC per well was used for GPI cleavage. 4 µl of PI-PLC storage buffer (20 mM Tris-HCl, pH 7.5, 1 mM EDTA, 0.01% sodium azide, 50% glycerol) was added to control samples. Treatment was carried out for 3 hours on an orbital shaker at 125 rpm, at 28°C. Cultures were spun down for 1 minute at 500 x g. The cell pellets were resuspended in 300 µl of cold PBS, pH 7.4, with 1% BSA. 100 µl of cell suspensions were transferred to a U-shaped 96-well plate. 4 µl of anti-V5-

AF647 antibody (R&D Systems, FAB8926R) was used for staining cells for 20 minutes on a shaker at 500 rpm (Thermo Microplate Shaker), at 4°C. Cultures were spun down for 1 minute at 500 x g, at 4°C and washed 3 times with 200 µl of PBS, pH 7.4, with 1% (w/v) BSA. Cells were analyzed using a BD Accuri C6 flow cytometer. 20,000 events were recorded per sample. The results were analyzed using FlowJo Software v10.8.1 (BD Life Sciences).

2.8.6 Cell aggregation assay with Sf9 cells

Sf9 cultures at the density of 2×10^6 cells/ml were placed in 6-well plates, 3 ml per well, and infected with baculoviruses encoding (N- to C-terminal) mScarlet, P2A sequence (ATNFSLLKQAGDVEENPGP) and V5-tagged Dpr, or EGFP, P2A sequence, and V5-tagged DIP. This construct design was chosen to leave unmodified C-termini for Dprs and DIPs, as that would be important for testing for a C-terminal GPI anchoring signal. Infected cultures were incubated for 48 hours on an orbital shaker at 125 rpm, at 28°C. Expression of V5-tagged Dprs and DIPs was confirmed using western blots with the anti-V5-AF647 antibody. Cultures were diluted 1:15 in Sf9 complete media (Gibco Sf-900 III SFM, with 10% FBS, 2 mM L-glutamine, and 20 µg/ml gentamicin). 200 µl of cultures expressing Dprs were mixed with 200 µl of cultures expressing DIPs in 24-well plates. The control samples included 200 µl of cultures expressing individual Dprs or DIPs mixed with 200 µl of non-infected Sf9 cultures. Samples were prepared in triplicates for each Dpr–DIP pair and each control culture expressing individual Dprs and DIPs. Cultures were left to aggregate for 30 minutes on an orbital shaker at 125 rpm, at 28°C. 4 µl of PI-PLC per well was used for GPI cleavage. 4 µl of PI-PLC storage buffer was added to control samples. Treatment was carried out for 1 hour on an orbital shaker at 125 rpm, at 28°C. Cultures were imaged in 24-well plates at 5x magnification. Three images were collected for every well. Cell aggregation was quantified using the cell aggregation index,

defined as the percentage of the total area occupied by cells that is comprised of aggregates (Boucard et al., 2012). The area occupied by cells and aggregates was determined using the 'Analyze particles' function in Fiji. Aggregates were defined as particles with areas of at least 2900 μm^2.

2.8.7 Tissue PLC experiment

Larvae were filleted, rinsed in PBS, and incubated while shaking for one hour in 1 ml of PBS with or without 1 µl of PI-PLC. Larvae were washed with PBS, fixed, and stained as above with a slight alteration: detergent was only used after staining for Dpr/DIP protein tags. After extensive washing in PBS, anti-DLG was diluted in PBST and incubated with larvae for 2 hours at room temperature. The subsequent washing and secondary antibody staining was as described above. The staining procedure for PLC-treated and untreated preparations was carried out in the same tube so that conditions were identical. Three muscle 4 Ib arbors were imaged per animal.

For quantification, images were collected from each experiment using identical imaging parameters. After measuring pixel sum of three terminal boutons per arbor, signal of the Dpr/DIP was normalized to DLG signal to control for any differences in staining conditions between replicates and because DLG should not be affected by PLC treatment. These values are reported as 'Relative Pixel Sum' representing Tag/DLG pixel sum.

2.8.8 Tissue Localization experiment

For localization experiments, crosses were maintained at 18°C in order to dampen protein expression levels. Samples to be compared were pooled and stained as above, omitting detergents in the first round of staining to label only proteins that were present on the cell surface

at the time of fixation.

Once images were collected, z-stacks were generated, and the relevant channel was converted to 8-bit format before a threshold was set to convert image to binary representation of the surface protein stain. The same threshold was used for all images. This image was then used to count particles. For presynaptic localization, particles of and surrounding three terminal boutons per arbor were measured. For postsynaptic localization, particles of the entire image were counted. These manipulations were performed using ImageJ FIJI (Schindelin et al., 2012).

2.8.9 Statistical Analysis

For tissue PLC experiments and tissue localization experiments, two-tailed Student's t-test was used to determine statistical significance (Prism 8). Cell aggregation experiments were evaluated using one-way ANOVA (Prism 9).

2.8.10 Tissue and cell imaging protocol

All in vivo images were obtained on a Zeiss LSM800 confocal microscope with a 40X plan-neofluar 1.3NA objective or 63X plan-apo 1.4NA objective. All images of Sf9 cells were obtained using a Leica THUNDER Imager 3D Cell Culture with Leica N Plan 5x/0.12 PH0 objective.

Antibodies	Source	Concentration
Chicken anti-V5	Bethyl/A190-118A	1:200
Mouse anti-V5	Invitrogen R960-25	1:200
Rabbit anti-V5	Glotzer Lab	1:10,000
Rabbit anti-DLG	Budnik Lab	1:40,000
Mouse anti-α-Tubulin	Sigma DM1A	1:5,000
Goat anti-Mouse 488	Invitrogen A11029	1:500
Goat anti-Rabbit 488	Invitrogen A11008	1:500
Goat anti-Chicken 488	Invitrogen A11039	1:500
Goat anti-Rabbit 568	Invitrogen A11036	1:500
Goat anti-HRP 647	Jackson ImmunoResearch /123-605-021	1:100
Goat anti-Mouse 680	Jackson ImmunoResearch /115-625-146	1:5,000
Goat anti-Rabbit 790	Jackson ImmunoResearch /111-655-144	1:5,000

Table 1.3 The antibodies used for this study.

Genotype	Description	Source
W1118	White controls	BDSC
Mef2-GAL4	Muscle GAL4 driver	(Ranganayakulu et al., 1998)
A8-GAL4	Is neuron GAL4 driver	(Venkatasubramanian et al., 2019; Wang et al., 2021)
UAS-V5-Dpr19	V5 tagged Dpr19	This study
UAS-V5-Dpr10	V5 tagged Dpr10	(Xu et al., 2018a)
UAS-Dpr10-CD4	First Ig domain from Dpr10, Ig5 and the TM from CD4	This study
UAS-CD4-Dpr10	First Ig from CD4, remainder of protein from Dpr10	This study
UAS-EGFP-DIP-ζ	sfGFP tagged DIP-ζ	This study
UAS-Myc-DIP-α	Myc tagged DIP-α (N)	This study
UAS-DIP-α-CD4	First Ig domain from DIP-α, Ig4+5 and the TM from CD4	This study

Table 1.4 The fly lines used for this study.

CHAPTER 3

DPR10 AND NOCTE ARE REQUIRED FOR *DROSOPHILA* MOTOR AXON PATHFINDING

Katherine DeLong identified the pathfinding phenotype and contributed to all aspects of this study. Rio Salazar and Ruiling Zhang aided in quantification of misrouting phenotypes. Yupu Wang was critical for shaping this work. This chapter was published in *Neural Development* in 2022.

3.1 Introduction

Assembling a functional neural circuit requires several steps: neurogenesis, axon pathfinding, synaptogenesis, and subsequent maintenance. The *Drosophila* larval neuromuscular junction is an excellent model to study these processes due to its relatively simple circuit architecture, its genetic accessibility, and the fact that many of the processes and molecules are conserved in vertebrates.

To assemble circuits, growth cones—specialized structures at the ends of developing axons—travel through dense extra-cellular milieus and use molecular signals to guide them to their final destinations. This sensing is mediated by cell surface proteins (CSPs) on the growth cone. Many proteins have been implicated in axon pathfinding, and they function as long- and short-range signals detected by cell surface receptors on the filapodial tips of the highly dynamic growth cone (Aberle, 2019; Stoeckli, 2018). Some of the best studied signals include the attractive cue Netrin-1, which signals through its receptors Frazzled and UNC-5 (Boyer and Gupton, 2018; Keleman and Dickson, 2001) and the Robo-Slit pathway that drives axon pathfinding through repulsion in the developing nervous system (Blockus and Chédotal, 2016;

Dickson and Gilestro, 2006; Pappu et al., 2011). Although these pathways are well characterized, they represent only a small fraction of the cues required to wire an entire nervous system (Kolodkin and Tessier-Lavigne, 2011; Stoeckli, 2018), and we still do not fully understand the entire repertoire of complex signaling molecules that mediate axon pathfinding (Stoeckli, 2018).

The immunoglobulin superfamily (IgSF) is a large family of soluble and CSPs implicated in all stages of circuit assembly and axon pathfinding (Maness and Schachner, 2007; Rougon and Hobert, 2003). An in vitro screen seeking to deorphanize ligand-receptor pairs revealed interactions between two *Drosophila* IgSF subfamilies: the Dprs and DIPs (Özkan et al., 2013). These IgSF CSPs interact heterophilically and some members also homodimerize; moreover, the unrelated Ig protein called Klingon and a leucine-rich repeat (LRR) protein called cDIP interact with a subset of Dprs and DIPs (Özkan et al., 2013). Dprs and DIPs are expressed throughout the nervous system and their functions are only beginning to be elucidated. Work from our lab and others have demonstrated Dpr-DIP function in cell survival (Carrillo et al., 2015; Xu et al., 2018a), synaptic partner preference (Xu et al., 2019), cell fate determination (Courgeon and Desplan, 2019), and axon guidance in olfactory neurons (Barish et al., 2018). Moreover, Dprs and DIPs are required for synaptic partner recognition in the adult brain (Bornstein et al., 2021; Carrillo et al., 2015; Courgeon and Desplan, 2019; Menon et al., 2019; Xu et al., 2018a) and in the neuromuscular junction (Ashley et al., 2019; Venkatasubramanian et al., 2019), suggesting multifaceted roles for Dprs and DIPs in nervous system development.

The larval neuromuscular junction is divided into highly stereotyped, segmentally repeated hemisegment units, and each hemisegment is comprised of 30 body wall muscles that are innervated by ~33 motor neurons. Most muscles are innervated by two glutamatergic motor neurons, the Ib (big) and Is (small) types, which can be distinguished by the size of their

postsynaptic membrane architecture as visualized with staining for Discs Large (DLG) (Guan et al., 1996). Most Ib motor neurons innervate single muscle targets, while Is motor neurons innervate groups of muscles. In this study, we examined the intersegmental nerve b (ISNb) consisting of efferent motor neuron axons that innervate a subset of the ventral muscle field (Figure 1A) and afferent sensory neuron axons that project into the ventral nerve cord (VNC). Dpr10 is required for olfactory neuron pathfinding but whether it also functions in motor neuron axon guidance is unknown. Here, we demonstrate that Dpr10 is required for ISNb pathfinding; loss of *dpr10* leads to misrouting of several motor axons in the ISNb, including those innervating muscles 12 and 13 (m12 and m13; also referred to as VL1 and VL2, respectively). To determine how Dpr10 mediates ISNb pathfinding, we performed Dpr10 immunoprecipitation-mass spectrometry from *Drosophila* larvae. Several proteins were identified, including cDIP, a previously identified Dpr10 interactor (Carrillo et al., 2015; Özkan et al., 2013), and the cytosolic protein Nocte.

To begin to uncover the role of Nocte in the neuromuscular synapse of junction, we examined *nocte* expression in larvae and found it in motor neurons, muscles, and glia. Anatomical analyses of *nocte* mutants revealed ISNb pathfinding defects, and cell-specific knockdown revealed that Nocte is required in motor neurons for proper ISNb pathfinding. Genetic analyses revealed that these *nocte* phenotypes were shared with *dpr10* mutants, and that they likely act in the same pathway. Overall, our work implicates a Dpr10–Nocte pathway in motor axon pathfinding and demonstrates that Dpr10 is required in several steps of circuit assembly, including pathfinding and synaptic partner matching.

3.2. Dpr10 is required for ISNb pathfinding and innervation

Dpr10 is a member of the *Drosophila* IgSF and instructs synaptic partner choice in the pupal neuromuscular junction (Venkatasubramanian et al., 2019) and innervation of specific medulla layers in the pupal visual circuit (Xu et al., 2018a). In the olfactory bulb, Dpr10 is required for axon pathfinding of olfactory neurons (Barish et al., 2018). Additionally, in the embryonic neuromuscular junction, Dpr10 is required for innervation of muscle 4 by the dorsal Is motor neuron (known as the dorsal common exciter, or dCE) (Ashley et al., 2019). *dpr10* is expressed in a large subset of embryonic and larval muscles and motor neurons (Ashley et al., 2019; Carrillo et al., 2015; Wang et al., 2022), suggesting that it may have additional functions in neuromuscular junction development.

Each hemisegment of the *Drosophila* larval body wall is innervated by three nerves: the intersegmental nerve (ISN), segmental nerve (SN), and transverse nerve (TN). The ISN and SN are further divided based on the muscle groups they innervate. For example, motor neuron axons in the ISNb innervate a subset of the ventral muscles. For this study, we focused on a subset of ventral muscles: m13 and m12 (Figure 3.1A). These muscles are innervated by a single Is motor neuron, the ventral common exciter (vCE, Figure 3.1A) and two Ib motor neurons, MN13-Ib, and MN12-Ib, respectively. The routes that these motor axons travel to reach their muscle targets and the innervation patterns are highly stereotyped. For example, in a dissected larva, the ISNb exits the VNC at specific locations, follows a defined trajectory under m6 and m7, emerges above m13, and finally reaches the dorsal side of m12. In control animals, this pattern is extremely hardwired with 97.8% of hemisegments revealing the correct ISNb trajectory (n = 90) (Figure 1B). In the small fraction of hemisegments with incorrect routing, we observed a variety

of phenotypes that include the nerve stalling before m13 or traveling underneath either m12, m13, or both muscles.

The expression of *dpr10* in embryonic and larval muscles and motor neurons prompted us to examine additional roles for Dpr10 in neuromuscular junction assembly. We used two *dpr10* alleles—a CRISPR generated null allele (*dpr10*^{CR}) (Xu et al., 2018a) and a T2A-GAL4 converted from a MiMIC insertion that contains transcriptional and translational stops (*dpr10-GAL4*) (Lee et al., 2018). RT-qPCR from *dpr10-GAL4* larvae revealed that *dpr10* mRNA levels were significantly reduced to approximately 6% relative to controls, suggesting the allele is a severe hypomorph (Wang et al., 2022). To determine if Dpr10 is required for motor axon pathfinding, we first examined ISNb pathfinding defects in the *dpr10*^{CR} null background. Loss of *dpr10* revealed significant ISNb pathfinding errors (23.2% defect, n = 55, ****p<0.0001) including the nerve traveling under m12 to innervate the incorrect dorsal side or missing innervations of Is and/or Ib motor neurons. To confirm that the phenotype was due to loss of *dpr10* and not a second site mutation, we examined the *dpr10-GAL4* hypomorph and observed comparable pathfinding defects (21.9% defect, n = 64, ****p<0.0001) (Figure 3.1C-E). In addition to these pathfinding errors, *dpr10* mutants exhibited a variety of muscle patterning defects, including missing muscles, muscle duplication, and incorrect attachment sites (Figure S3.1). Altered muscle patterning can affect motor neuron pathfinding and innervation (Cash et al., 1992; Chang and Keshishian, 1996) so only hemisegments with normal muscle patterns were quantified.

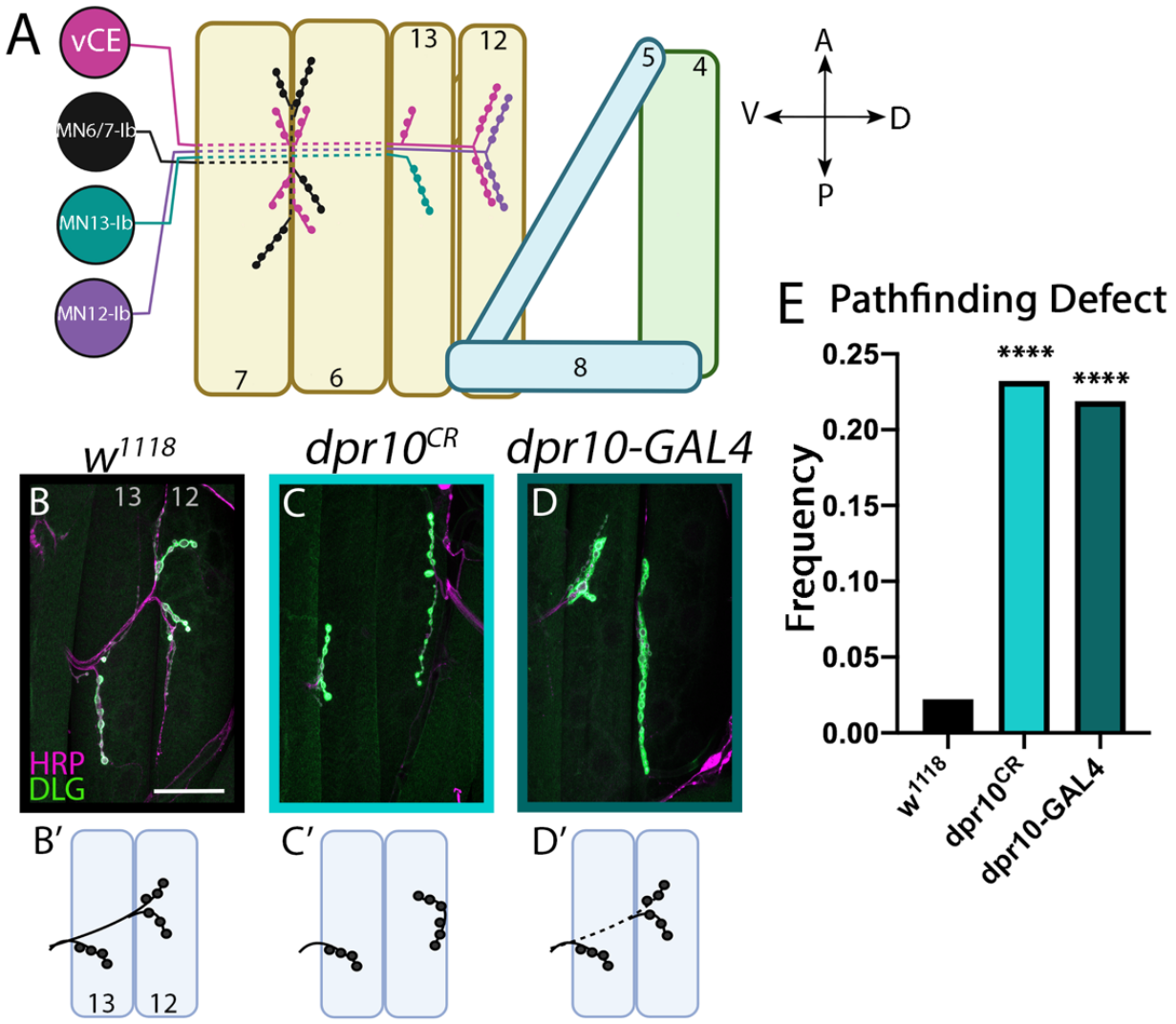

Figure 3.1 Dpr10 is required for ISNb pathfinding
(A) Schematic of innervation pattern of the ventral muscle field. The Is motor neuron, vCE, is shown in magenta and Ib neurons are shown in black, teal, and purple. Solid lines indicate the nerve is traveling above muscles while dotted line indicates the nerve is travelling below muscles. (B-D) Innervation of m13 and m12 with neurons labeled by HRP staining (magenta) and postsynapses labeled with DLG staining (green). Scale bar = 50μm. (B) Control w^{1118} animal with the normal innervation pattern. (C) $dpr10^{CR}$ animals (light blue) display significant ISNb pathfinding defects. Here, m12 is innervated from distal side. (D) *dpr10-GAL4* animals (dark green) display significant ISNb pathfinding defects. Here, the nerve travels underneath m13 to innervate m12. (E) Quantification of ISNb pathfinding defects of control and *dpr10* mutant animals. ****p<0.0001.

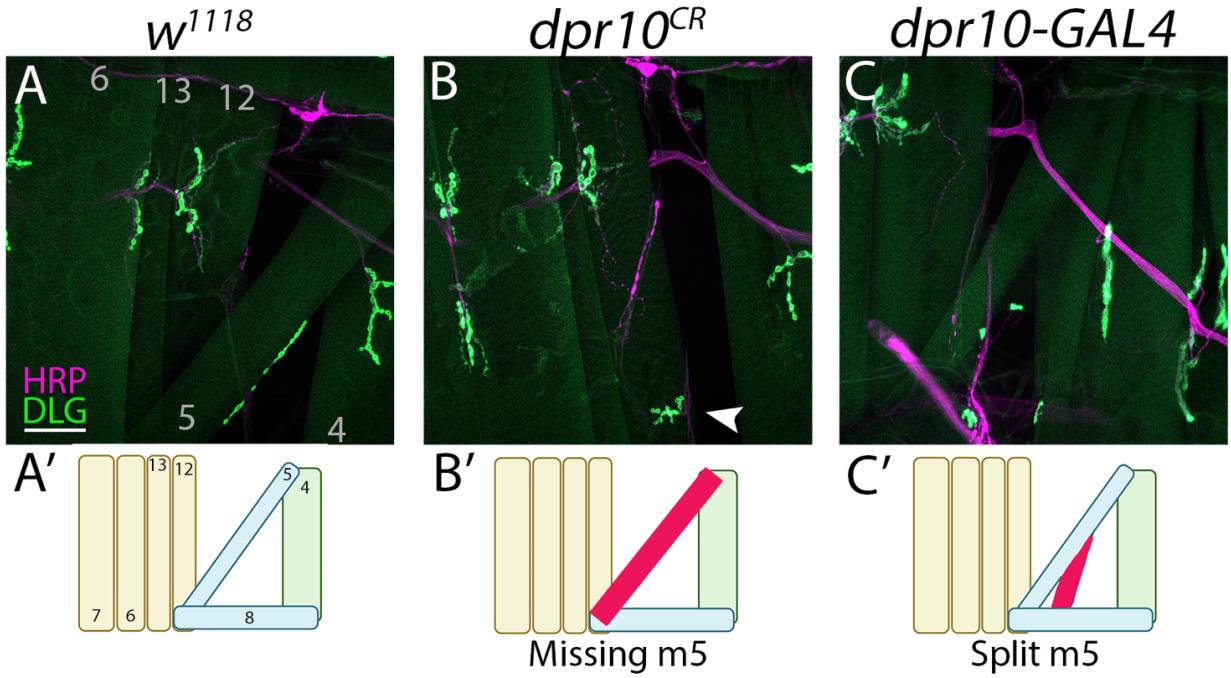

Figure S3.1 Muscle patterning defects in *dpr10* mutants
(A) A control w^{1118} animal depicting the normal muscle patterns in the ventral field. Neurons were labeled by staining for HRP (magenta) and postsynapses were labeled by staining for DLG (green). Note that the GFP channel also outlines individual muscles. (B) A $dpr10^{CR}$ animal with a missing m5. Ectopic innervation of m12 by MN5-Ib indicated with arrowhead. (C) A *dpr10-GAL4* animal with a split m5. (A'-C') Cartoon schematics of muscle patterning observed in A-C. Aberrant muscles highlighted in red. Scale bar = 50µm.

3.3 Dpr10 interacts with Nocte and cDIP in vivo

Previous in vitro studies determined that Dpr10 binds four Ig proteins: DIP-α, DIP-β, DIP-λ, and Klingon, and one LRR protein, cDIP (Carrillo et al., 2015; Cosmanescu et al., 2018; Özkan et al., 2013). However, in vivo interacting partners of Dpr10 and putative downstream signaling pathways have not been thoroughly examined. To identify direct and indirect interactors in an unbiased manner, we performed immunoprecipitation of a tagged Dpr10, followed by mass spectrometry in order to identify putative components of a Dpr10 signaling pathway.

Dpr10 is expressed in a subset of larval neurons and muscles (Carrillo et al., 2015; Wang et al., 2022). We used the GAL4-UAS system to drive expression of a V5 tagged Dpr10 (Dpr10-V5) with *dpr10-GAL4* and isolated larval brains; this preparation reveals Dpr10 interactors in the cell bodies, axons, and dendrites of motorneurons and interneurons (Figure 3.2A). In addition, we expressed Dpr10-V5 in muscles (*Mef2-GAL4*) and collected larval body walls; this preparation reveals Dpr10 interactors in muscles (Figure 3.2B). For both experiments, we ran complimentary controls by expressing mCD8-GFP with the same drivers and continuing with the same experimental pipeline. Here, we only report Dpr10 interacting proteins that appeared in the experimental conditions and not in controls.

In the body wall preparations, mass spectrometry analysis revealed cDIP as a Dpr10 interactor, confirming the previous in vitro Dpr10–cDIP binding (Figure 3.2C) (Özkan et al., 2013). Additionally, we identified a novel interactor, Nocte (Figure 3.2C). Strikingly, Nocte was the only protein pulled down with Dpr10 in both brain and body wall preparations (Figure 3.2C). Absent from our immunoprecipitation experiments were other known binding partners of Dpr10: DIP-α, DIP-β, and DIP-λ. One possibility is that these DIPs are part of an insoluble membrane

fraction. Indeed, multiple attempts at solubilizing DIP-α from tissue failed. Also, in our immunoprecipitation experiments we did not include cross-linking reagents, which could contribute to loss of weaker interactions such as Dpr-DIP binding. Overall, Nocte and cDIP are the first non-IgSF proteins to interact with the Dprs and DIPs in vivo and may be components of the Dpr10 signaling pathway.

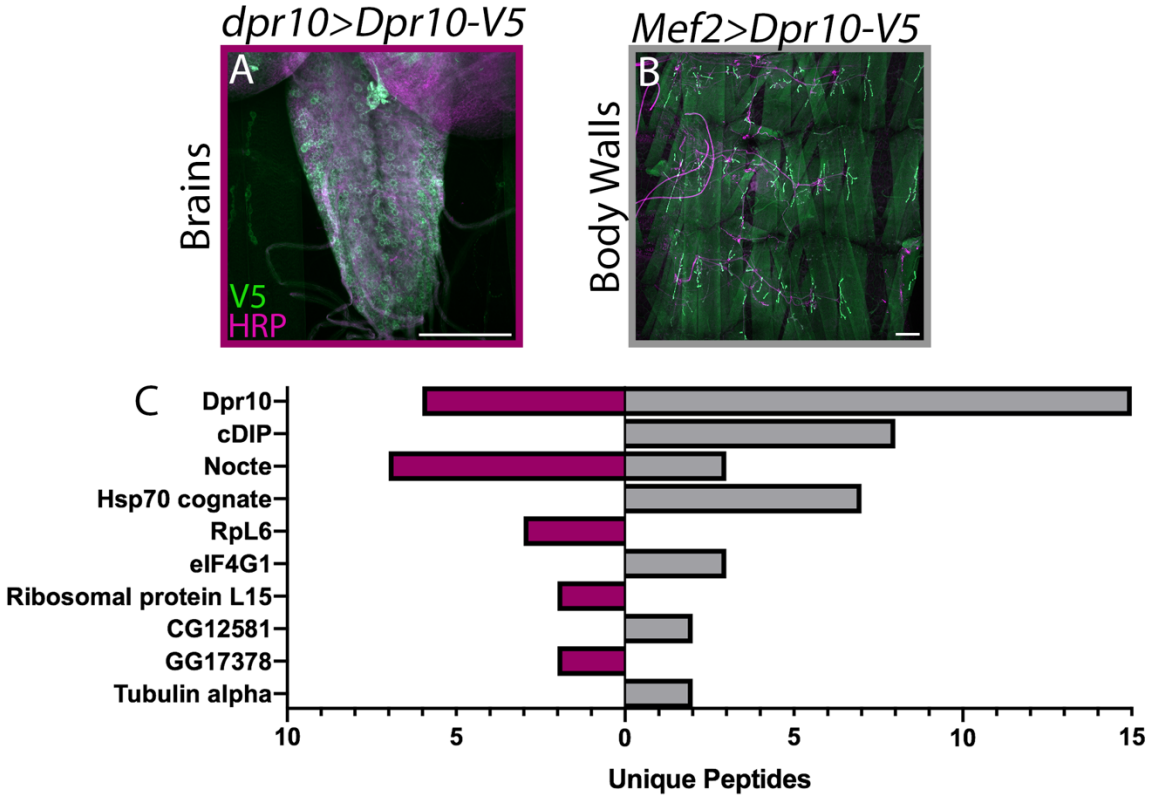

Figure 3.2 Immunoprecipitation followed by Mass Spectrometry of Dpr10 uncovers in vivo interactors

(A) Larval brain of Dpr10-V5 expressed with *dpr10-GAL4*. Preps were stained for V5 (green) to visualize Dpr10 and HRP (magenta) to visualize neurons. (B) Larval body wall of Dpr10-V5 expressed in muscles (*Mef2-GAL4*). Scale bars = 100µm. (C) Unique peptides recovered from immunoprecipitation of Dpr10-V5 and analyzed by mass spectrometry from brain samples (left, plum) and muscles (right, gray). Note that Nocte is the only associated protein recovered from both samples.

3.4 Nocte is required for motor neuron pathfinding

Nocte has been extensively studied in the adult fly for its role in circadian clock entrainment (Chen et al., 2018; Glaser and Stanewsky, 2005; Sehadova et al., 2009); however, to our knowledge, no published studies have examined its function in other systems (George and Stanewsky, 2021). Our biochemical data in larval tissues suggest that Nocte may function in Dpr10-dependent processes. To examine Nocte function, we used *nocte*^{P}, a hypomorphic allele generated by imprecise p-element excision (Sehadova et al., 2009).

In the neuromuscular junction, Dpr10 is required for m4 innervation by the dCE motor neuron (Ashley et al., 2019) and ISNb pathfinding (Figure 3.1). Based on our biochemical data (Figure 3.2), Dpr10 may mediate these processes through interaction with Nocte. First, we compared m4 innervation in control and *nocte*^{P} mutants. In control larvae, the m4 innervation by the dCE occurred in 95.18% of hemisegments (n = 83) and *nocte*^{P} showed a similar penetrance (m4 innervation by the dCE occurred in 88.57% of hemisegments, n = 70, p = 0.145), suggesting that Nocte is not required for motor neuron-muscle synaptic partnerships at m4 (Figure S3.3A). We then examined ISNb pathfinding in control and *nocte*^{P} larvae. As discussed above, the trajectory and innervation of the ISNb is nearly invariant in control flies (Figure 3.3A,E); however, in *nocte*^{P} hypomorphs this pattern is disrupted (9.4% defect, n = 192, *p = 0.043) (Figure 3.3B,E). To confirm a role for Nocte in ISNb pathfinding, we examined a second allele, *nocte*^{1}, a mutation that induces a stop codon after amino acid 1706 (Sehadova et al., 2009). In this mutant background we observed a defect in 14.7% of hemisegments (n = 102). Similar to *nocte*^{P}, *nocte*^{1} animals displayed normal m4 innervation by the dCE (91.30% of hemisegments, n = 69, p = 0.513) (Figure S3.3A). Finally, a previous study co-expressed two *nocte* RNAi constructs and showed a significant reduction in *nocte* RNA (Sehadova et al., 2009). We used the

same line to knockdown *nocte* using *nocte-GAL4* and found ISNb misrouting in 15.6% (n = 96, **p = 0.002) of hemisegments examined (Figure 3D-E). Similar to the hypomorphs, we observed ISNb pathfinding errors at m12 and m13 (Figure 3.3A-D). Strikingly, disrupting *nocte* also resulted in muscle patterning defects similar to loss of *dpr10* (Figure S3.3B-E). Overall, these data reveal a novel role for Nocte in motor axon pathfinding, similar to those found in the putative upstream partner, Dpr10.

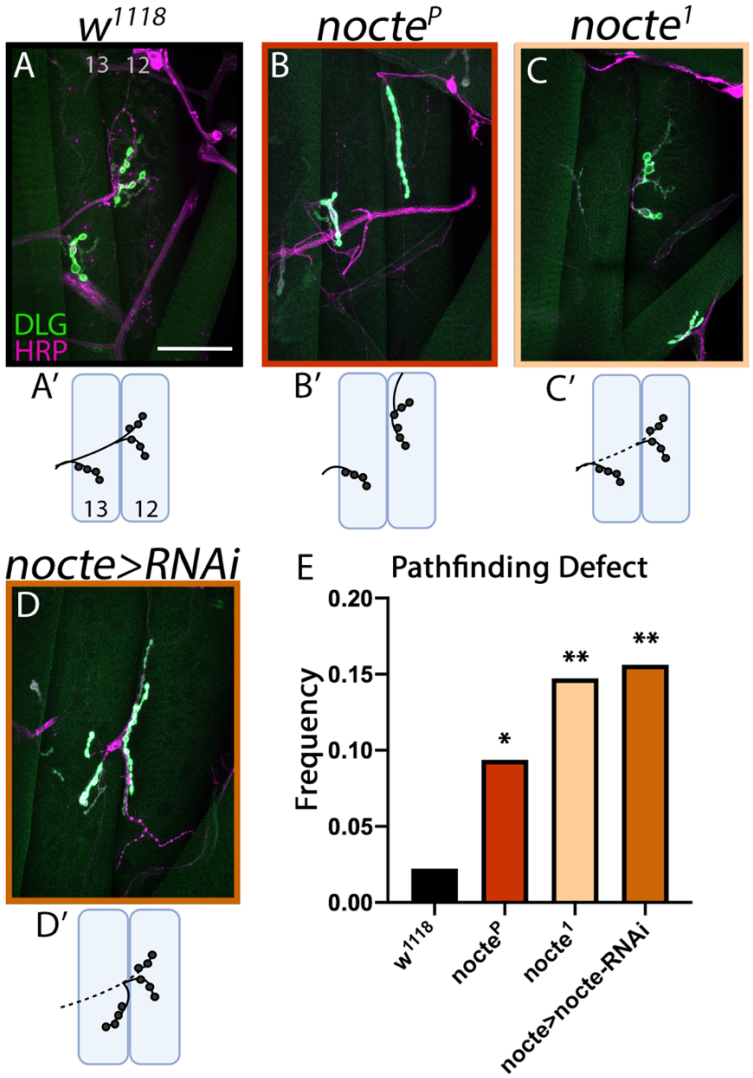

Figure 3.3 *nocte* mutants exhibit ISNb pathfinding errors
(A-D) m13 and m12 NMJs from respective genotypes. Neurons were visualized by staining for HRP (magenta) and the postsynapses were visualized by staining for DLG (green). Scale bar = 50µm. (A,A') Control w^{1118} animals with normal pathfinding. Note that the ISNb travels above m13. (B, B') $nocte^{P}$ animals (red) revealed pathfinding defects. Here, MN12-Ib traveled in a different nerve (likely the TN) and m12 lacked innervation by vCE. (C,C') $nocte^{1}$ animals (cream) showed innervation defects. Here, m12 was innervated from below m13 and m13 is innervated by only the vCE not the Ib NMJ. (D,D') *nocte-GAL4 x UAS-nocte-RNAix2* animals (cinnamon) also showed significant pathfinding defects. Here, m12 and m13 are innervated after the nerve incorrectly traveled underneath m13. (E) Quantification of the frequency of pathfinding defects in the respective genotypes. Knockdown of *nocte* increased the frequency of ISNb pathfinding defects. *p<0.05, **p<0.01.

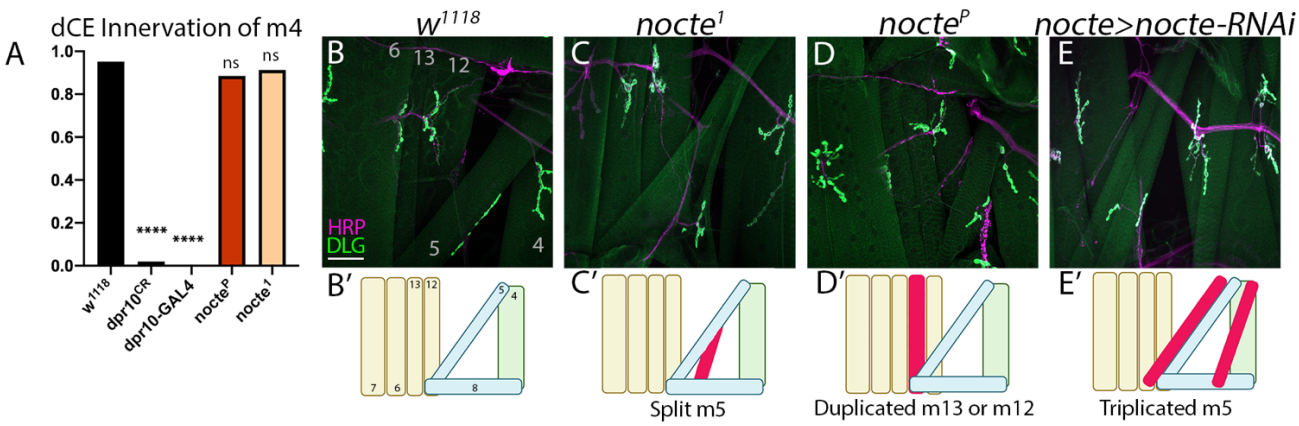

Figure S3.3 *nocte* mutants exhibit normal innervation of m4 but display muscle defects
(A) Innervation frequency of m4 by the dCE (Is neuron that innervates the dorsal muscles) in respective genotypes. Loss of *nocte* does not affect dCE innervation of m4. ****p<0.0001. (B) A control w^{1118} animal with normal muscle patterns. Neurons were labeled by staining for HRP (magenta) and postsynapses were labeled by staining for DLG (green). (C) A $nocte^{1}$ animal with a split m5. (D) A $nocte^{P}$ animal with duplicated m13 or m12. (E) A *nocte-GAL4 x nocte-RNAi* animal with a triplicated m5. (B'-E') Cartoon schematics of muscle patterns observed in B-E. Aberrant muscles shown in red. Scale bar = 50µm.

3.5 Nocte mutant embryos exhibit delayed nerve innervation

Motor axon pathfinding occurs during embryonic development when axons exit the VNC, navigate the periphery, and finally innervate their target muscles. The ISNb pathfinding defects we observed in *nocte* and *dpr10* mutants in third instar larvae could originate during the initial routing of axons or from axon retraction and subsequent misrouting in the larvae. To determine if pathfinding defects were present before larval development, we examined late stage 16 embryos, when most motor axon terminals have reached their target muscles.

Indeed, $nocte^{P}$ embryos exhibited ISNb pathfinding defects. To delineate ISNb development more accurately in control and mutant larvae, we used immunohistochemistry against Fasciclin 2 to determine the ISNb terminal position and scored the ISNb as i) reaching m13, ii) traversing m13 and reaching m12, and iii) innervating m12. An axon terminal was classified as reaching its target when filipodia extended along the muscle edge, and innervation occurred once varicosity-like structures appeared over the muscle surface (Yoshihara et al., 1997), (Figure 3.4D). In late stage 16 control embryos, 6.82% of ISNb terminals reached m13, 25% traversed m13 and reached m12, and 68.18% formed varicosity-like structures on m12 (Figure 3.4A, E) compared to 25.53%, 25.53%, and 48.93%, respectively, in $nocte^{P}$ embryos. Thus, perturbing *nocte* resulted in ISNb pausing, or stalling, and delayed m12 innervation (Figure 3.4B, E). On the other hand, overexpression of *nocte* expedited ISNb pathfinding and innervation; 2.33% of ISNb terminals reached m13, 6.98% traversed m13 and reached m12, and 90.70% innervated m12 (Figure 3.4C, E). Taken together, these data suggest that Nocte is required for axonal pathfinding at embryonic stages and that *nocte* mutant growth cones reach their targets more slowly than controls.

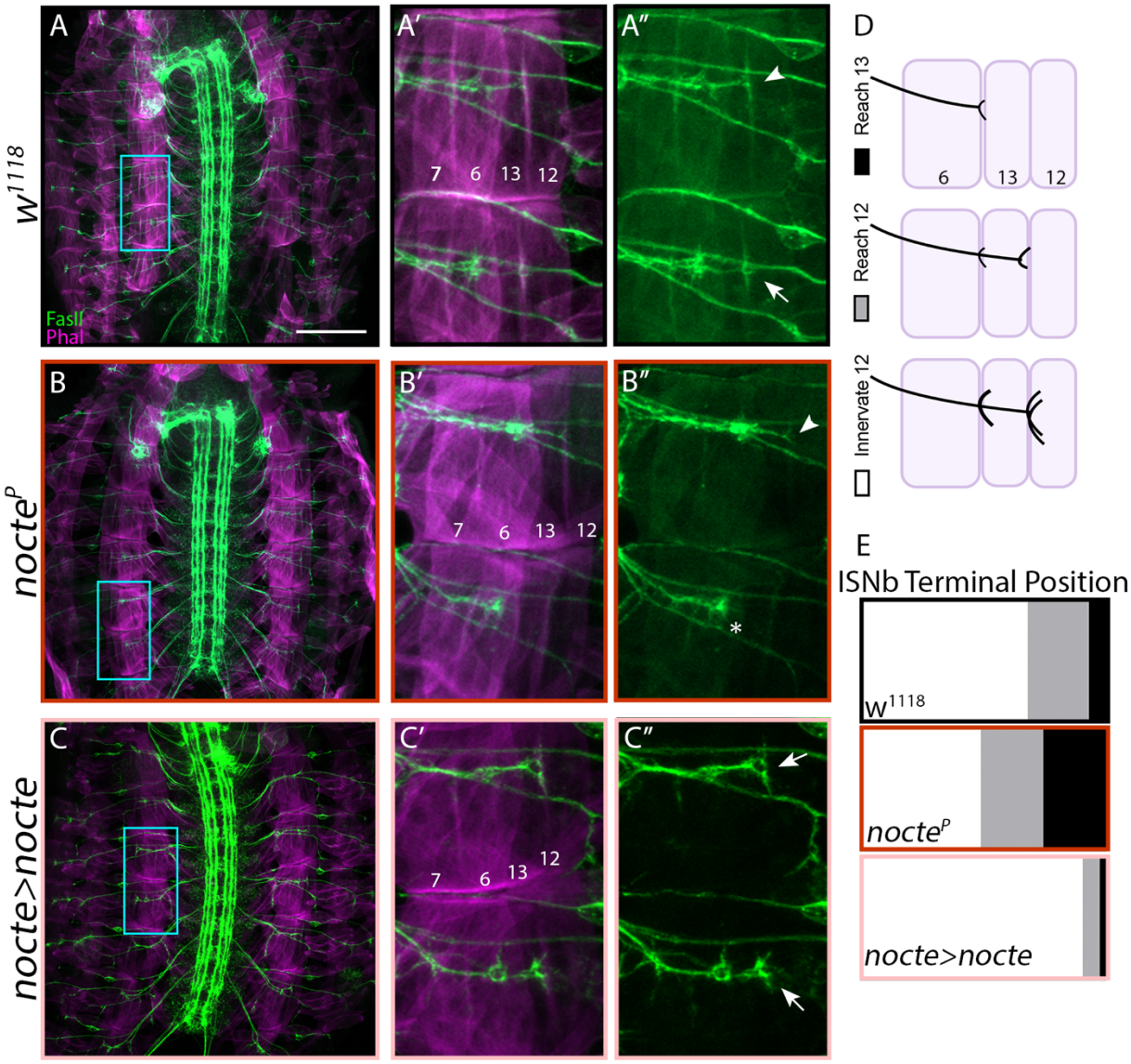

Figure 3.4 Loss of *nocte* causes stalling of ISNb before reaching terminal muscle targets
(A-C) Stage 16 embryo fillets stained for FasII (labels nerves, green) and phalloidin (labels muscles, magenta). Scale bar = 100µm. (A'-C') insets from A-C (cyan rectangle), expanded to show ISNb terminal extension. (A''-C'') FasII stain of previous insets. Asterisk indicates terminal that reached and stalled at m13, arrowhead indicates terminal that traversed m13 and reached m12, and arrow indicates terminal that innervated m12. (D) Schematic of ISNb nerve terminals reaching or innervating m13 and m12. (E) Quantification of ISNb terminal position of genotypes in A-C. The bar graphs are represented as parts of a whole with the key given in D. Note that in *nocte*^{p} embryos the ISNb stalls at m13 with greater frequency than in either control or overexpression contexts (black bar).

3.6 Nocte is expressed in subsets neurons, muscles, and glia

Motor axon pathfinding requires interactions between neurons, muscles, and glia (Abrell and Jäckle, 2001; Jeong, 2021; Wu et al., 2010). To understand how Nocte controls ISNb axon pathfinding, we examined the expression pattern of *nocte*.

To examine *nocte* expression in larvae, we used *nocte-GAL4* (Sehadova et al., 2009) to drive a nuclear localized green fluorescent protein (*nocte>NLS-GFP*), and cell types were verified by co-staining with specific markers. *nocte* was widely expressed in the larval VNC (Figure 3.5A-E). Co-staining with Elav, a panneuronal marker, revealed substantial overlap with GFP, suggesting that *nocte* is expressed in neurons (Figure 3.5A). Moreover, co-staining with a pan-motor neuron marker pMad and the transcription factor Eve revealed that a subset of motor neurons and interneurons express *nocte* (Figure 3.5 B-C). Finally, some *nocte*+ cells in the VNC were not labeled with Elav, suggesting that *nocte* is also expressed in non-neuronal cells (Figure 3.5A, arrowheads); co-staining with the glial maker, Repo, identified these as glial cells (Figure 3.5D).

The analyses above only revealed *nocte* expression in 3rd instar larvae. However, Nocte is required for pathfinding, suggesting that it is expressed in earlier developmental stages. To examine *nocte* temporal expression, we used the G-TRACE system to permanently label a cell with one fluorophore (GFP) and transiently with another fluorophore (RFP) (Evans et al., 2009; Wang et al., 2022). Thus, cells that are only GFP+ expressed *nocte* earlier in development. In the larval VNC, we observed broad overlap between red and green nuclei but also a significant number of GFP+ only nuclei, suggesting that nocte is temporally expressed in earlier developmental stages (Figure 3.5E).

We also characterized *nocte* expression outside the VNC. In *nocte>NLS-GFP* larvae, we observed GFP+ nuclei along peripheral nerves where glial cell bodies reside, and we confirmed glial expression by co-localization with Repo (Figure 3.5F). However, only a subset of glial cells expressed *nocte*. Examination of the larval body wall revealed *nocte* expression in a large subset of muscles (Figure 3.5G), including m13 and m12. Furthermore, we found a cluster of GFP+ cells posterior to m8 (Figure S3.5A). Based on the location of these cells, the absence of Repo staining, and overlap with Cut staining, we identified these cells as adult muscle precursor cells (AMPs), specifically Lateral-AMPs (Figeac et al., 2010; Lavergne et al., 2020). Finally, *nocte* is expressed in other tissues including the fat body (FB), and gut (Figure S3.5B-C). Similar to peripheral glia, only a subset of FB cells expressed *nocte* (Figure S3.5C), suggesting that *nocte* can subdivide FB tissue at the molecular level.

Taken together, *nocte* is expressed in subsets of cells in a variety of larval tissues including the nervous system, muscles, and the fat body with subset of these cells temporally expressing *nocte* throughout development.

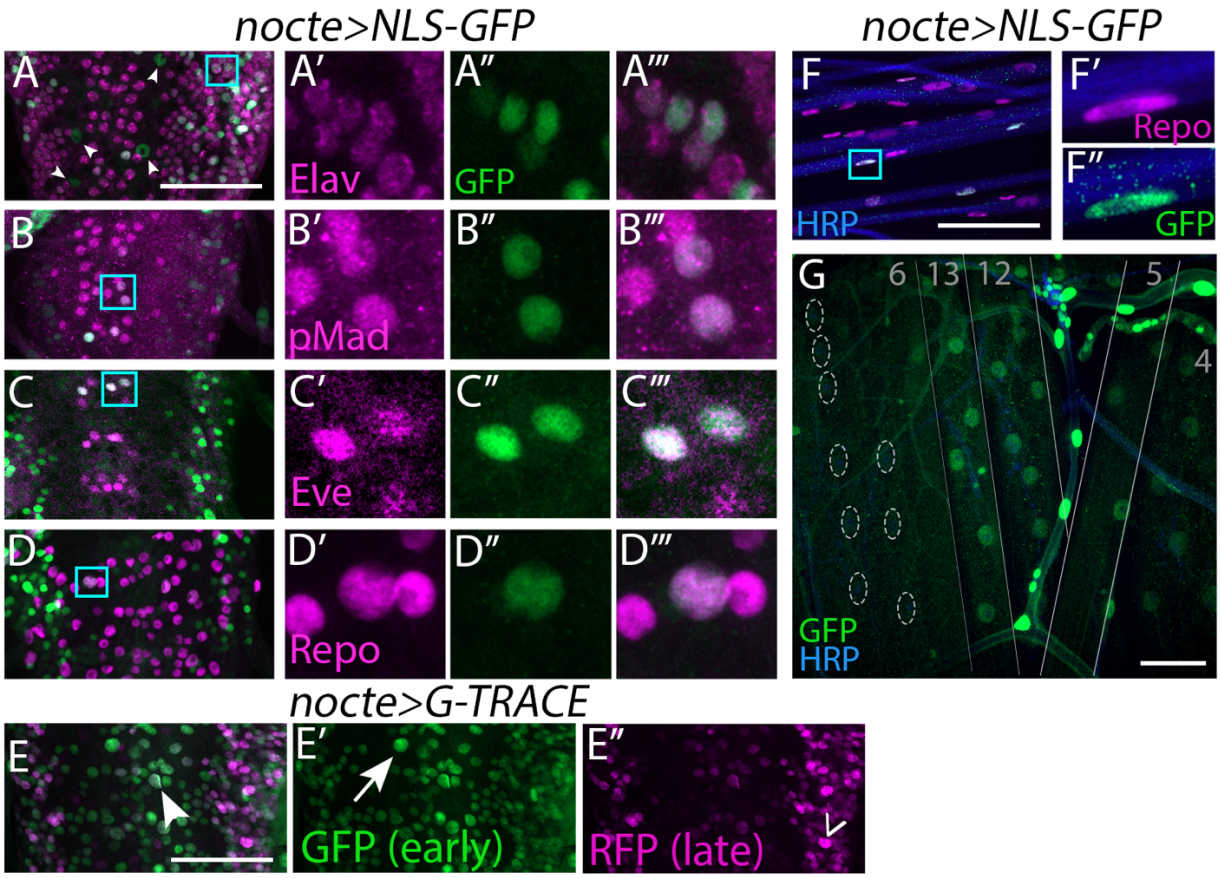

Figure 3.5 *nocte* is broadly expressed in larvae
(A-D) Larval VNCs from *nocte-GAL4 x UAS-NLS-GFP* animals stained for GFP (green) and cell specific markers (magenta). (A'-D''') Insets of A-D (cyan rectangles) showing co-localization of GFP and the cell specific markers. (E-E'') VNC of *nocte-GAL4 x UAS-G-TRACE* larva stained for GFP (green) indicating only early expression (arrow) and RFP (magenta) indicating only late expression (caret). Cell expressing both GFP and RFP (arrowhead) suggest *nocte* is constitutively expressed. (F-G) *nocte-GAL4 x UAS-NLS-GFP* animals stained for GFP (green) and neuronal tissue (HRP, blue). (F-F'') Peripheral nerves stained for the glial marker Repo (magenta). (F'-F'') Insets of cyan rectangle in F. Note that only a subset of glial cells express *nocte*. (G) Ventral muscle field showing expression in m13, 12, 5, 4 but not m6 (nuclei lacking GFP outlined in dotted ellipses). All scale bars = 50μm.

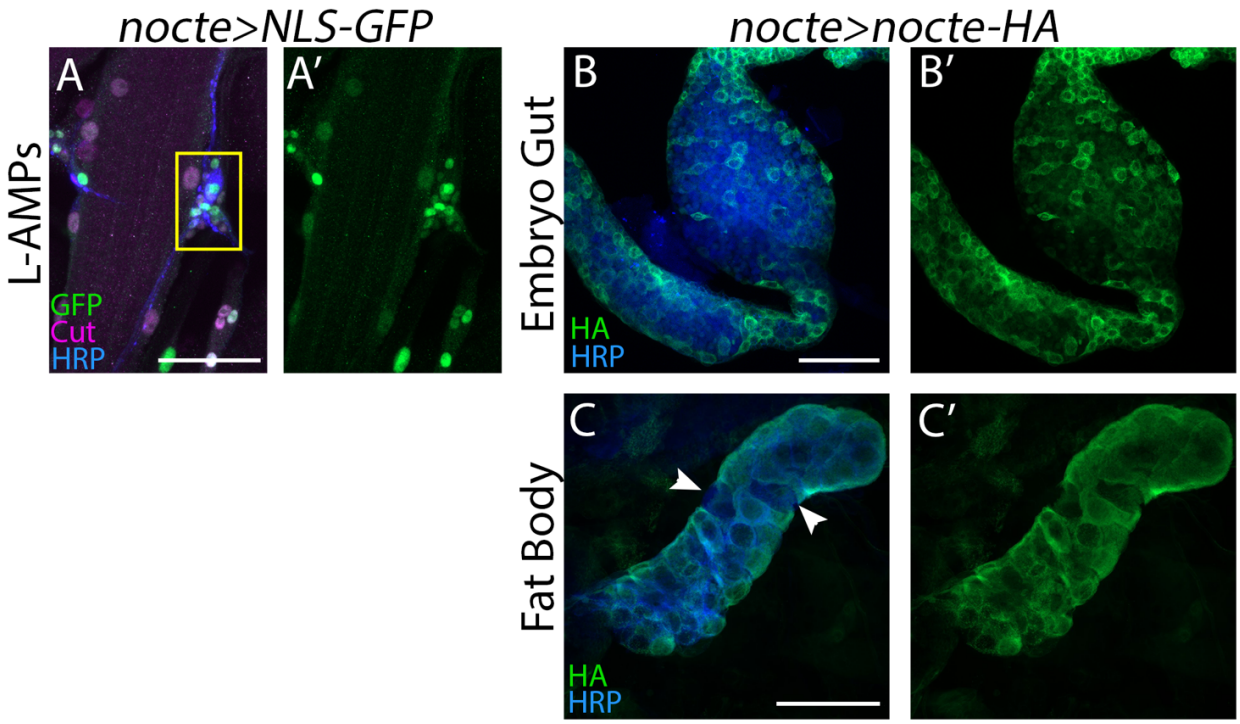

Figure S3.5 Nocte peripheral expression
(A) *nocte-GAL4 x UAS-NLS-GFP* larvae. Lateral adult muscle precursor cells (L-AMPs) highlighted by a yellow rectangle. Preps were co-stained for the transcription factor Cut (magenta) and HRP (blue). (B') GFP channel. (B-C) *nocte-GAL4 x UAS-nocte-HA* larvae. (B) Embryonic gut dissected away from rest of embryo. Nocte localization labeled with HA (green) and gut outline shown in HRP (magenta). (C) Larval fat body cells. Nocte localization labeled with HA (green) and FB outline shown in HRP (magenta). Cells lacking *nocte* expression indicated with arrowhead. All scale bars = 50μm.

3.7 Nocte localizes to the cytoplasm and nucleus

We lack insight into where Nocte is found inside the cell. Structural prediction of Nocte using Alphafold did not reveal any known protein motif (Jumper et al., 2021) (Figure S3.6A). Nocte lacks a signal peptide, suggesting that it functions intracellularly. To gain insight into Nocte sub-cellular localization, we used a *UAS-HA-nocte* transgenic line (Chen et al., 2015). Expression of *HA-nocte* with *nocte-GAL4* resulted in lethality at larval and pupal stages; to circumvent this, we overexpressed *HA-nocte* in a $nocte^{P}$ hypomorphic background. We used antibodies against HA to visualize Nocte localization and found significant staining around the outer nuclear envelope marker, LamC, in both glia and muscle cells (Figure 3.6A-B). In addition, we observed that Nocte localizes in striated patterns in the muscle (Figure 3.6A), mirroring the alternating muscle A- and I-bands (Poovathumkadavil and Jagla, 2020). Thus, these experiments suggest that Nocte is distributed throughout the cytoplasm and is concentrated around the nucleus.

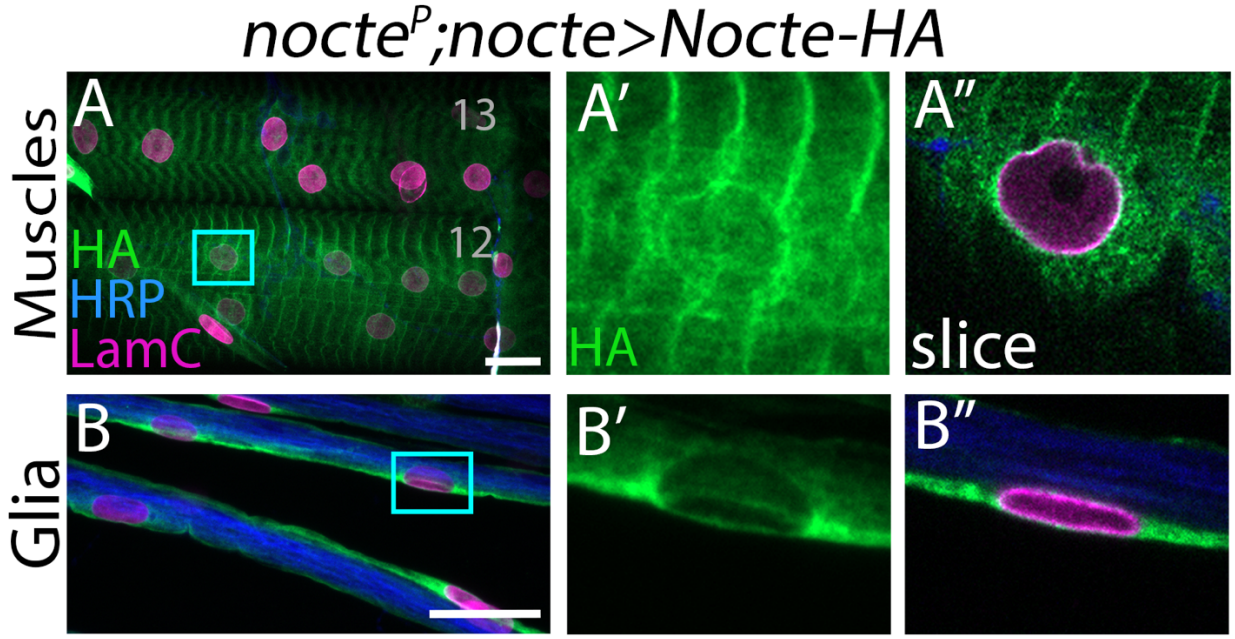

Figure 3.6 Sub-cellular localization of Nocte
(A,B) *UAS-Nocte-HA* was expressed by *nocte-GAL4* in a *nocte*^{P} mutant background. Nuclear lamina was stained with LamC (magenta), neuronal tissue was visualized by staining with HRP (blue), and Nocte was localized by staining for HA (green). (A) In m12 and m13, Nocte was localized around the nucleus and at I-bands. (B) In nerves, Nocte was localized in glial cells surrounding axons. (A'-B') Inset of A-B (cyan rectangle), enlarging a nucleus and showing only the green channel. (A''-B'') Single z-plane confocal slice of nucleus in A'-B 'with all channels present. All scale bars = 20μm.

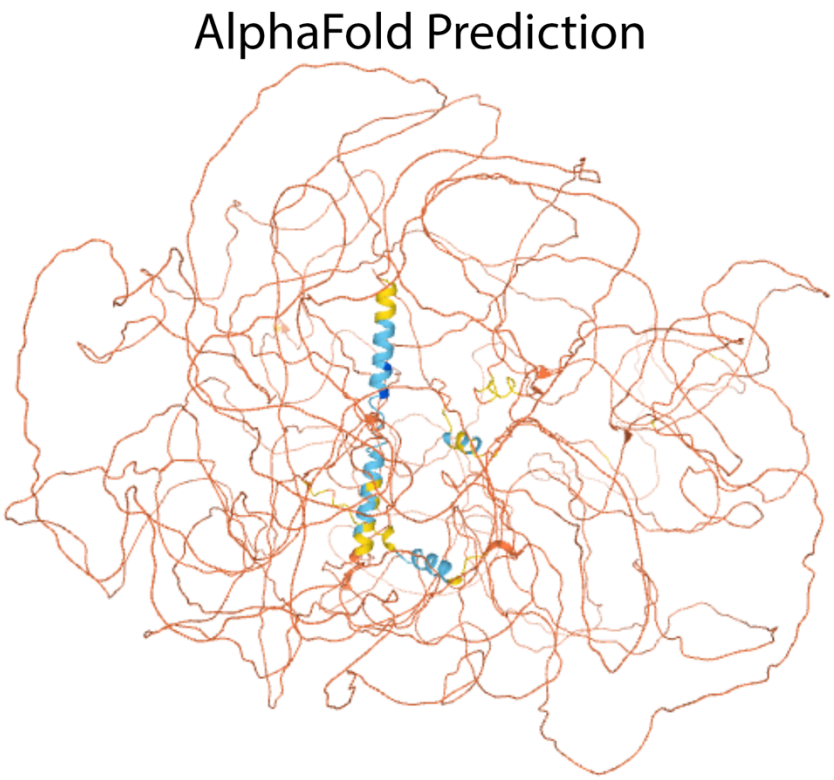

Figure S3.6 AlphaFold structural prediction of Nocte
The orange lines are predicted unstructured regions with fragments of alpha helices visible in the center.

3.8 Nocte is required in neurons to instruct axon pathfinding

To determine where Nocte functions for motor axon pathfinding, we used RNAi to knock down *nocte* pre- and postsynaptically. Reducing *nocte* levels in muscles did not significantly affect ISNb pathfinding compared to controls (*Mef2>nocte-RNAi* = 8.0%, n = 125, p = 0.079; Figure 7A-B, D). However, many of these animals displayed muscle patterning defects with concomitant innervation defects (Figure S3.7). Knockdown of *nocte* in neurons lead to significant ISNb pathfinding defects (w^{1118} = 2.2%, n = 135; *Elav>nocte-RNAi* = 15.7%, n = 134, **p = 0.001) (Figure 3.7A, C, D). Knockdown of *nocte* in all *nocte* expressing cells (*nocte-GAL4*) resulted in similar ISNb pathfinding errors (15.6%, n = 96) compared to neuronal knockdown (Figure 3.3D-E). Neither *GAL4* nor the *UAS-nocte-RNAi* alone had significant pathfinding defects (Figure 3.7D). Overall, these data suggest that Nocte functions presynaptically in motor neurons to mediate ISNb pathfinding.

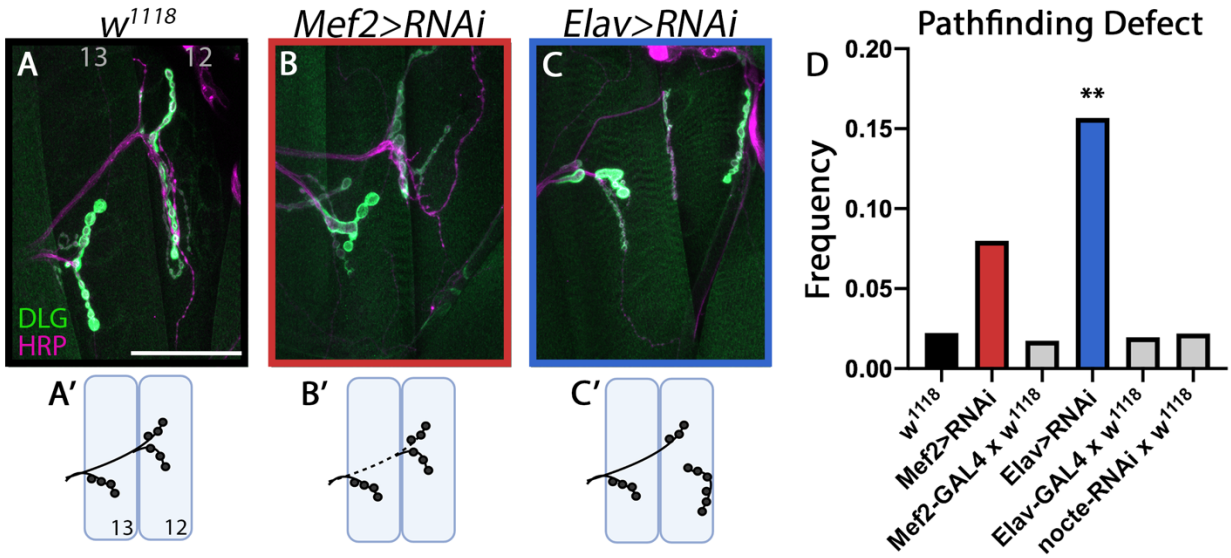

Figure 3.7 Tissue specific knockdown of *nocte* using RNAi

(A-A') w^{1118} control animals depicting the normal ISNb projection over m13 before innervating m12. Neurons were labeled by staining for HRP (magenta) and postsynapses labeled by staining for DLG (green). Scale bar = 50µm. (B-B') *Mef2-GAL4 x UAS-nocte-RNAix2* results in modest misrouting. Here, the m12 ISNb branch for travels under m13. (C-C') *Elav-GAL4 x UAS-nocte-RNAix2* led to significant misrouting of the ISNb. Here, the MN12-Ib innervates from the dorsal side rather than the ventral side. (D) Quantification of the frequency of ISNb pathfinding defects in the respective genotypes. Note that knockdown of *nocte* in neurons (*Elav>RNAi*) significantly increased pathfinding defects. **p<0.01.

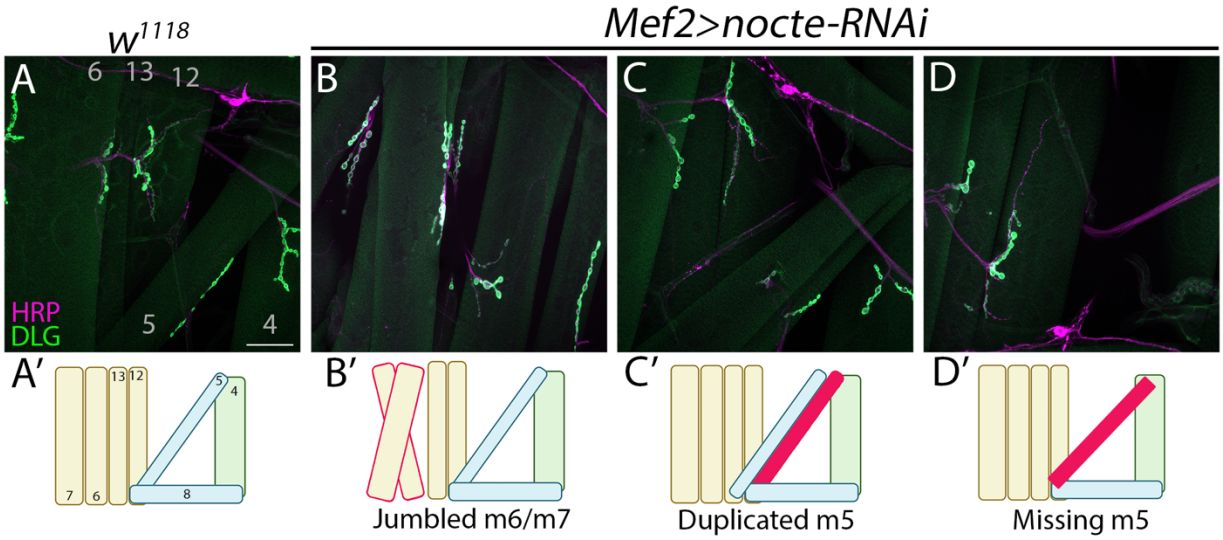

Figure S3.7 Muscle patterning defects caused by knockdown of *nocte* in muscles
(A) A control w^{1118} animal depicting the normal muscle pattern. Neurons are labeled by HRP staining (magenta) and postsynapses by DLG staining (green). Note that the outline of muscles can be clearly visualized in the green channel. Scale bar = 50µm. (B-D) *Mef2-GAL4 x UAS-nocte-RNAix2* animals revealed several defects including (B) crisscrossing of m6 and m7, (C) duplication of m5, and (D) absence of m5. (A'-D') Cartoon schematics of muscle patterns observed in A-D. Aberrant muscles shown in red. Scale bar = 50µm.

3.9 Nocte and Dpr10 genetically interact

Dpr10 is a cell surface protein, and like Nocte, it is expressed in motor neurons and muscles (Ashley et al., 2019; Wang et al., 2022). Dpr10 and Nocte also interact biochemically in vivo (Figure 3.2) and loss of each resulted in ISNb pathfinding defects. Here, we tested whether Dpr10 and Nocte function in the same pathway.

dpr10 mutants alone exhibited ISNb pathfinding and innervation defects at levels higher than *nocte* mutants (Figure 3.8). Specifically, $dpr10^{CR}$ larvae displayed innervation defects in 23.2% of examined hemisegments (n = 90) compared to 9.4% in $nocte^{P}$ larvae (n = 192) (Figure 3.8C). We reasoned that if *dpr10* and *nocte* are in the same pathway, double mutants would exhibit defects similar to the single *dpr10* mutant. Indeed, in $nocte^{P};;dpr10^{CR}$ double mutants, ISNb misrouting was not statistically different than $dpr10^{CR}$ mutants (28.3%, n = 120, p = 0.584) (Figure 3.8B-C). Moreover, the double mutants exhibited muscle patterning defects akin to single mutant animals (Figure S3.8). Taken together, these data suggest that Dpr10 and Nocte function in the same pathway to instruct ISNb pathfinding and innervation.

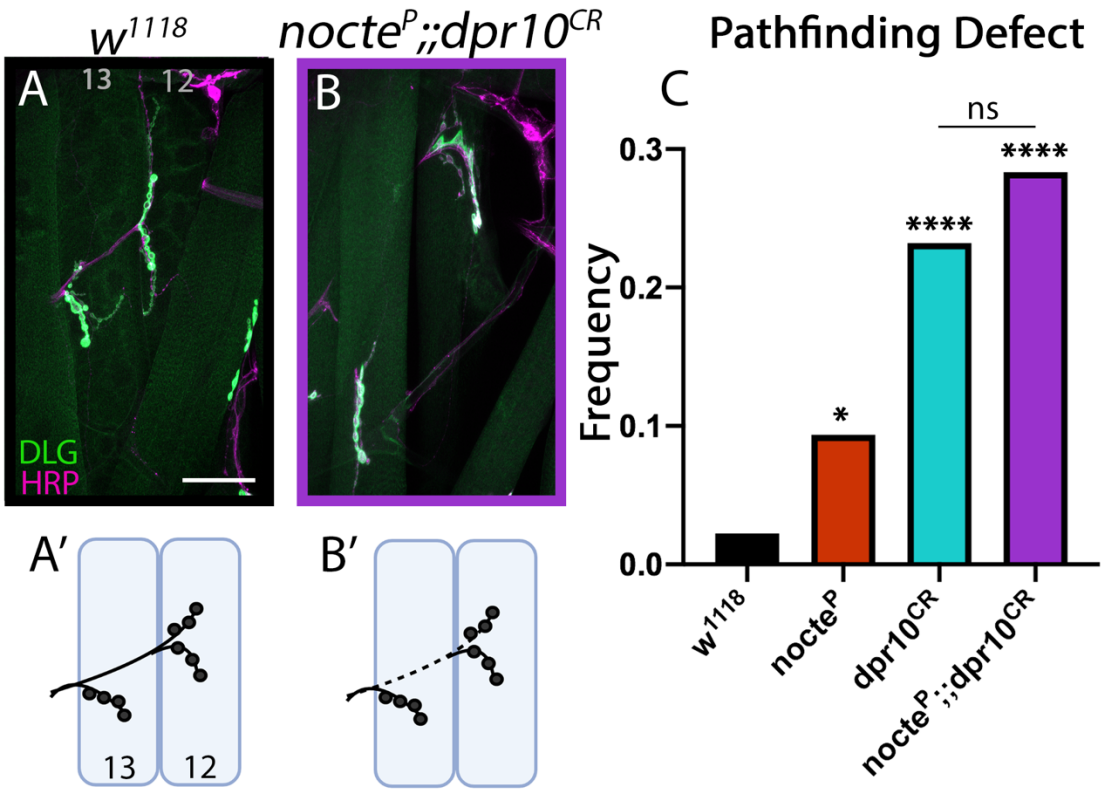

Figure 3.8 *nocte*^{P} and *dpr10*^{CR} double mutants are indistinguishable from *dpr10*^{CR} single mutants

NMJs of m13 and m12, with neurons shown in magenta (HRP) and postsynapses in green (DLG). Scale bar = 50µm. (A-A') Normal pathfinding in a *w*^{1118} control animal. (B-B') In a *nocte,dpr10* double mutant, the ISNb traveled under m13 before innervating m12. (C) Quantification of misrouting frequencies of control, single, and double mutant animals. *p<0.05, ****p<0.0001.

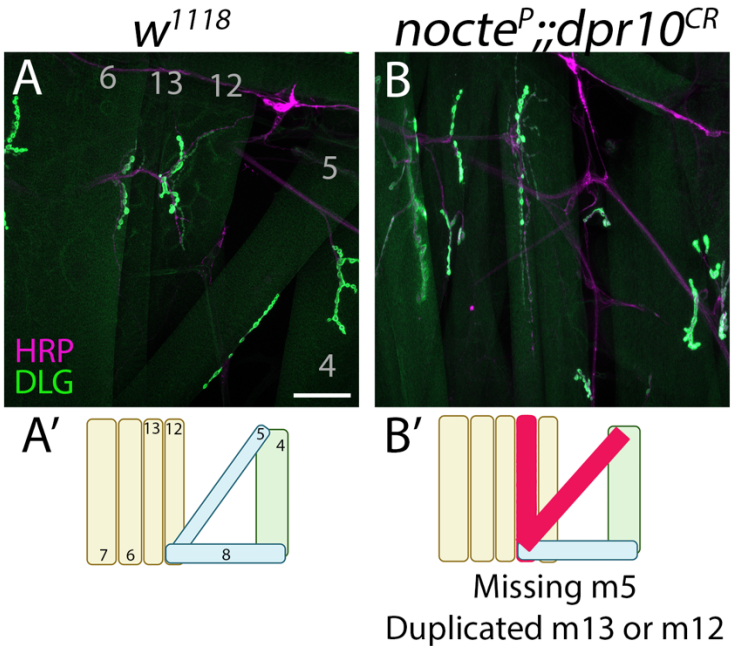

Figure S3.8 Muscle defects in *nocte,dpr10* double mutants
(A) A control w^{1118} animal depicting the normal muscle pattern. Neurons are labeled by HRP staining (magenta) and postsynapses by DLG staining (green). Note that the outline of muscles can be clearly visualized in the green channel. Scale bar = 50µm. (B) $nocte^{P};;dpr10^{CR}$ double mutant animals showed various muscle patterning defects including duplication of m13 or m12 and missing m5. (A'-B') Cartoon schematics of muscle patterns observed in A-B. Aberrant muscles shown in red. Scale bar = 50µm.

3.10 Discussion

The Dpr and DIP subfamilies of the IgSF have been implicated in several steps of *Drosophila* nervous system development. In this study, we revealed a novel function for Dpr10 in motor axon pathfinding. To understand the Dpr10 molecular pathway that underlies this role, we identified Nocte as a novel Dpr10 interactor. In support of Dpr10 and Nocte being in the same molecular pathway, loss of *nocte* led to ISNb pathfinding defects, and *nocte,dpr10* double mutants did not exacerbate the *dpr10* phenotype. Knockdown of *nocte* in neurons caused significant axon misrouting, suggesting that Nocte and Dpr10 interact presynaptically to mediate ISNb pathfinding. Overall, our data identified new interactors of Dpr10 and revealed novel roles for Nocte and Dpr10 in motor neuron pathfinding.

3.10.1 Examining Dpr-DIP mediated mechanisms

Several CSP families have been implicated in circuit assembly, but the signaling pathways are much less understood. The *Drosophila* Dprs and DIPs instruct synaptic connectivity in the optic lobe and neuromuscular junction and other neurodevelopmental processes including motor axon terminal morphology, olfactory axon pathfinding, and cell survival. In this study, we demonstrate that Dpr10 is also required for motor axon pathfinding. Thus, in the neuromuscular junction, Dpr10 is used for motor axon pathfinding (this study) and later for synaptic connectivity (Ashley et al., 2019). Together, these studies suggest that Dprs and DIPs may use multiple signaling pathways to mediate their pleotropic functions.

At the larval NMJ, loss of *dpr11* and *DIP-γ* revealed exuberant satellite boutons (Carrillo et al., 2015), reminiscent of BMP signaling overactivation (O'Connor-Giles et al., 2008; O'Connor-Giles and Ganetzky, 2008). Genetic interaction tests and BMP pathway reporters

confirmed that *dpr11* and *DIP-γ* modulate BMP signaling (Carrillo et al., 2015). How Dprs and DIPs interact with BMP ligands and/or receptors in not known. The vertebrate orthologs of the Dprs and DIPs, the IgLONs, are required for normal neurite outgrowth in forebrain (Akeel et al., 2011) and hippocampal neurons (Singh et al., 2018). One member of the IgLON family, Negr1, signals through the FGF pathway to promote neuronal arborization (Pischedda and Piccoli, 2016). In the *Drosophila* larval neuromuscular junction, one of the FGF receptors, Heartless, is required for NMJ development (Sen et al., 2011). Whether the Dpr/DIP and FGF pathways interact is not known. Elucidating signaling pathways of the Dprs and DIPs may contribute to our understanding of IgLON mechanisms during nervous system development.

To uncover potential Dpr/DIP signaling pathways, we sought to identify proteins that interact with Dpr10. We immunoprecipitated Dpr10 and found several interactors including cDIP, an LRR protein previously identified in an in vitro screen as a Dpr10 binding protein (Carrillo et al., 2015; Özkan et al., 2013). cDIP binds many Dprs and DIPs, and in the *Drosophila* visual system, cDIP is required in glial cells for synaptic refinement (Shimozono et al., 2019); a role in the neuromuscular junction has not been reported. cDIP may be involved in a Dpr10-mediated pathway, but as a putative secreted protein, it would not be able to signal directly into the cell.

Another Dpr10 interactor identified in our screen was Nocte, a glutamine-rich protein that is predicted to be an unstructured intracellular protein. Previous work implicated Nocte in temperature-dependent entrainment of circadian rhythm (Sehadova et al., 2009). In this study, we collected body wall and brain tissues to perform Dpr10 immunoprecipitations, and in both samples, we isolated Nocte; however, we cannot distinguish between direct or indirect interactions. The association between Dpr10 and Nocte, whether direct or indirect, suggests that

Nocte must also localize at or near the cell membrane. A previous study found that in the adult head, Nocte was enriched in the membrane associated fraction of a mass spectrometry experiment (Aradska et al., 2015), suggesting that Nocte endogenously binds proteins at or in the cell membrane. Furthermore, when Nocte was expressed with *timeless-GAL4* in adult fly heads and immunoprecipitated, the transmembrane receptor Ir25a was identified as an interactor. Thus, Nocte is known to interact with membrane associated proteins.

Functionally, *dpr10* and *nocte* mutants exhibited similar pathfinding defects and *nocte,dpr10* double mutants displayed misrouting at a similar frequency to *dpr10* single mutants, suggesting these two genes are in the same ISNb pathfinding pathway. How they work together at a mechanistic level is unknown but binding of Dpr10 with an extracellular ligand could modify its interaction with Nocte to activate or inhibit downstream signaling.

3.10.2 ISNb pathfinding is mediated by multiple pathways

During axon pathfinding, growth cones must recognize multiple attractive and repulsive cues that instruct the axons to their appropriate destinations. In addition to the challenges of interpreting these cues, some axons must traverse long distances to find their correct targets (Jeong, 2021; Kolodkin and Tessier-Lavigne, 2011). The synaptic connections that are finally established are critical for all behaviors, learning, and memory, and thus, axon pathfinding is tightly regulated. Identifying the cues that regulate this process is challenging, in part, because of molecular redundancy (Stoeckli, 2018). In *Drosophila* embryos, the ISNb innervates muscles 7, 6, 28, 14, 13, and 12. However, the cell bodies for the axons in the ISNb are located in the VNC. These axons must exit the VNC in defined locations, ignore incorrect target cells, make precise decisions about where to defasciculate, and ultimately innervate their respective muscles.

Previous studies have implicated multiple signaling pathways in ISNb pathfinding. Not surprisingly, many of the identified genes code for CSPs.

In (Kurusu et al., 2008), the Zinn lab conducted a screen of LRR CSPs that mediate synaptic pathfinding and target selection. Loss- and gain-of-function analyses revealed multiple LRR proteins, such as Tartan (Trn), Capricious (Caps), and Hattifattener (Haf), as mediators of ISNb pathfinding. For example, manipulation of *trn* levels showed multiple ISNb mistargeting and pathfinding phenotypes in embryos and larvae including stalling and misrouting under m13 and m12 leading to innervation of m12 on the dorsal side. These defects mimic those we observed after loss of *dpr10* and *nocte*. Moreover, the same study reported similar frequencies of the misrouting defect, with *caps* mutants exhibiting ~15% defects, and *trn* nulls mistargeting in ~40% of hemisegments. Interestingly, loss of *trn* and *caps* also lead to muscle patterning defects, akin to loss of *dpr10* and *nocte*.

In another study, Tolloid-related 1 (Tlr1) was also implicated in motor axon pathfinding. In *tlr1* mutants, m12 is incorrectly innervated from the dorsal rather than the ventral side (Meyer and Aberle, 2006). Tlr1 is a metalloprotease that functions together with Sidestep, an IgSF CSP, for proper ISNb defasciculation (Meyer and Aberle, 2006). Taken together, these studies and our work support the model that multiple CSP families act combinatorically and/or redundantly to mediate ISNb pathfinding.

3.10.3 Putative function of Nocte in axon pathfinding

Our current study identified Nocte as an interactor of Dpr10 in larval brains and body walls. To gain insight into Nocte structure and function, we used the structure prediction software AlphaFold (Jumper et al., 2021); however, it was unable to resolve clear domains for

Nocte. Other prediction software programs (Rosetta, RaptorX) were unable to run predictions as Nocte is a relatively large protein with 2,309 amino acids. Given the lack of clear structure, we cannot infer the molecular function of Nocte or how it may bind Dpr10.

Based on our genetic and biochemical data, Nocte functions in either a repulsive or attractive axon pathfinding cascade mediated through Dpr10. In either model, when Nocte is removed the nerve cannot distinguish between the correct and incorrect trajectories. Similar observations were made when disrupting the repulsive Semaphorin-Plexin pathway: loss of either the ligand or receptor perturbs axon defasciculation and axon guidance (Koropouli and Kolodkin, 2014; Winberg et al., 1998). Similarly, when the attractive cue Netrin, or its receptor Unc5, is removed, defasciculation does not occur and the motor neurons that reach the periphery fail to innervate their target muscles properly (Keleman and Dickson, 2001; Mitchell et al., 1996).

In vertebrates, Proline rich coiled-coil 2a (Prrc2a) is the ortholog of Nocte (Hu et al., 2011) and functions as a N^6-methyladenosine (m^6A) reader (Wu et al., 2019). m^6A is the most abundant mRNA modification found in eukaryotes and regulates mRNA stability, splicing, and translation (Jiang et al., 2021). In glial cells, Prrc2a modulates mRNA stability and is required for cell specification and maintenance (Wu et al., 2019). In *Drosophila*, m^6A modifications are critical for sex determination and neuronal function and are upregulated during embryogenesis and pupal stages (Haussmann et al., 2016; Lence et al., 2016). If Nocte is an m^6A reader, Nocte could regulate the temporal expression of pathfinding molecules at specific choice points. In support of this model, *nocte* knockdown and overexpression delayed and expedited, respectively, the innervation of m12 by the ISNb. In a similar model, the Hox gene *Ultrabithorax* (*Ubx*)

regulates ISNb routing by controlling expression of pathfinding molecules (Hessinger et al., 2016).

An open question is why Nocte interacts with cell surface CSPs, including Dpr10 and Ir25a. One possibility is that interactions with CSPs may regulate Nocte by sequestering it. Alternatively, CSPs could transduce an extracellular signal to Nocte to regulate relevant mRNAs. Future studies will examine if Nocte, like its vertebrate ortholog Prrc2a, regulates mRNAs though m^6A modifications. Moreover, it is unknown how Nocte associates with Ir25a and Dpr10, and if these interactions influence Nocte function. Taken together, this study identified in vivo interactors of Dpr10 and novel functions for Nocte and Dpr10 in motor axon pathfinding.

3.11 Methods

3.11.1 Drosophila melanogaster stocks and reagents

All flies were maintained at 25℃. Crosses were kept at medium density and vials were flipped every day to achieve a standard level of egg laying and rearing conditions. The Stanewsky Lab (University of Münster) generously provided all Nocte fly reagents.

3.11.2 Scoring Misrouting Defect

We scored ISNb pathfinding defects at m13 and m12 including motor axons aberrantly traveling under m13, under m12, or under both, and loss of innervation of any of the Is or Ib terminals on m13 or m12. These phenotypes were collectively reported as a 'pathfinding defect' as pathfinding can be aberrant by the path the axon takes and subsequently which muscles it innervates. Additional misrouting phenotypes were observed at other NMJs, but in this study we focus specifically on the ISNb at m12 and m13.

3.11.3 Larval Dissections

Larval dissections and immunostaining were performed as described previously (Ashley et al., 2019). Briefly, third instar larvae were dissected in PBS on Sylgard dishes and fixed with 4% paraformaldehyde for 30 minutes. Fillets were washed with Phosphate Buffered Saline (PBS) and placed in tubes with PBST (PBS + 0.05% TritonX100) for three 15-minute washes on a nutator, before blocking for an hour in 5% Normal Goat Serum in 0.05% PBST block. Samples were incubated with primary antibodies overnight in block (5% Goat serum in 0.05% PBST) at 4°C. After incubation, samples were washed in PBST and incubated for two hours with secondary fluorescent antibodies in block at room temperature. Samples were washed and then

mounted in Vectashield (Vector Laboratories). Representative images were acquired on a Zeiss LSM800 confocal microscope and processed with ImageJ.

3.11.4 Biochemistry

50 brains per sample were collected from *dpr10>Dpr10-V5* and *dpr10>CD8-GFP* larvae. Similarly, 50 body walls were collected from *Mef2>Dpr10-V5* and *Mef2>CD8-GFP* larvae. All dissections were performed in ice cold PBS and tissue was kept on ice for no more than ten minutes before transferring to the -80°C freezer. Samples were homogenized in NP-40 Buffer with Pierce Protease Inhibitor Mini (A32955) using Fisherbrand RNase-FREE Disposable Pellet Pestles (12-141-368).

Tissue lysate was first cleared with Protein G Magnetic Beads (New England Bio Labs S1430S) and then immunoprecipitation was performed using fresh beads incubated with either mouse anti-V5 or mouse anti-GFP antibodies (1:8 antibody to bead ratio per sample). Samples were thoroughly washed before boiling in 2x SDS loading buffer. Samples were then run in a 12% acrylamide gel, stained with Coomassie Blue, and fragments were excised and placed in Eppendorf Tubes. Mass Spectrometry was run by the Northwestern Proteomics Core Facility.

3.11.5 Embryos

Embryo dissections were performed as outlined by (Lee et al., 2009). Briefly, embryo cages were setup in collection chambers, with grape plates at the bottom for egg laying. Each batch of grape plates is made by dissolving 12g agar in 300ml water and adding 100ml grape juice, 5.35g sucrose, and 8ml Tegosept (Genesee Scientific 20-258). Yeast paste (dry yeast, water) was added to the center of grape plates to encourage egg laying and to feed adult flies.

Plates were collected after a two-hour egg laying period at 25°C in darkness. Embryos reached stage 16 after incubation in humid environment at 25°C for 15 hours. Staging was confirmed by shape of the gut after chorion was removed using a dull metal probe and two-sided tape (Lee et al., 2009). Embryos were staged on a slab of agar before being transferred, dorsal side up, to two-sided tape on a glass slide. Embryos were submerged in filter sterilized PBS. Using a sharp tungsten probe, embryos were removed from vitellin membrane and placed onto Superfrost Plus Slides. Embryos were fillet, fixed, and stained, similar to the larval protocol above, the only difference is that primary and secondary antibodies are incubated overnight at 4°C and that samples were not placed on a nutator at any point.

3.11.6 Immunohistochemistry

The primary antibodies used for this study are: Chicken anti-GFP (1:500, Invitrogen A10262), Rabbit anti-GFP (1:10,000, Glotzer Lab), Chicken anti-mCherry (1:1000, Novus NBP 2-25158), Mouse anti-HA (1:1000, BioLegend 901501), Rabbit anti-HA (1:300, Cell Signaling 3724S), Rabbit anti-FLAG (1:200, Novus NBP-1-06712), Rat anti-FLAG (1:200, Novus Biologicals), Mouse anti-Repo (1:100, DSHB 8D12), Rabbit anti-DLG (1:40,000, Budnik Lab), Mouse anti-LamC (1:100, DSHB LC28.26), Mouse anti-V5 (1:200, Invitrogen R960-25), Mouse anti-Cut (1:100, DSHB LC28.26), Rabbit anti-pmad (1:300, Abcam EP823Y), Mouse anti-Eve (1:100, DSHB 3C10), and Mouse anti-FasII (1:100, DSHB 1D4).

The conjugated primary antibodies used for this study are: Goat anti-Phalloidin 405 (1:100, Invitrogen A30104), Goat anti-HRP 405 (1:100, Jackson ImmunoResearch 123-475-021), Goat anti-HRP TRITC (1:100, Jackson ImmunoResearch 123-025-021), and Goat anti-HRP 647 (Jackson ImmunoResearch 123-605-021).

The secondary antibodies used for this study are: Goat anti-Mouse 488 (1:500, Invitrogen A11029), Goat anti-Rabbit 488 (1:500, Invitrogen A11008), Goat anti-Chicken 488 (1:500, Invitrogen A11039), Goat anti-Rat 488 (1:500, Invitrogen A11006), Goat anti-Rat 568 (1:500, Invitrogen A11077), Goat anti-Mouse 568 (1:500, Invitrogen A11031), Goat anti-Rabbit 568 (1:500, Invitrogen A11036), Goat anti-Chicken Cy3 (1:500, Jackson Immunological Research 123-605-021), Goat anti-Rabbit 647 (1:500, Invitrogen A32733), and Goat anti-Mouse 647 (1:500, Invitrogen A32728).

3.12.7 Imaging Protocols

Quantification of innervation and misrouting phenotypes were conducted using a Zeiss Axiolmager M2 and a 40X plan-neofluar 1.3NA objective. NMJs were examined using HRP and DLG stains. The DLG signal allowed for scoring Is presence, as Is boutons have smaller postsynaptic membrane structures and appear smaller and dimmer than Ib boutons. All images were captured on a Zeiss LSM800 confocal microscope with a 20X plan-apo 0.8NA objective, a 40X plan-neofluar 1.3NA objective, or 63X plan-apo 1.4NA objective.

3.12.8 Analysis

Statistical analysis was performed using GraphPad (Prism). Each data group was collected from a minimum of two experiments of six animals each, using the abdominal body wall segments 2-5. Data significance was determined through Chi Squared Test with Fisher's exact test. Images were prepared using ImageJ FIJI (Schindelin et al., 2012).

Genotype	Description	Source
nocte^{P}	Mutant (transposon excision)	(Sehadova et al., 2009)
nocte^{1}/ FM7	Mutant (EMS)	(Sehadova et al., 2009)
UAS-nocte-RNAi 2:1b;UAS-nocte-RNAi 1:3	RNAi	(Sehadova et al., 2009)
nocte-Gal4	Nocte GAL4 driver	(Sehadova et al., 2009)
UAS-Flag-Strep-nocte-HA	FLAG and HA tagged nocte	(Chen et al., 2015)
dpr10^{CR}	Mutant (CRISPR)	(Xu et al., 2018b)
Mef2-GAL4	Muscle GAL4 driver	(Ranganayakulu et al., 1998)
Elav-GAL4	Neuronal GAL4 driver	BDSC: 8765
Repo-GAL4	Glial GAL4 driver	BDSC: 7415
dpr10-T2A-GAL4	Dpr10 MiMIC GAL4 insertion	(Lee et al., 2018)
UAS-GFP::LacZ NLS	Nuclear localized GFP	BDSC: 6451
W^{1118}	White control	BDSC
UAS-nRedStinger, UAS-FLP, Ubi-p63E(FRT.STOP)-nStinger	G-TRACE	BDSC: 28280
UAS-mCD8::GFP	Membrane GFP	BDSC: 32184

Table 2.1. The fly lines used in this study.

CHAPTER 4

DIP-α AND DPR10 SUPPRESS SYNAPTIC ARBOR GROWTH THROUGH DRAPER AND LAR AT THE *DROSOPHILA* NMJ

Yupu Wang helped with study design. Darian Estevez aided in quantification of affinity phenotypes. Violet Sorrentino identified initial phenotype. James Ashley helped with quantification. This work is unpublished.

4.1 Introduction

To form functional nervous systems, neurons extend their axons to the general area of their synaptic targets (axon pathfinding), discriminate correct from incorrect partners (synaptic partner matching), and then elaborate their processes until they have reached the appropriate, functional size (synaptic arbor growth). Each of these steps is regulated by soluble factors and cell surface proteins (CSPs) that allow the neuron to gain information about its environment. The *Drosophila melanogaster* larval neuromuscular system is an excellent model to examine these developmental steps because (1) it is a relatively simple, mapped circuit that is easily imaged, (2) the molecules that regulate these processes are largely conserved with vertebrates, and (3) the robust genetic access.

Synaptic arbor growth occurs after the correct synaptic partners have matched and the synaptic transmission machinery is assembled. At the larval NMJ, this machinery is housed in bead like structures called boutons (Figure 4.1). As the animal grows, boutons are added to keep pace with the drastic expansion of muscle surface area to maintain synaptic efficacy (Menon et al., 2013). Bouton number does not scale directly with muscle size, and as with other steps in neural circuit assembly, multiple factors have been implicated in synaptic growth. There are two

types of glutamatergic motor neurons (MNs) in the larval neuromuscular system, the Is- and Ib-type, which are easily distinguished based on the size of the subsynaptic reticulum that surrounds the boutons (Is = small, Ib = big) (Guan et al., 1996). While Ib neurons innervate single muscle targets (for example, motor neuron 4-Ib innervates only muscle 4; m4-Ib), Is MNs innervate muscle groups and are therefore known as common exciters (for example, the ventral common exciter, vCE, innervates a large subset of the ventral muscles).

Many signaling pathways and cellular processes have been implicated in shaping synaptic arbor growth (Menon et al., 2013). Signaling can come from the neuron and muscle, and the arbor size can also be shaped by activity (Harris and Littleton, 2015) A transsynaptic pathway with both forward and retrograde signaling that impacts synaptic growth is the bone morphogenic pathway (BMP). BMP activation is required both in the neuron and the muscle for the development and growth of NMJs (Dudu et al., 2006; Fuentes-Medel et al., 2012; Keshishian and Kim, 2004; Marqués et al., 2002; O'Connor-Giles and Ganetzky, 2008). BMP dependent synaptic growth defects can be restored with muscle derived glass bottom boat (Gbb), a BMP ligand (McCabe et al., 2003). However, neuronal Gbb is required to restore synaptic activity, suggesting that both are required for synapse function (Goold and Davis, 2007). An example of activity dependent regulation of synaptic arbor size is the voltage-gated calcium channel, which allows calcium to enter the boutons and causes neurotransmitter release, and mutants exhibit smaller synaptic arbor sizes (Rieckhof et al., 2003). In these examples, cells use CSPs and receptors to sense the ligands or ions in their environment.

The Dprs and DIPs are two related families of immunoglobulin (Ig) superfamily CSPs which function in various steps of nervous system development. Dprs and DIPs have two and three Ig domains, respectively, bind hetero- and homophilically through the first Ig domain

(Carrillo et al., 2015; Cosmanescu et al., 2018; Özkan et al., 2013), and are tethered to the outer leaflet of the cell membrane through a GPI anchor (Lobb-Rabe et al., 2023). Although Dpr-DIP interactions have been extensively implicated in synaptic partner matching (Ashley et al., 2019; Bornstein et al., 2021; Carrillo et al., 2015; Courgeon and Desplan, 2019; Menon et al., 2019; Venkatasubramanian et al., 2019; Xu et al., 2019, 2022, 2018a), they also function in axonal pathfinding (Barish et al., 2018; Lobb-Rabe et al., 2022), link stochastic and deterministic partner matching (Courgeon and Desplan, 2019; Menon et al., 2019), and cell survival (Carrillo et al., 2015; Courgeon and Desplan, 2019; Menon et al., 2019; Xu et al., 2019, 2022). The wide range of functions mediated by Dpr-DIP binding suggest that signaling may be required. However, to date only DIP-γ and Dpr11 have been shown to genetically interact with the BMP pathway to function in NMJ presynaptic terminal development (Carrillo et al., 2015). If signaling is a part of Dpr/DIP biology, their GPI anchor would necessitate a co-receptor that traverses the cell membrane and allows for information to be transduced into the cell.

Here, we demonstrate a novel role for Dprs and DIPs in synaptic arbor growth and show that this occurs with previously characterized molecular pathways, LAR and Draper. Specifically, DIP-α and Dpr10 inhibit synaptic arbor growth of the Is-type vCE as both mutants display exuberant m12-Is growth. Unlike synaptic innervation, which can be tuned with Dpr-DIP binding affinity, synaptic growth is insensitive to binding affinity below a threshold. To identify candidate co-receptors, we performed transheterozygous analyses with CSPs containing transmembrane domains and found that *DIP-α* and *dpr10* genetically interact with *draper* and *LAR* to instruct synaptic arbor growth. This work reveals that DIP-α and Dpr10 function in synaptic arbor growth and mediate this function through transmembrane CSPs that likely act as co-receptors to signal into the cell.

4.2 DIP-α inhibits growth of the motor neuron terminal

After a motor neuron terminal finds its correct partner, it must grow to a size that allows it to elicit muscle contractions without overgrowing and wasting resources. We previously showed that many Dprs and DIPs, including *DIP-α*, continue to be expressed after synapses are formed, suggesting a role in synaptic growth or maintenance (Wang et al., 2022). Upon examining *DIP-α* mutants, we noticed that the vCE terminals on m12 were overgrown, with significantly more boutons than controls, suggesting that DIP-α functions to restrict m12-Is growth (Figure 4.1). We confirmed the role of *DIP-α* in NMJ growth with two independently generated alleles and each allele over a deficiency (Df)—large genomic deletion containing our gene of interest (Figure 4.1B-E) (Venkatasubramanian et al., 2019). Thus, DIP-α inhibits m12-Is growth.

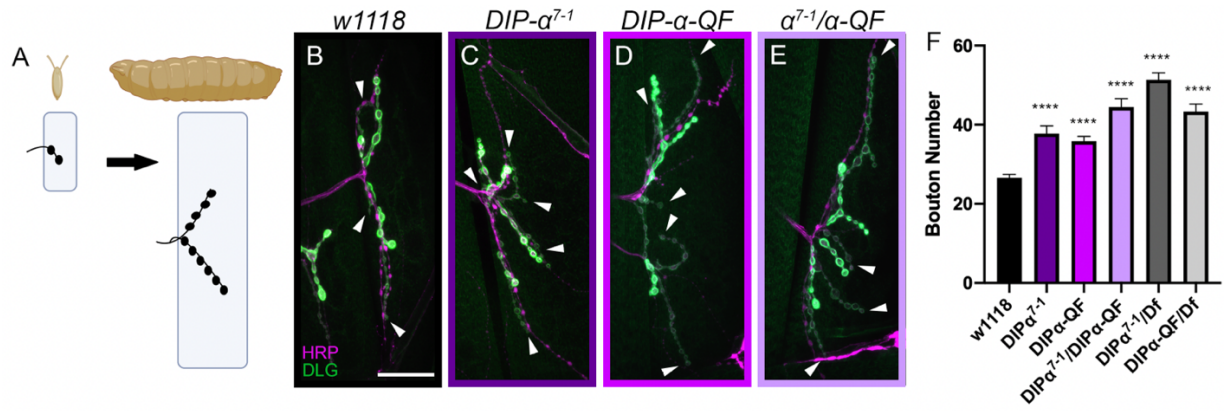

Figure 4.1 DIP-α inhibits growth of motor neuron terminal.
(A) Schematic of synaptic growth at the *Drosophila* NMJ from embryo to third instar larva. (B-E) Larval m12 NMJ with neuronal tissue in magenta (HRP) and postsynaptic staining in green (DLG); Is arbors marked with arrowheads. Scale bar 50 µm. (A) Typical arbor seen on m12 in *w1118* control animals (n=115/16). (B) *DIP-α$^{7-1}$* animals exhibit increased m12-Is arbor size (n=86/15). (C) *DIP-α-QF* animals exhibit increased m12-Is arbor size (n=114/21). (D) Transheterozygous *DIP-α$^{7-1}$/ DIP-α-QF* animals exhibit increased m12-Is arbor size (n=135/18). (E) Quantification of A-D in addition to *DIP-α$^{7-1}$/Df* (n=88/12) and *DIP-α-QF/Df* (n=68/10). Numbers of n reported as n=a/b where a=segments and b=animals. ****p<0.0001; Ordinary one-way ANOVA with multiple comparisons.

4.3 Dpr10 inhibits growth of the motor neuron terminal

DIP-α binds Dpr6 and Dpr10 (Carrillo et al., 2015; Cosmanescu et al., 2018; Özkan et al., 2013). We previously demonstrated that DIP-α interacts with Dpr10 to instruct synaptic partner matching at the larval NMJ (Ashley et al., 2019). We sought to determine if Dpr10 inhibits NMJ growth on m12 and so we examined *dpr10* mutants. Indeed, *dpr10* mutants exhibited similar overgrowth phenotypes relative to controls as *DIP-α* mutants (Figure 4.2). Dpr10's role in inhibiting synaptic growth was confirmed with multiple alleles individually and in heteroallelic combination (Figure 4.2B-E). To examine if Dpr6 is involved in m12-Is growth, we examined *dpr6-dpr10* double mutants. If Dpr6 inhibits growth, we would expect that the double mutants would exacerbate the phenotype observed in *dpr10* single mutants. However, *dpr6-dpr10* double mutants showed no exacerbation of the phenotype, suggesting that Dpr6 does not inhibit m12-Is growth (Figure 4.2E).

To examine if Dpr10 and DIP-α function in the same molecular pathway for synaptic growth, we performed transheterozygous analyses, where depleting each individual component by roughly half has no or a very mild phenotypic readout but when depleting both genes in the same pathway, the phenotype is stronger. Consistent with Dpr10 and DIP-α function in the same molecular pathway, the transheterozygote of *DIP-α* and *dpr10* showed increased Is bouton numbers on m12. Thus, *DIP-α* and *dpr10* inhibit exuberant synaptic growth of the m12-Is NMJ.

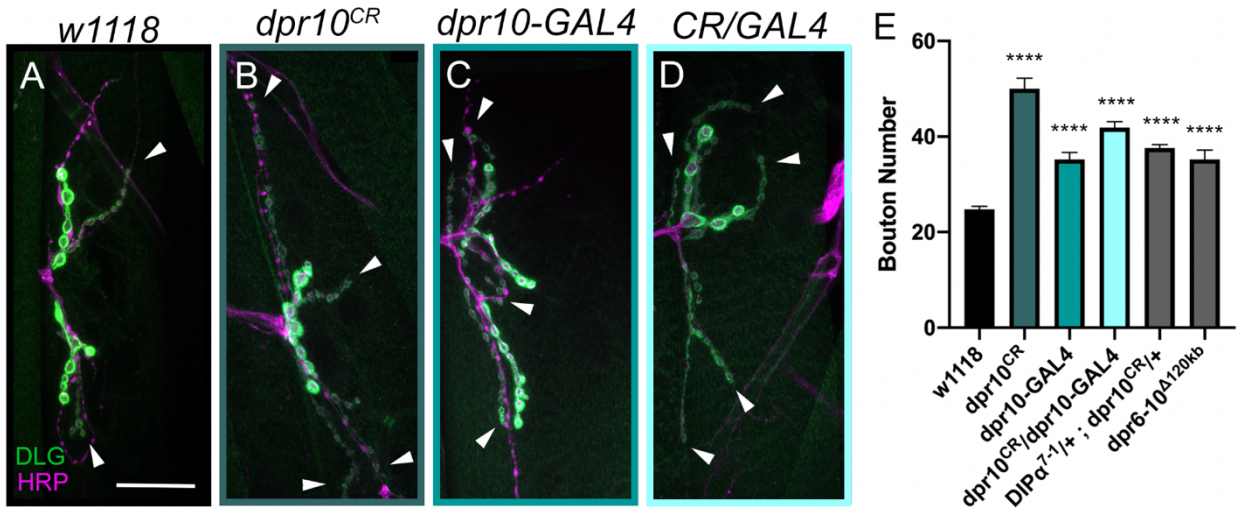

Figure 4.2 Dpr10 inhibits growth of motor neuron terminal.
(A-D) Larval m12 NMJ with neuronal tissue in magenta (HRP) and postsynaptic staining in green (DLG); Is arbors marked with arrowheads. Scale bar 50 µm. (A) Typical arbor seen on m12 in *w1118* control animals (n=115/16). (B) *dpr10^{CR}* animals exhibit increased m12-Is arbor size (n=87/13). (C) *dpr10-GAL4* animals exhibit increased m12-Is arbor size (n=77/12). (D) Transheterozygous *dpr10^{CR}/ dpr10-GAL4* animals exhibit increased m12-Is arbor size (n=112/15). (E) Quantification of A-D in addition to *DIP-α$^{7-1}$/+ ;; dpr10^{CR}/+* (n=127/17) and *dpr6-10^{Δ120kb}* (n=46/6). Numbers of n reported as n=a/b where a=segments and b=animals. ****p<0.0001; Ordinary one-way ANOVA with multiple comparisons.

4.4 Dpr10 is required in muscles to inhibit synaptic growth

We demonstrated that loss of *dpr10* results in increased synaptic bouton number on m12. However, *dpr10* is expressed presynaptically (in the vCE) and postsynaptically in the muscle (Wang et al., 2022). To determine which cell type requires Dpr10 to inhibit synaptic growth, we used tissue specific knock down with a Is specific driver, *A8-GAL4*, and a muscle specific driver, *Mef2-GAL4* (Ranganayakulu et al., 1998; Venkatasubramanian et al., 2019; Wang et al., 2021).

Muscle specific knock down of *dpr10* resulted in signficantly more boutons than all controls suggesting that this population of Dpr10 is, at least in part, responsible for the Dpr10 dependent growth phenotype observed at m12-Is NMJs (Figure 4.3). Interestingly, the *A8-Gal4/+* and *UAS-dpr10-RNAi/+* heterozygoous controls had significantly fewer boutons than the *w1118* control (Figure 4.3A,E). Because these controls themselves have fewer boutons than *w1118* animals, it is difficult to interpret the decreased bouton number observed when depleting *dpr10* in Is MNs (Figure 4.3B,E). The increased number of vCE boutons on m12 is consistent with DIP-α in the neuron interacts with Dpr10 in the muscle to instruct synaptic arbor growth.

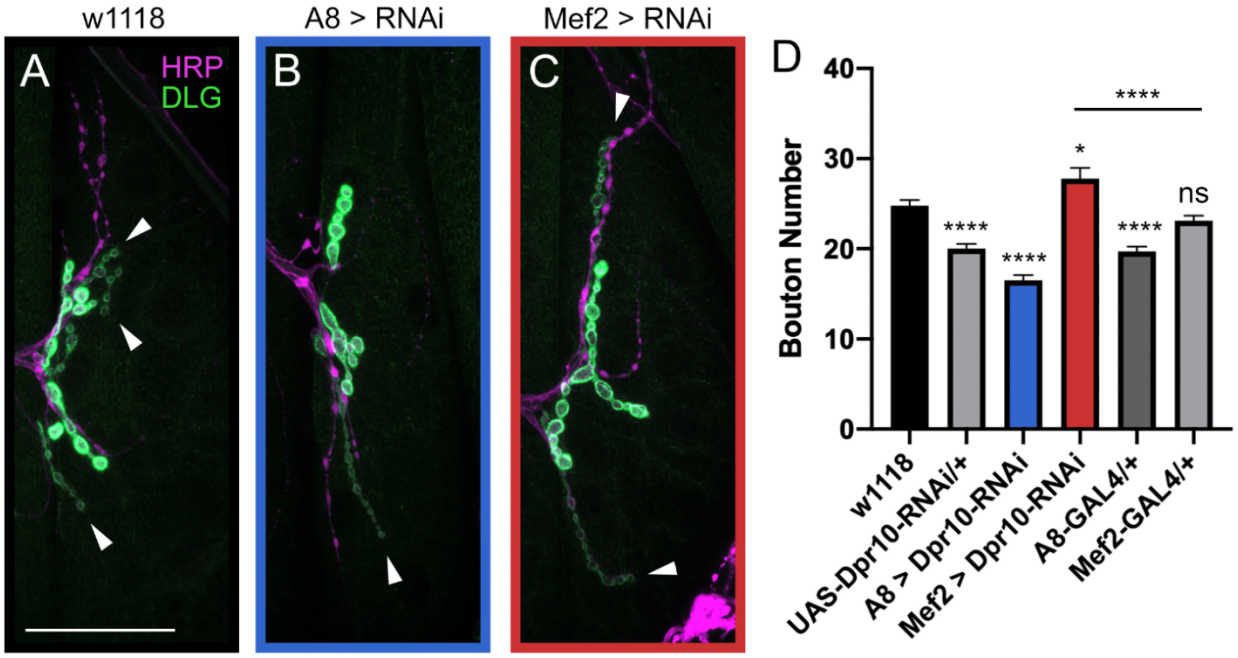

Figure 4.3 Dpr10 is required in muscles to inhibit synaptic growth.
(A-C) Larval m12 NMJ with neuronal tissue in magenta (HRP) and postsynaptic staining in green (DLG); Is arbors marked with arrowheads. Scale bar 50 µm. (A) Typical arbor seen on m12 in *w1118* control animals (n=115/16). (B) Animals with *A8-GAL4* driving *UAS-dpr10-RNAi* animals exhibit decreased m12-Is arbor size (n=126/18). (C) Animals with *Mef2-GAL4* driving *UAS-dpr10-RNAi* animals exhibit decreased m12-Is arbor size (n=134/18). (D) Quantification of A-C in addition to *UAS-Dpr10-RNAi/+* (n=140/18), *A8-GAL4/+* (n=137/18) and *Mef2-GAL4/+* (n=139/18). Numbers of n reported as n=a/b where a=segments and b=animals. *p=0.438, ****p<0.0001; Ordinary one-way ANOVA with multiple comparisons.

4.5 DIP-α–Dpr10 binding affinity influences growth and innervation differently

DIP-α and Dpr10 are required in sequential steps of neuromuscular development: synaptic partner matching (Ashley et al., 2019; Venkatasubramanian et al., 2019) and synaptic arbor growth (this study). Similarly, in the fly visual circuit, Dpr10-DIP-α interactions are required for multiple developmental processes: cell survival and synaptic partner matching (Carrillo et al., 2015; Courgeon and Desplan, 2019; Menon et al., 2019; Xu et al., 2019, 2022, 2018a). Interestingly, Xu and colleagues found that cell survival and synaptic connectivity have different binding affinity thresholds with connectivity being more sensitive to affinity reduction than cell survival(Xu et al., 2022). We reasoned that neuromuscular circuit connectivity and NMJ growth may also differ in their sensitivity to Dpr10–DIP-α binding affinity.

We examined the affinity mutants generated by Xu and colleagues (Xu et al., 2022) and unlike in the pupal eye, the larval NMJ has a threshold; when binding affinity falls above that threshold the NMJ is indistinguishable from controls, but below the threshold, NMJs exhibit increased Is boutons on m12 (Figure 4.4A-E; Figure 4.5A-E).

To determine whether this insensitivity to binding affinity was due to a difference in the nature underlying synaptic growth or if the binding affinity of Dprs and DIPs generally acts as a threshold at the NMJ, we examined m4-Is innervation in affinity mutants. Like in pupal eye innervation, m4-Is innervation scaled with DIP-α and Dpr10 binding affinity (Figure 4.4F-H, Figure 4.5F-H): when affinity was increased, m4-Is innervation frequency was increased and as DIP-α and Dpr10 binding affinity was lowered, innervation decreased. Therefore, innervation in pupa and larvae can be tuned by binding affinity, whereas synaptic growth in larvae exhibits a threshold. In other words, at the larval NMJ, innervation but not growth scales with Dpr-DIP binding affinity.

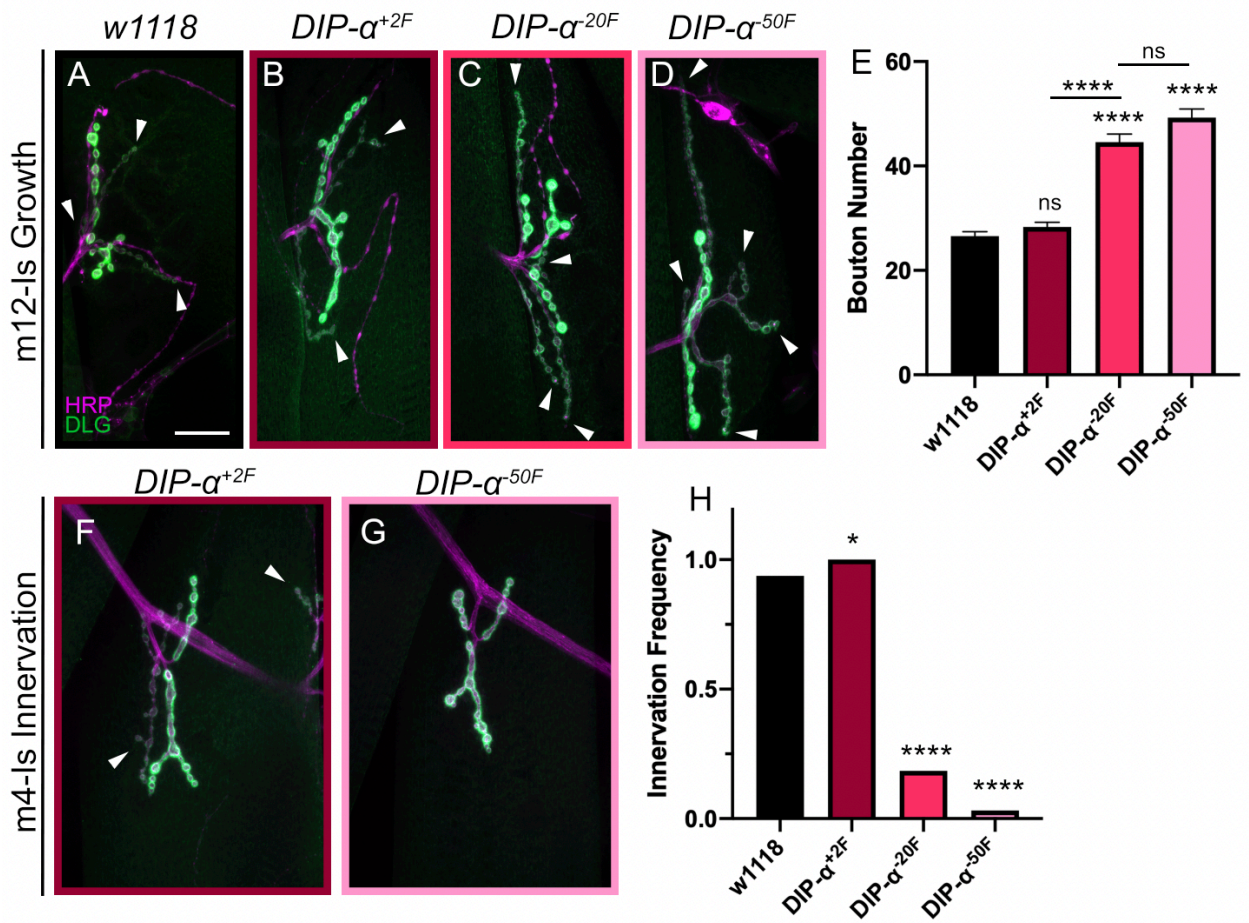

Figure 4.4 DIP-α–Dpr10 binding affinity influences growth and innervation differently
(A-E) m12-Is growth phenotypes of *DIP-α* affinity alleles, neuronal tissue in magenta (HRP) and postsynaptic staining in green (DLG). Is arbors marked with arrowheads, scale bar 50 µm. (A) Typical arbor seen on m12 in *w1118* control animals (n=115/16). (B) *DIP-α*$^{+2F}$ m12-Is arbors are indistinguishable from controls (n=105/17). (C) *DIP-α*$^{-20F}$ m12-Is arbors contain significantly more boutons than controls (n=71/11). (D) *DIP-α*$^{-50F}$ m12-Is arbors contain significantly more boutons than controls (n=78/13). (E) Quantification of A-D. (F-G) m4-Is innervation examples exhibited by *DIP-α* affinity alleles. (F) m4-Is innervation frequency is increased in *DIP-α*$^{+2F}$ (n=113/17). (G) m4-Is innervation frequency is increased in *DIP-α*$^{-50F}$ (n=94/14). (H) Quantification of m4-Is frequency in F-G, in addition to *w1118* (n=127/16) and *DIP-α*$^{-20F}$ (n=73/11). Numbers of n reported as n=a/b where a=segments and b=animals. (A-E) ****p<0.0001; Ordinary one-way ANOVA with multiple comparisons. (F-H) *p=0.0114, ****p<0.0001; Fisher's exact test.

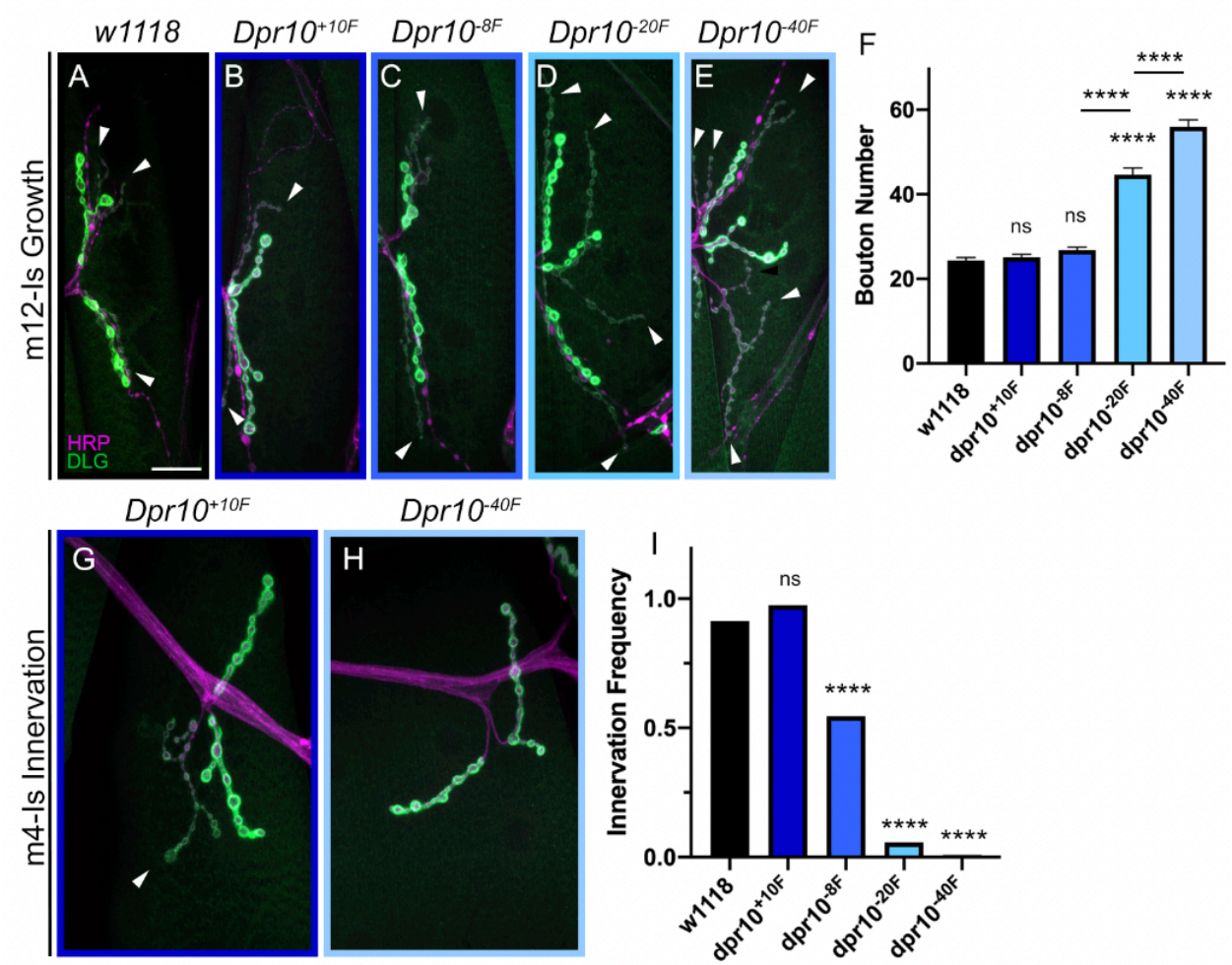

Figure 4.5 Dpr10–DIP-α binding affinity influences growth and innervation differently. (A-E) m12-Is growth phenotypes of *dpr10* affinity alleles, neuronal tissue in magenta (HRP) and postsynaptic staining in green (DLG). Is arbors marked with arrowheads, scale bar 50 μm. (A) Typical arbor seen on m12 in *w1118* control animals (n=115/16). (B) *dpr6*$^{-}$*,dpr10*$^{+10F}$ m12-Is arbors are indistinguishable from controls (n=). (C) *dpr6*$^{-}$*,dpr10*$^{-8F}$ m12-Is arbors contain significantly more boutons than controls (n=104/15). (D) *dpr6*$^{-}$*,dpr10*$^{-20F}$ m12-Is arbors contain significantly more boutons than controls (n=119/16). (E) *dpr6*$^{-}$*,dpr10*$^{-40F}$ m12-Is arbors contain significantly more boutons than controls (n=120/16). (F) Quantification of A-E. (F-G) m4-Is innervation examples exhibited by *dpr10* affinity alleles. (F) m4-Is innervation frequency is increased in *dpr6*$^{-}$*,dpr10*$^{+10F}$ (n=112/16). (G) m4-Is innervation frequency is increased in *dpr6*$^{-}$*,dpr10*$^{-40F}$ (n=123/16). (H) Quantification of m4-Is frequency in G-H, in addition to *w1118* (n=127/16), *dpr6*$^{-}$*,dpr10*$^{-8F}$ (n=110/15), and *dpr6*$^{-}$*,dpr10*$^{-20F}$ (n=121/16). Numbers of n reported as n=a/b where a=segments and b=animals. (A-F) ****p<0.0001; Ordinary one-way ANOVA with multiple comparisons. (G-I) ****p<0.0001; Fisher's exact test.

4.6 Dpr10 is required for normal active zone number

Loss of both *dpr10* and *DIP-α* led to larger Is NMJs on m12. When NMJs are structurally altered, homeostasis can lead to compensation so that the overall strength of the synapse is maintained. One way to examine compensation is through the central active zone protein, Bruchpilot (BRP), whose number is tightly regulated and responsive to perturbations (Goel et al., 2019; Wang et al., 2021). To determine if BRP is altered in response to overgrowth in *DIP-α* and *dpr10* mutants, we examined BRP staining at m12-Is NMJs. Compared to controls, *DIP-α* mutants exhibited no difference in the number of puncta per bouton or BRP puncta size (Figure 4.6A-B, D-E). Surprisingly, *dpr10* mutants had fewer puncta per bouton and a concomitant increase in BRP puncta size relative to controls (Figure 4.6A, C-E). However, *dpr10* is expressed both pre- and postsynaptically (Wang et al., 2022), and so this function could be coming from the presynaptic pool of Dpr10 or through DIP-α independent retrograde signaling from the muscle pool of Dpr10. Taken together, *dpr10* but not *DIP-α* is required for BRP localization.

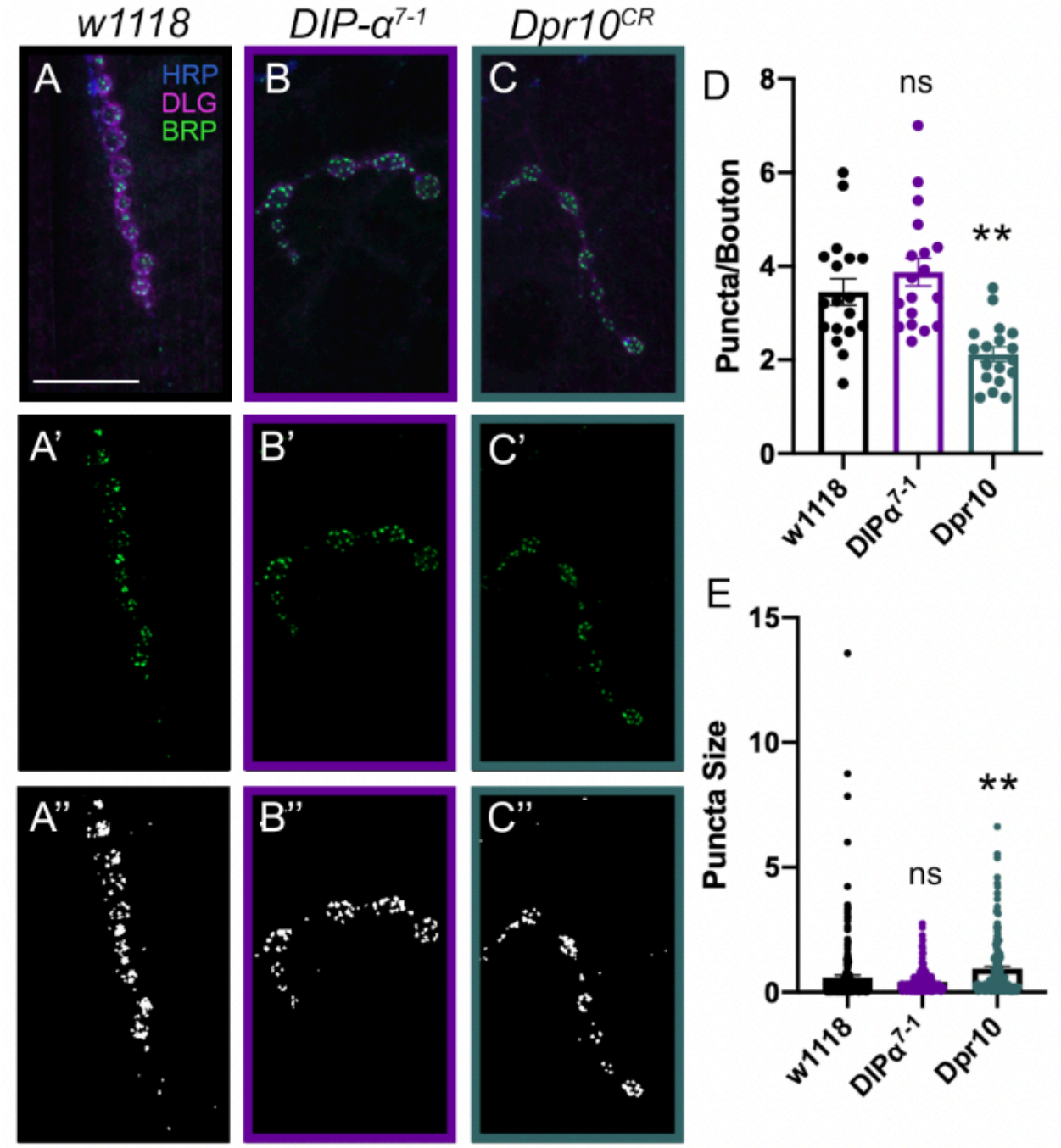

Figure 4.6 Dpr10 is required for normal active zone number.
(A-C) m12-Is arbors with neuronal membrane in blue (HRP), postsynaptic membrane in magenta (DLG), and active zones in green (BRP), scale bar 50 µm. (A'-C') BRP channel of A-C. (A''-C'') Thresholded representations of A'-C'. (D-E) Quantification of genotypes shown in A-C. (D)**p=0.0013, (E)**p=0.0044; One-way ANOVA with multiple comparisons.

4.7 *draper* genetically interacts with *DIP-α* and *dpr10* to regulate synaptic growth

Because Dprs and DIPs are GPI-anchored they cannot transduce information directly into the cell (Lobb-Rabe et al., 2023). In addition, the only mechanism for Dpr-DIP function is in NMJ presynaptic terminal development, where Dpr11 and DIP-γ interact with the BMP pathway (Carrillo et al., 2015). No signaling pathways have been identified for how Dprs and DIPs mediate their multifaceted functions. Using transheterozygous analyses, we sought to identify candidate co-receptors that interact with Dpr10 and DIP-α to inhibit synaptic arbor growth. We examined transmembrane proteins that have known roles in synaptic arbor growth.

Draper is the Drosophila homologue of MEGf10, a single pass transmembrane protein that signals for engulfment of cells through phagocytosis and apoptosis. At the larval NMJ, *draper* mutants exhibit decreased bouton numbers but increased synaptic debris, demonstrating that Draper functions in synaptic growth (Fuentes-Medel et al., 2009).

We examined transheterozygotes of *DIP-α* and *dpr10* in combination with *draper*; each individual heterozygote showed no phenotype, but in *draper/+, dpr10/+* and *DIP-α/+ ;; draper/+* larvae m12-Is NMJ growth was significantly higher (Figure 4.7A-D). These data suggest that *DIP-α, dpr10*, and *draper* are in the same genetic pathway that controls synaptic arbor growth.

Next, we examined known downstream components of Draper signaling. Draper binds CED-6, an adaptor protein involved in signal transduction. If DIP-α and Dpr10 signal through the canonical Draper pathway, then we predict that transheterozygotes with *CED-6* should also display overgrowth of the m12-Is NMJ. Indeed, transheteozygotes of *DIP-α* and *dpr10* with two different *CED-6* alleles resulted in overgrowth suggesting that DIP-α and Dpr10 interact with Draper/CED-6 for m12-Is NMJ growth (Figure 4.7E-H).

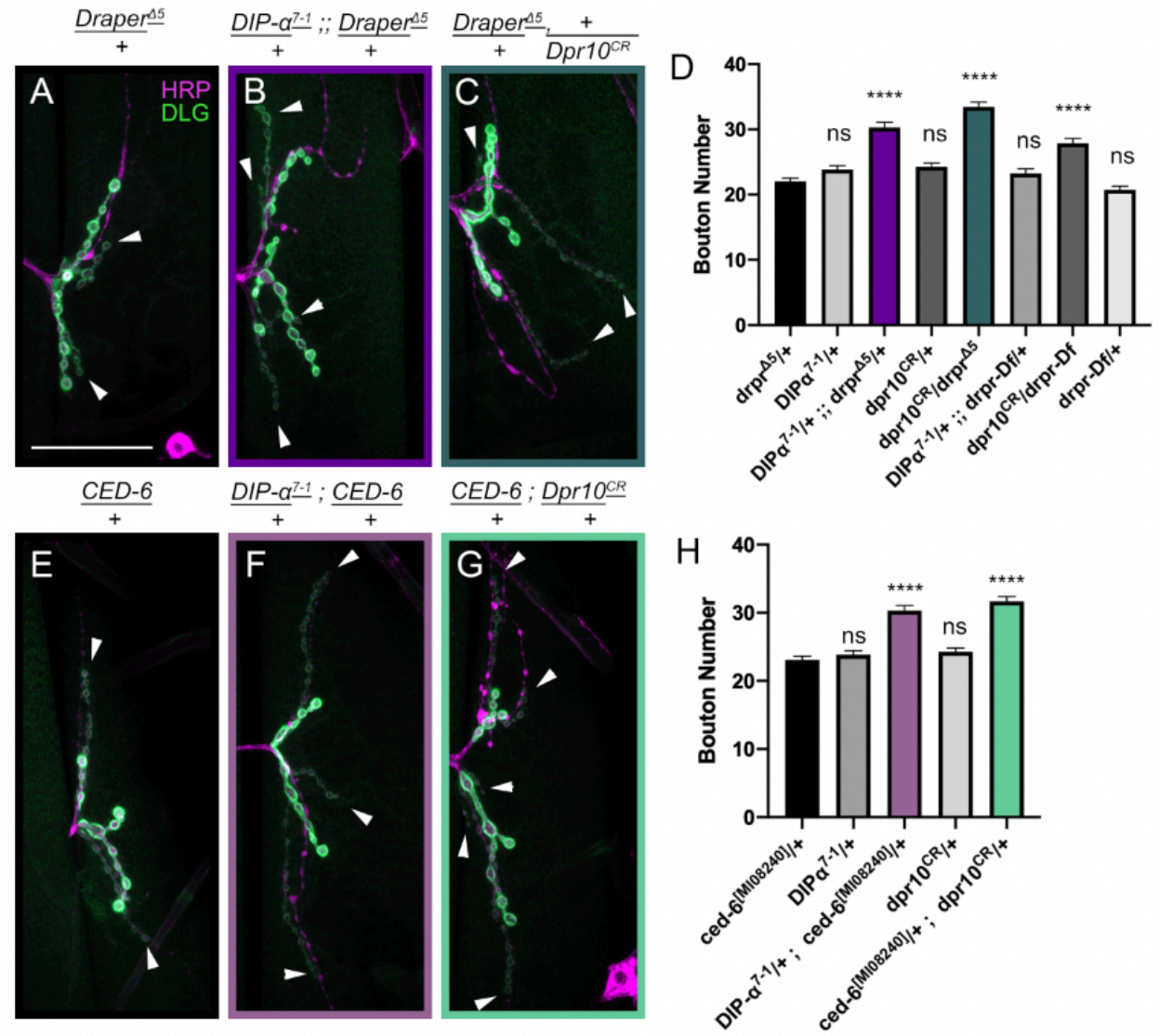

Figure 4.7 *Draper* genetically interacts with *DIP-α* and *dpr10* to regulate synaptic growth. (A-C) Larval m12 NMJ with neuronal tissue in magenta (HRP) and postsynaptic staining in green (DLG), Is arbors marked with arrowheads. Scale bar 50 µm. (A) Typical arbor seen on m12 in *draper* $^{\Delta 5}$/+ animals (n=132/17). (B) *DIP-α* $^{7-1}$/+ *;; draper* $^{\Delta 5}$/+ transheterozygous animals exhibit increased m12-Is arbor size (n=114/16). (C) *draper* $^{\Delta 5}$*/dpr10* ^{CR} transheterozygous animals exhibit increased m12-Is arbor size (n=119/17). (D) Quantification of A-C in addition to *DIP-α* $^{7-1}$/+ (n=139/18), *dpr10* ^{CR}/+ (n=131/18), *DIP-α* $^{7-1}$/+ *;; draper-Df*/+ (n=137/18), *dpr10* ^{CR}*/draper-Df* (n=135/18), and *draper-Df*/+ (n=121/16). (E) Typical arbor seen on m12 in *CED-6*/+ animals (n=135/8). (F) *DIP-α* $^{7-1}$/+ *; CED-6*/+ transheterozygous animals exhibit increased m12-Is arbor size (n=114/15). (G) *CED-6*/+ *; dpr10* ^{CR}/+ transheterozygous animals exhibit increased m12-Is arbor size (n=126/17). (H) Quantification of E-G in addition to *DIP-α* $^{7-1}$/+ (n=139/18) and *dpr10* ^{CR}/+ (n=131/18). Numbers of n reported as n=a/b where a=segments and b=animals. ****p<0.0001; Ordinary one-way ANOVA with multiple comparisons.

4.8 *LAR* genetically interacts with *DIP-α* and *dpr10* to inhibit synaptic growth

In addition to Draper, we examined Leukocyte-antigen-related-like (LAR), a single pass transmembrane protein tyrosine phosphatase which has been implicated in a multitude of biological processes, including motor axon guidance, embryogenesis, and cell migration. At the larval NMJ, *LAR* mutants exhibit decreased synaptic growth (Johnson et al., 2006). To determine if *LAR* functions in the same genetic pathway as *DIP-α* and *dpr10*, we performed transheterozygous analysis examining vCE growth on m12. We observed increased bouton number of vCE on m12 in transheterozygotes of both *DIP-α* and *dpr10* in combination with *LAR* compared to single heterozygotes (Figure 4.8A-D). We confirmed that *LAR* genetically interacts with *DIP-α* and *dpr10* with a deficiency panning the *LAR* locus (*Lar-Df*).

At the NMJ, Lar is activated by the membrane protein Syndecan (Sdc) and inhibited by the ligand Dallylike protein (Dlp) (Johnson et al., 2006). However, we are interested in the downstream mechanisms of Dpr10 and DIP-α and therefore focused on potential intracellular messengers. We examined Liprin-α and Ena, but none showed an interaction with either *dpr10* or *DIP-α* suggesting that signaling must occur through different downstream messengers (Supplementary Figure 4.1). In summary, *dpr10* and *DIP-α* genetically interact with *LAR* to instruct synaptic arbor size at m12-Is.

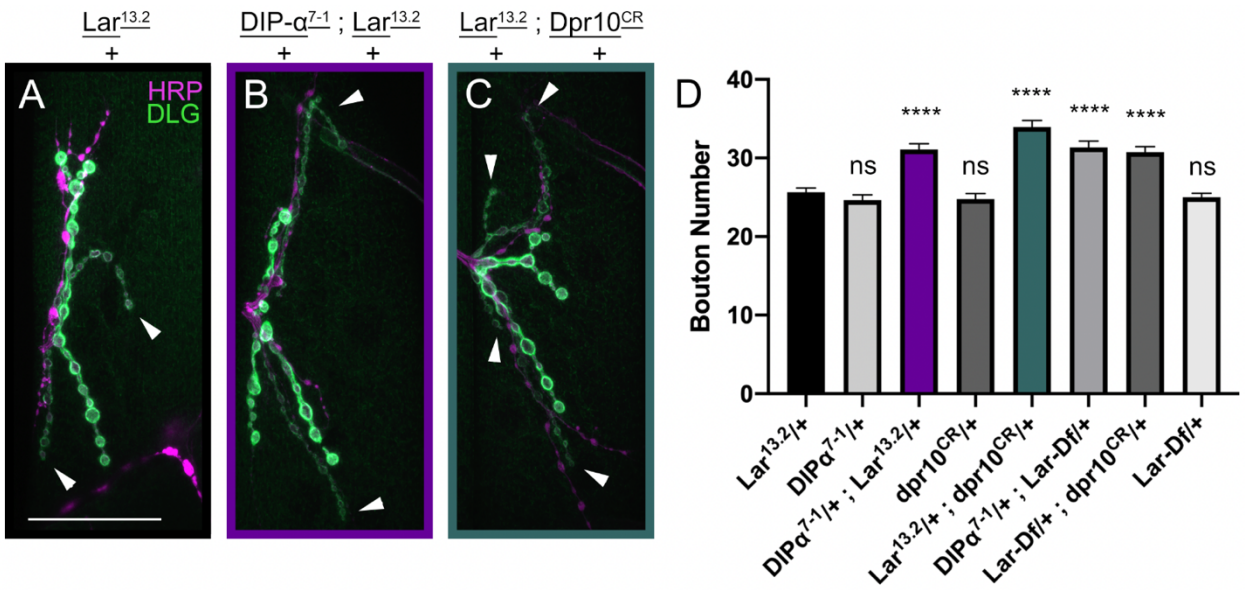

Figure 4.8 *LAR* genetically interacts with *DIP-α* and *dpr10* to inhibit synaptic growth.
A-C) Larval m12 NMJ with neuronal tissue in magenta (HRP) and postsynaptic staining in green (DLG), Is arbors marked with arrowheads. Scale bar 50 µm. (A) Typical arbor seen on m12 in $Lar^{13.2}$/+ animals (n=129/17). (B) $DIP\text{-}\alpha^{7\text{-}1}$/+ *;* $Lar^{13.2}$/+ transheterozygous animals exhibit increased m12-Is arbor size (n=117/16). (C) $Lar^{13.2}$/+ ; $dpr10^{CR}$/+ transheterozygous animals exhibit increased m12-Is arbor size (n=125/16). (D) Quantification of A-C in addition to $DIP\text{-}\alpha^{7\text{-}1}$/+ (n=139/18), $dpr10^{CR}$/+ (n=131/18), $DIP\text{-}\alpha^{7\text{-}1}$/+ *;* *Lar-Df*/+ (n=123/16), *Lar-Df*/+ ; $dpr10^{CR}$/+ (n=130/17), and *Lar-Df*/+ (n=139/18). Numbers of n reported as n=a/b where a=segments and b=animals. ****p<0.0001; Ordinary one-way ANOVA with multiple comparisons.

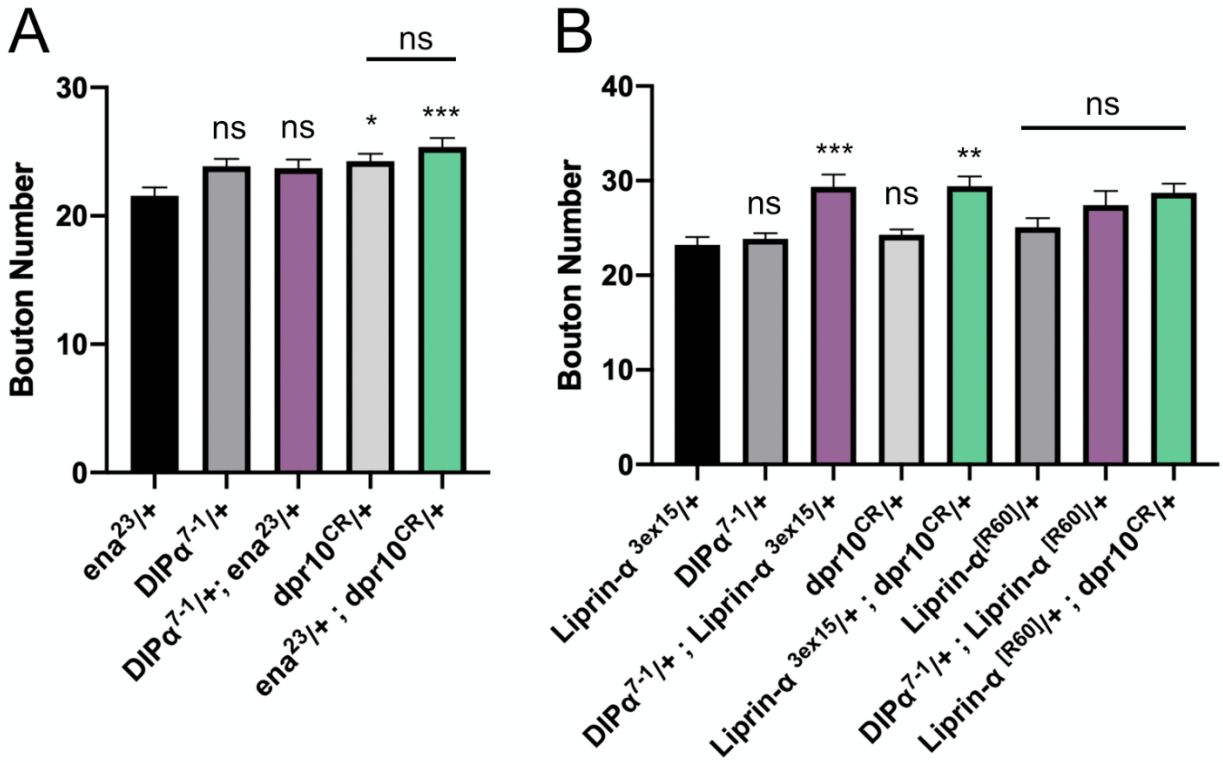

Figure S4.1 Neither Ena nor Liprin-α interact with Dpr10 and DIP-α.
(A) Transheterozygous analysis of *ena* with *DIP-α* and *dpr10*. *p=0.0165; ***p=0.0002; Ordinary one-way ANOVA with multiple comparisons.
(B) Transheterozygous analysis of *Liprin-α* with *DIP-α* and *dpr10*. Although the 3ex15 allele shows mild interaction, the R60 allele shows no interaction and so this was ruled out as an interactor. ***p=0.0010; **p=0.0019; Ordinary one-way ANOVA with multiple comparisons.

4.9 Discussion

Here, we demonstrate a novel role for two members of the Dprs and DIPs, Dpr10 and DIP-α, in suppression of NMJ arbor growth. Unlike their role in innervation, Dpr10- DIP-α function in growth does not scale with their binding affinity. Rather, there is a threshold above which the NMJ exhibits no growth phenotype and below which increased bouton numbers are observed for m12-Is. Moreover, *dpr10* mutants but not *DIP-α* mutants exhibit fewer and larger BRP puncta, suggesting impairment of the presynaptic active zones. Lastly, using genetic interactions we demonstrate that Dpr10 and DIP-α function in the same pathway as Draper and LAR to specify synaptic growth. Future research will focus on whether this interaction is direct and what regulates binding of Dpr10/DIP-α and potential co-receptors.

4.9.1 Dprs and DIPs are reused for sequential steps of neural circuit assembly

Dprs and DIPs have almost exclusively been examined in the context of developing neural circuits and are best known for instructing matching between neurons and correct postsynaptic targets. Combined with previous studies implicating Dpr10 in axon pathfinding (Barish et al., 2018; Lobb-Rabe et al., 2022), Dpr10 is utilized for three sequential steps of neural circuit assembly: axon pathfinding, synaptic partner matching, and synaptic growth. The Dpr10 interactor, DIP-α, is required for both synaptic partner matching and synaptic growth. Reusing the same molecules for different steps in development is an efficient way for the cell to regulate these steps, especially given the specificity of gene expression patterns of each cell found in the peripheral nervous system of *Drosophila* larvae (Wang et al., 2022).

Utilizing the same proteins for sequential steps in neural development has been observed for several key genes. In mammals, 14-3-3 proteins are reused in sequential steps of brain

development – neurogenesis, neuron migration, and synaptogenesis (Cornell and Toyo-oka, 2017). In *Drosophila*, Teneurins influence axon guidance, synaptic partner matching, and synaptogenesis (DePew et al., 2019; Hong et al., 2012; Mosca et al., 2012; Young and Leamey, 2009; Zheng et al., 2011). For all of these examples, what causes the switch from one function to another (e.g. axon guidance to synaptic partner matching) is not well understood. A future interesting avenue of research will be to understand what drives the switch for Dprs and DIPs to function in different developmental processes. In other words, which molecules are the CSPs interacting with and do these interactions dictate their function?

4.9.2 Dprs and DIPs require co-receptors

Although Dprs and DIPs have been implicated in several aspects of neural development, how they achieve this mechanistically has largely remained elusive. Moreover, they are GPI-anchored—tethered to the outside of the cell membrane by a lipid anchor that is covalently attached to the protein after translation (Lobb-Rabe et al., 2023). Therefore, if any signaling occurs, it must be through a co-receptor containing a transmembrane and intracellular domains.

The IgLONs, the vertebrate orthologs of Dprs and DIPs, are also GPI-anchored and similarly function in neural development, including neurite arbor outgrowth and neuronal arborization (Akeel et al., 2011; Pischedda and Piccoli, 2016; Reed et al., 2004; Sanz et al., 2015). The IgLONs have a known receptor, which mediates their function: FGFR2, an FGF pathway receptor, binds one of the four IgLONs, Negr1, and mediates its role in neuronal arborization (Pischedda and Piccoli, 2016). In the future, it should be examined if Dprs and DIPs also interact with the FGF pathway and if the IgLONs interact with the vertebrate orthologs of Draper and LAR.

4.9.3 CSPs are integrating different pathways with similar functions

Most important developmental processes are regulated by several signaling pathways; this redundancy allows for the developmental process to occur, even if one or two genes are mutated. Redundancy can be found in the vertebrate retina, where members of the cadherin (Cdh) family promote specific connectivity of neurons that synapse onto ON-OFF direction-selective retinal ganglion cells (ooDSGCs) (Duan et al., 2018). Connectivity is only disrupted in triple mutants of *Cdh6-9-10*, and not in single or double mutants, demonstrating that when one or two of these proteins are lost, the third can compensate (Duan et al., 2018). Redundancy exists outside of a single protein family as well, with multiple molecular pathways shaping crucial steps in neural development. Such an example can be found in the *Drosophila* ventral nerve cord, where multiple molecular pathways regulate axonal midline crossing, including Robo-Slit, Semaphorins and Plex, and Hedgehog and its receptor Ptc (Howard et al., 2019; Kidd et al., 1998; Ricolo et al., 2015; Simpson et al., 2000; Zlatic et al., 2009).

Here we demonstrate that members of the *dpr* and *DIP* families genetically interact with two receptors, *draper* and *LAR*, which regulate distinct signaling pathways. These pathways have not previously been linked. However, previous work has linked Dpr11 and DIP-γ with the BMP pathway in synaptic maturation at the NMJ (Carrillo et al., 2015). One attractive hypothesis for how Dprs and DIPs can have such varied functions in different cell types and developmental stages is integration with known transmembrane proteins of varying developmental functions. Future work will focus on how these interactions are regulated and if Dprs and DIPs interact with additional signaling pathways.

4.10 Methods

4.10.1 *Drosophila* husbandry, reagents, and dissections

All flies were kept at 25°C. Crosses were set at a medium density and flipped daily. Dissections were performed as previously described (Cheng et al., 2019a). Briefly, crawling third instar larvae were dissected on Sylgard dishes in phosphate buffered saline (PBS) and then fixed in 4% paraformaldehyde for 30 minutes. Samples were then washed in PBS before being transferred to block in a 0.5ml Eppendorf with 5% Normal goat serum in PBST (PBS + 0.05% Triton X100). Samples were incubated in primary antibodies diluted in block and agitated on a nutator at 4C overnight. Samples were then extensively washed in PBST, incubated in secondary antibodies, and covered on a nutator at room temperature for 2 hours. Samples were again washed and then mounted on a microscope slide in Vectashield (Vector Laboratories).

4.10.2 Imaging Protocol

Quantification of synaptic arbor growth was performed with a Zeiss AxioImager M2 and a 63x plan-neofluar 1.3NA objective. Is MN arbors were distinguished using DLG and HRP stains; Is boutons are smaller than Ib boutons and have less elaborate DLG staining (Guan et al., 1996), while Type II and Type IIIs have no DLG staining. We define Type I boutons as swellings of the axon terminal that are surrounded by DLG.

Images for BRP quantification were captured using a Zeiss LSM800 confocal microscope with a 63X plan-apo 1.4NA objective. Images were thresholded in ImageJ and particles (BRP puncta) were counted. All samples to be compared were pooled after fixation and thus received the same staining and imaging parameters.

All images were captured on a Zeiss LSM800 confocal microscope with either a 40X

plan-neofluar 1.3NA objective or 63X plan-apo 1.4NA objective.

4.10.3 Analysis

Statistical analysis was performed using GraphPad (Prism). All experiments were performed in biological triplicates. Data were collected from body wall segments A2-A5. P-values were calculated using Chi Squared Test or ANOVA. All images were prepared using ImageJ Fiji (Schindelin et al., 2012).

Genotype	Description	Source
W1118	Control	BDSC
DIP-α$^{7-1}$	*DIP-α* mutant	(Venkatasubramanian et al., 2019)
DIP-α-QF	*DIP-α* mutant	(Venkatasubramanian et al., 2019)
DIP-α-Df	*DIP-α* deficiency	BDSC 27886
dpr10^{CR}	*dpr10* mutant	Xu et al., 2018
dpr10-GAL4	*dpr10* mutant with GAL4 driver	Lee et al., 2018
A8-GAL4	Is neuron GAL4 driver	(Venkatasubramanian et al., 2019; Wang et al., 2021)
Mef2-GAL4	Muscle GAL4 driver	(Ranganayakulu et al., 1998)
UAS-dpr10-RNAi	*dpr10* RNAi under UAS	
DIP-α^{+2F}	DIP-α with 2-fold stronger binding to Dpr10	(Xu et al., 2022)
DIP-α^{-20F}	DIP-α with 20-fold weaker binding to Dpr10	(Xu et al., 2022)
DIP-α^{-50F}	DIP-α with 50-fold weaker binding to Dpr10	(Xu et al., 2022)
Dpr6^{-},dpr10^{+10F}	Dpr10 with 10-fold stronger binding to DIP-α, Dpr6 mutant	(Xu et al., 2022)
Dpr6^{-},dpr10^{-8F}	Dpr10 with 10-fold stronger binding to DIP-α, Dpr6 mutant	(Xu et al., 2022)
Dpr6^{-},dpr10^{-20F}	Dpr10 with 20-fold weaker binding to DIP-α, Dpr6 mutant	(Xu et al., 2022)
Dpr6^{-},dpr10^{-40F}	Dpr10 with 40-fold weaker binding to DIP-α, Dpr6 mutant	(Xu et al., 2022)
Drpr^{Δ5}	*Draper* mutant	BDSC 67033
Drpr-Df	*Draper* deficiency	BDSC 9292
CED-6$^{[MI08240]}$	*CED-6* mutant	BDSC 44761
Lar$^{13.2}$	*Lar* mutant	BDSC 8774
Lar-Df	*Lar* deficiency	BDSC 8679
ena^{23}	*ena* mutant	BDSC 25405
Liprin-α^{3ex15}	*Liprin-α* mutant	BDSC 8563
Liprin-α$^{[R60]}$	*Liprin-α* mutant	BDSC 8561

Table 3.1 The fly lines used for this study.

Antibody	Concentration	Source
Mouse anti-BRP	1 : 50	DSHB NC82
Rabbit anti-DLG	1 : 40,000	Guan et al., 1996
Goat anti-Mouse 488	1 : 500	Invitrogen A11029
Goat anti-Rabbit 488	1 : 500	Invitrogen A11008
Goat anti-Rabbit 568	1 : 500	Invitrogen A11036
Goat anti-HRP TRITC (568)	1 : 100	Jackson ImmunoResearch 123–025-021
Goat anti-HRP 647	1 : 100	Jackson ImmunoResearch 123-605-021

Table 3.2 The antibodies used for this study.

CHAPTER 5

DISCUSSION AND FUTURE DIRECTIONS

5.1 Summary

In this thesis, I demonstrated that most, if not all, Dprs and DIPs are GPI anchored. This post-translational modification has implications for their trafficking, localization, and downstream signaling. I also found that Dpr10 is involved in motor axon pathfinding. Immunoprecipitation and mass spectrometry identified Nocte, a large, unstructured protein as a Dpr10 interactor, and Nocte is also required for axon guidance. Finally, Dpr10 and DIP-α inhibit NMJ growth and genetically interact with Lar and Draper to influence synaptic arbor growth.

5.2 Dprs and DIPs function in neural circuit assembly

Dprs and DIPs have been implicated in neuronal survival, axon pathfinding, synaptic partner matching, and synaptic growth in several fly neural circuits. Although our understanding of Dpr/DIP function has expanded greatly since discovery of the Dpr-DIP interactome (Özkan et al., 2013), fundamental knowledge gaps remain. Here, I will examine general modes that have emerged in the near decade since the interactome discovery and some of the questions that remain unanswered.

5.2.1 Expression patterns of Dprs and DIPs

Dprs and DIPs are expressed throughout the *Drosophila* nervous system (Brovero et al., 2021; Carrillo et al., 2015; Cosmanescu et al., 2018; Kurmangaliyev et al., 2020; Tan et al., 2015; Wang et al., 2022). These expression patterns were elucidated through direct GAL4 reporters or by RNA-seq of whole tissues and animals. In all datasets, DIPs have a more specific and restricted expression pattern compared to expression patterns of Dprs.

In some of the expression studies, the temporal expression of Dprs and DIPs was also evaluated. For example, in the larval motor and sensory circuits, most family members are expressed from embryo through larval development (Wang et al., 2022). This is perhaps no surprise given the role of Dprs and DIPs in different steps of nervous system development. In contrast, in a single-cell RNA-seq experiment examining pupal brains at different stages, some Dpr/DIP expression is highly variable across time points and cell types (Kurmangaliyev et al., 2020). For example, Dpr17 expression in Tm1 neurons in the optic lobe spikes at 48hrs before falling sharply, while expression in C3 neurons increases slowly and is relatively stable for the latter part of pupal development. Given these different expression profiles (maintained vs restricted), an appealing is that the expression patterns correspond to the utility of the protein in those cells. In other words, if the protein is expressed for only a 12-hour window, perhaps its only function is synaptic partner matching, whereas if expression extends from embryonic stage to late third instar stage, the protein may be involved in multiple steps. The pupal fly eye has been used extensively to examine Dpr-DIP function, where the primary role that has been characterized is synaptic partner matching and neuronal survival. It will be interesting to examine if additional roles are uncovered in the optic lobe.

Based on their expression patterns, likely complex regulatory networks instruct Dpr/DIP expression. In instances where the Dpr or DIP expression is maintained across developmental stages, this could be achieved by terminal transcription factors, which are required for inducing and maintaining expression of genes necessary for cell function and identity. For the Dprs and DIPs that are temporally expressed, the regulatory mechanisms are likely more elaborate, requiring repressors or down regulation of transcription factors. The only studies, to my knowledge, showing transcriptional regulation of Dprs or DIPs is in pupal visual system, where the transcription factor spineless promotes expression of DIP-γ in yR7 cells (Courgeon and Desplan, 2019; Menon et al., 2019). In addition, the transcription factor dFezf regulates expression of multiple *dprs* (Peng et al., 2018). Additional work elucidating how cell specific expression of Dprs and DIPs is achieved will provide important insights into Dpr-DIP biology.

5.2.2 Dprs and DIPs are utilized in sequential neural developmental steps

As mentioned in the introduction, the same proteins and signaling pathways can be reused for different developmental processes, for instance synaptic partner matching and synaptogenesis as is the case with Ten-a and Ten-m (Mosca et al., 2012).

Another example are Semaphorins and Plexins, which function in axon guidance and synaptic partner matching. In *Drosophila*, there are 5 Semas and 2 Plexins (Rozbesky et al., 2019). In both the CNS and PNS, Sema-Plex are required for proper axon guidance (Winberg et al., 1998; Yu et al., 1998). In the olfactory bulb, Semas function in both axon guidance and target selection (Joo et al., 2013). In adult stages, Semas and Plexes are continuously expressed, and this expression is required for MN survival and normal motility (Chithran et al., 2023). In

summary, Sema-Plex CSPs are required for several steps in *Drosophila* nerves system development.

The work from several labs, including ours, demonstrated that Dprs and DIPs function in sequential steps of neural development. For example, Dpr10 is used for motor axon pathfinding of the ISNb as it travels below m6/m7 over m13 and terminates on m12 (Lobb-Rabe et al., 2022). *dpr10* mutants exhibit innervation defects at these muscles, especially at m13. However, these innervation defects could also be due to errors of axon guidance. At other NMJs, the role of Dpr10 in synaptic partner matching is clear, as the dCE axon requires Dpr10 for specific innervations while still navigating the correct route (Ashley et al., 2019). Later in larval neuromuscular development, Dpr10 restricts synaptic arbor growth, and genetic interaction tests suggest that Dpr10 functions in the same molecular pathway as LAR and Draper. Thus, Dpr10 has roles in different developmental processes.

5.2.3 Structure of Dprs and DIPs informs their function

A central dogma in biology is that the structure equals function. Dprs and DIPs are no exception—at minimum their function is to tether two opposing membranes together. These CSPs are anchored into the outer cell membrane leaflet and extend two or three Ig domains into the extracellular space. Dpr-DIP interactions occur at the first (most distal) Ig domains. One outstanding question is whether other Ig domains bind unknown proteins. Preliminary data from our lab suggest that the D2/D3 Ig domains of DIP-α are required for its function. Ongoing work utilizing proximity ligation and mass spectroscopy will aid in identifying such interactions.

Another open question is whether cleavage plays a role in Dpr/DIP function. The vertebrate orthologs, the IgLONs, are secreted from the cell surface after being cleaved by

ADAM metalloproteases to promote neurite outgrowth of cortical neurons (Sanz et al., 2015). Given the similarities between IgLONs and Dprs/DIPs, it begs the question of whether Dprs and DIPs are sensitive to metalloproteases and whether shedding is a part of their function. With Viola Nawrocka, we examined some candidate metalloproteases but did not observe any cleavage of Dprs and DIPs (data not shown). However, a subset of Dprs and DIPs were identified in a secretome screen as soluble factors in larval hemolymph (Personal Communication, Norbert Perrimon and Justin Bosch). Given the large repertoire of metalloproteases, the possibility still exists that Dprs and DIPs are substrates for cleavage.

Altogether, the structural information available for Dpr/DIP family members is incredibly rich. This, paired with improved prediction tools will allow for the computational assessment of metalloprotease cleavage sites and additional binding interactions. However, as our evaluation of GPI prediction methods shows, any predictions should be experimentally validated.

5.3 Insights from GPI anchor status of Dprs and DIPs

As stated above, we have gained significant information from the structural data available for Dpr-DIP interactions. In this section, I will discuss how my work describing that Dprs and DIPs have GPI anchors influences our understanding of their underlying biology.

5.3.1 GPI-anchored proteins require co-receptors for signaling

Given the multifaceted functions of Dprs and DIPs throughout nervous system development, it is intriguing to posit that they signal into the cell about their binding status. This would explain why, when binding does not occur, the cell often dies. Until we discovered that most if not all Dprs and DIPs have GPI anchors, we believed that this signaling could be direct.

However, now we know that they must interact with other CSPs that contain transmembrane domains to achieve intracellular signaling. My work in Chapter 4 suggests that LAR and Draper may be such receptors, although it is unclear whether this interaction is direct or indirect. Regardless, an exciting model is that different co-receptors interact with specific members of the Dpr/DIP family to instruct their respective functions.

5.3.2 Localization

GPI anchored proteins are thought to localize to lipid microdomains called lipid rafts in the cell membrane. Like other forms of phase separation, there is much debate about the biological relevance of these domains and how stable these compartments are (Levental et al., 2020). I will not delve into the debate here but will move forward with the assumption that GPI anchors alter localization of proteins in the membrane (something we saw in our own experiments at the fly NMJ).

An intriguing question about GPI anchors is why have them at all? The synthesis of the anchor alone requires 13 steps and at least 20 proteins (Kinoshita, 2020). Then, once on the protein, the GPI anchor limits the proteins signaling capabilities. One attractive hypothesis for attaching GPI anchors to proteins is to instruct localization to sub-compartments where functionally relevant proteins, or co-receptors, are clustered. Lipid rafts are thought to increase the local concentration of proteins that prefer lipid microdomains, thereby acting akin to a scaffolding protein.

5.3.3 Missing insights into GPI-anchored protein QC/trafficking/regulation

Although GPI anchor synthesis is well understood (Kinoshita 2020), there are still open questions in our understanding of GPI anchored protein biology. Our discovery that Dprs and DIPs are GPI anchored contributed to the difficulty in working with them biochemically. Here, I will briefly discuss the aspects of GPI anchored protein biology that are currently incomplete.

GPI anchor attachments sites lack a consensus motif, contributing to the difficulty of predicting whether a protein is GPI anchored. Moreover, in some cases, if a GPI attachment site is mutated, a secondary, upstream site can be used. We observed this firsthand when, in collaboration with Ruiling Zhang and Viola Nawrocka, deletion of the putative GPI anchor site still produced a GPI anchored protein (data not shown).

Another striking difference between TM and GPI proteins is the difference in amount of protein that makes it to the cell surface (Lobb-Rabe et al., 2023). We expressed a DIP-α transgene with either a TM domain or a GPI anchor from identical genome insertion sites, and found that larger quantities of the TM DIP-α was present on the cell surface compared to the GPI anchored version. It seems unlikely that this difference is transcriptional in nature and more likely that the difference is due to protein processing and trafficking. Indeed, in yeast, TM and GPI proteins are sorted and exit the ER separately (Lopez et al., 2019; Mayor and Riezman, 2004). Expanding GPI protein trafficking studies in *Drosophila* will help elucidate the mechanisms driving these differences.

Lastly, the C-terminally tagged DIP-α provides puzzling data. A Myc epitope was inserted at the C-terminus of the protein, which should be cleaved upon GPI anchor addition. However, we observed that some of the Myc tag is trafficked to boutons and expressed on the cell surface (Ashley et al., 2019); this is not the case for a similarly tagged DIP-ζ-Myc transgene

suggesting the DIP-α-Myc transgene is eluding quality control (QC) mechanisms and localizes to the cell surface as a pre-processed membrane associated protein.

Although incomplete, we have some insights into the QC of GPI anchored proteins. For instance, the GPI anchored Prion protein (PrP) has been used to study GPI anchored protein QC mechanisms. In HEK293T cells, almost 90% of misfolded Prp made it to the cell surface before being endocytosed and trafficked to the lysosome for degradation (Zavodszky and Hegde, 2019). In addition, yeast cells with GPI anchor lipid remodeling mutantions (e.g. the lipid moiety of the anchor is improperly formed) were targeted for degradation while still in the ER (Sikorska et al., 2016). Although informative, these examples deal with actual structural defects of the GPI anchor or attached proteins. In the case of DIP-α-Myc, it appears that the protein is functional and folded correctly, but C-terminal cleavage did not occur suggesting the GPI anchor was not attached. These data suggest that there may be a leakiness for DIP-α that allows some protein to exit the ER and Golgi without being fully processed.

With our characterization of 33 GPI anchored proteins coupled with the highly tractable model system that is *Drosophila*, this provides an power system to study aspects of GPI protein processing and trafficking in an animal model.

5.4 Conclusion

Here, I presented my thesis research to better understand how cells utilize cell surface proteins to assemble complex, stereotyped, functional neural circuits. I demonstrated that Dprs and DIPs are reused for sequential steps in nervous system development: motor axon pathfinding, synaptic partner recognition, and NMJ elaboration. Finally, in a collaboration with the Özkan lab, I revealed that Dprs/DIPs are GPI anchored, which changes the way we approach

their signaling capabilities, and more importantly, provides a model to study open questions in GPI anchored protein biology.

CHAPTER 6: APPENDICES

6.1 APPENDIX A
CHARACTERIZING DIP-α-GAL4

I want to start by thanking Violet Sorrentino who started the DIP-α growth project before I even rotated in the Carrillo lab. Her initial work on this project was invaluable, and I am thankful to have worked with her. When I started the DIP-α project, we and others were using a *DIP-α-GAL4* line. This GAL4 was generated by randomly inserting mobile genetic elements into the *Drosophila* genome and then determining where they were inserted. These cassettes are called Minos-mediated integration cassettes (MiMICs) and are inserted at random to provide tools to the *Drosophila* community (Nagarkar-Jaiswal et al., 2015; Venken et al., 2011). These cassettes can then be transformed to GAL4 drivers with translational stops using recombinant mediated cassette exchange—functionally generating gene traps (Lee et al., 2018).

The *DIP-α-GAL4* line was supposed to be a conversion of the MiMIC insertion line MI02031, which would place the translational stop just downstream of the signal peptide, thereby generating a *DIP-α* null allele. In addition to the m4-Is innervation defect observed in *DIP-α* nulls, this GAL4 allele also showed pronounced undergrowth of Is arbors in a dosage dependent manner (Figure A1). This phenotype was extremely severe, yielding only a few boutons in homozygous animals.

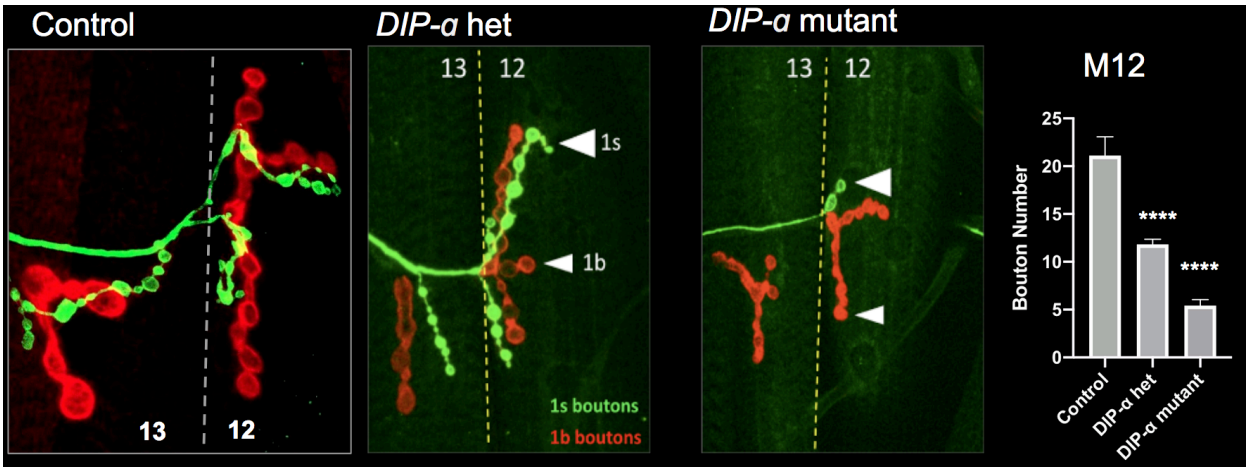

Figure A1: Quantification of Is boutons on m12 and m13 in controls versus DIP-α-GAL4 heterozygous and homozygous animals. First three panels show confocal images of control and DIP-α-GAL4 animals. Last panel quantifies the bouton number on m12 for these genotypes.

However, when compared with other *DIP-α* alleles, this undergrowth was not observed and in fact, other *DIP-α* mutants exhibited significant overgrowth of Is arbors (see Chapter 4). I set out to determine why this *DIP-α-GAL4* allele produced this severe undergrowth phenotype. Using PCR, I determined that the insertion was not MI02031 as previously thought. Next, I checked all possible insertions sites and found that the GAL4 cassette was actually at MI1680, placing it precisely between the second and third Ig domains of DIP-α. Thus, rather than a clean null allele this allele likely generated a secreted fragment of DIP-α consisting of the first two Ig domains. However, staining with a DIP-α antibody showed no clear signal in larval VNCs (the caveat here being that it's not clear where exactly the antibody binds DIP-α) (Figure A2).

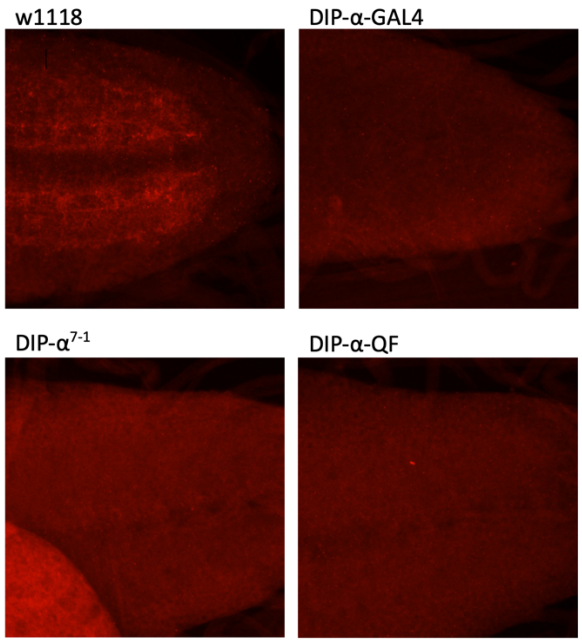

Figure A2: Larval VNC staining of DIP-α antibody.
Example images of VNC stained with the DIP-α antibody. Top left panel shows w1118 controls with visible dendrites. Other three panels depict DIP-α alleles, all of which lack dendritic staining in the VNC.

I next set out to determine if (1) truncating the protein after the first two Ig domains resulted in a secreted protein and if (2) secreting that peptide in vivo showed the same undergrowth observed in the *DIP-α-GAL4* allele. I generated UAS constructs with truncated DIP-α fragments containing, one, two, or three Ig domains. When expressing them in S2 cells and saving the supernatant, I determined that these are indeed secreted into the supernatant (Figure A3).

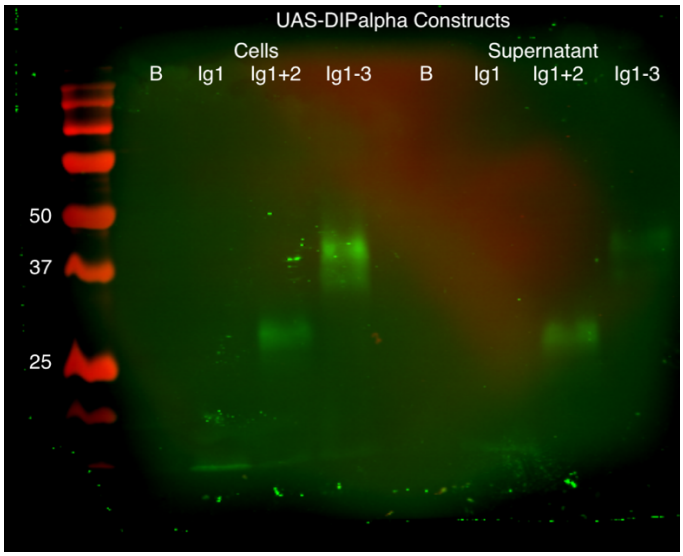

Figure A3: Western gel of UAS-DIP-α constructs expressed in S2 cells.
Both cell lysate (left lanes) and supernatant (right lanes) were examined.

Using the Is specific GAL4 driver *A8-GAL4*, I expressed these constructs in larvae. Surprisingly, I did not observe the undergrowth phenotype seen in the *DIP-α-GAL4* line and in some cases observed significantly more boutons than in controls. Due to time constraints and lack of results, I stopped working on this project.

6.1 APPENDIX B

IN VIVO EVIDENCE FOR C-TERMINAL RETENTION OF WOULD-BE GPI-ANCHORED DIP-α

Glycosylphosphatidylinositol (GPI) anchored proteins are cell surface proteins that have been implicated in many important biological processes and are attached to the membrane through a lipid anchor. As the anchor is covalently attached to the protein, the C-terminus is cleaved. Recently, the Dprs and DIPs, a family of CSPs involved in neural development in *Drosophila*, were demonstrated to be GPI anchored. Here, we demonstrate that a subpopulation of tagged DIP-α retains its C-terminus in vivo suggesting that it is incompletely processed and that a subpopulation of DIP-α is trafficked to the surface of the axon terminal with its C-terminus intact.

GPI anchored proteins are cell surface proteins (CSPs) that are tethered to the outer leaflet of the cell membrane through a sugar-lipid moiety that is covalently linked to the ω site, a small residue toward the C-terminus of the amino acid chain (Kinoshita, 2020). GPI anchor synthesis and addition are complex pathways that require multiple sequential steps carried out inside the endoplasmic reticulum (ER) and Golgi (Kinoshita, 2020; Kinoshita and Fujita, 2016). The GPI anchor is synthesized through a series of chemical reactions; separately, the protein to be anchored is synthesized and imported into the ER (Kinoshita, 2020; Kinoshita and Fujita, 2016). Once partially inserted into the ER membrane through the stretch of hydrophobic amino acids at its C-terminus, the protein is then tethered to the ER lumen membrane until it encounters GPI transamidase, which attaches the GPI anchor to the protein (Kinoshita, 2020; Kinoshita and Fujita, 2016). As the GPI anchor is covalently attached, the amino acids downstream of the C-terminus are cleaved and released from the now GPI-anchored protein. Thus, correctly processed GPI anchors should lose their C-terminus. Canonically, it is thought that GPI anchors are signals

for proteins to begin export from the ER and begin their journey through the secretory pathway. Misfolded GPI anchored proteins have previously been demonstrated to trafficked to the plasma membrane before undergoing endocytosis and degradation (Zavodszky and Hegde, 2019). Moreover, a point mutation in a yeast protein that prevented the GPI-anchor addition resulted in a type 1 transmembrane protein (Sikorska et al., 2016). Additionally, in mammalian cells, C-terminally anchored CD55 precursor protein was found to mostly reside in the ER (Liu et al., 2023).

The Dpr-DIP family of CSPs form selective hetero- and homophilic interactions that drive various processes in *Drosophila* circuit assembly including axon pathfinding, synaptic partner matching, and cell survival (see Chapter I for a comprehensive description). More recently, Dprs and DIPs were described to be GPI anchored (Lobb-Rabe et al., 2023). In a previous study examining the role of DIP-α in neuromuscular system development (Ashley et al., 2019), we utilized a C-terminal tagged DIP-α before determining DIP-α was GPI anchored. If canonically processed, this C-terminal tag should be removed. In this brief study, we demonstrate that a subpopulation of DIP-α is trafficked to the correct location while retaining its C-terminus, suggesting that a fraction of this protein population escapes the secretory pathway without GPI anchor addition, but with the C-terminus exposed to the extracellular space.

C-terminal tagged DIP-α (DIP-α-Myc) displays punctate surface labeling when expressed presynaptically using *A8-GAL4* (Venkatasubramanian et al., 2019; Wang et al., 2022), suggesting that some DIP-α-Myc is trafficked to the surface of boutons and retains its C-terminus (Figure B1). Additionally, this C-terminally tagged protein is sufficient to rescue the innervation defect observed in *DIP-α* mutants (Ashley et al., 2019). We did not see any surface expression with a C-terminally tagged DIP-ζ. The sparse labeling of the C-terminally tagged

DIP-α suggests that a subpopulation of DIP-α-Myc is not GPI anchored, but rather anchored to the cell surface through its unprocessed C-terminus, which contains hydrophobic residues (Figure B1). Importantly, this surface labeling likely represents only a fraction of the DIP-α present on the cell surface, as presumably the majority of this protein is processed correctly, thereby losing its tag. It is unclear how the C-terminally attached proteins are trafficking properly. Moreover, all of the produced DIP-ζ appears to efficiently lose its C-terminus even though the tag identity is the same and the insertion site is similar. Whether proper localization and trafficking of unprocessed would-be GPI-anchored proteins is a more general phenomenon or whether DIP-α presents a unique exception remains to be determined.

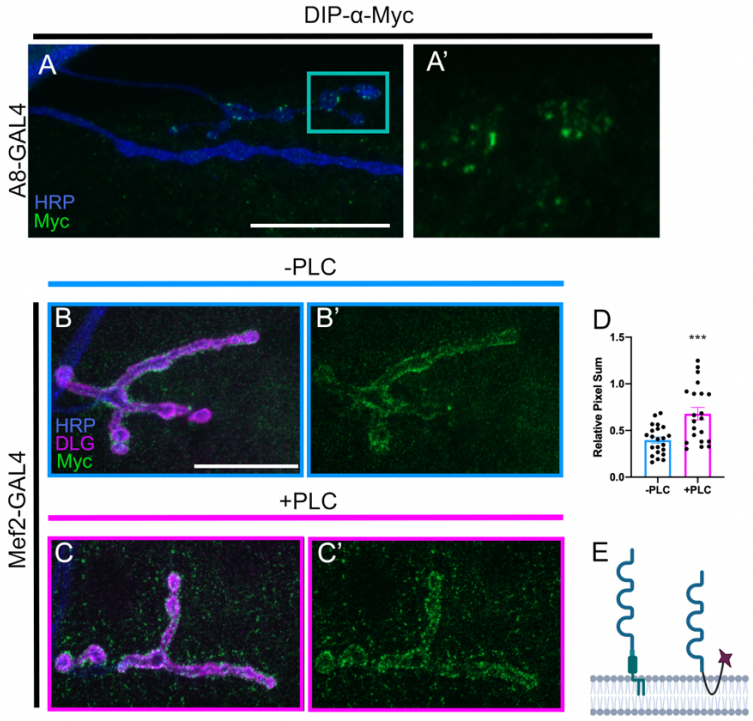

Figure B1. In vivo evidence for C-terminal retention of GPI-anchored DIP-α.
(A) C-terminally tagged DIP-α is present at the cell surface of Is neurons when expressed with A8-GAL4, neuronal membrane visualized in blue (HRP) and DIP-α-Myc in green. (A') Green channel only. (B-C') In vivo PLC experiment with neuronal membrane visuzlied in blue (HRP), postsynaptic membrane visualized in magenta (DLG), and DIP-α-Myc visuzlized in green. (B-B') Control samples that did not get treated with PLC. (C-C') Samples treated with PLC. (D) Quantification of experiment in (B-C). (E) Model of wildtype GPI-anchored DIP-α (left) and unproccesed C-terminally tagged DIP-α (right).

6.3 APPENDIX C

DEVELOPMENTAL TIMING OF BOUTON ADDITION IN *DROSOPHILA* LARVAE

The *Drosophila* nervous system has been used as a model for neurodevelopment for decades. In some cases, observations made long ago with technology available at the time stands as fact and are now starting to be examined with modern tools. I want to thank my colleague Dr. Yupu Wang for encouraging this type of thinking in the lab—to follow our data even if it challenges some existing ways of thinking.

One belief held in the field was that the number of boutons at NMJs decreases from anterior to posterior segments. In other words, the m6 NMJ of abdominal segment 2 (A2) has many more boutons than does A3, which has more than A4 and so on. Yupu showed that this observation is likely due to the existence of an additional motor neuron innervating m6/m7 in A2—this MN does not exist in other segments (Wang et al., 2022). I expanded on this work, examining bouton numbers in segments A2-A5 on muscles 12 and 13. I used the endogenously labeled DIP-α to quantify Is terminals on these muscles and found no significant difference in the number of boutons of different segments (Figure C1). There was no difference 24 hours after the embryos were laid and no difference in third instar, 96 hours after the embryo was laid.

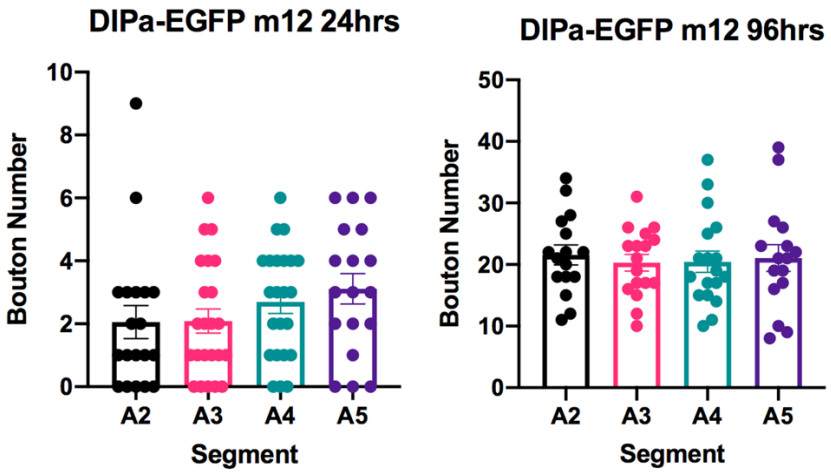

Figure C1. Quantification of boutons on m12 on different segments at 24 and 96 hours after embryos are laid.

In order to generate a more detailed timeline of NMJ development, and specifically synaptic growth, at the larval NMJ, we examined bouton numbers every 8 hours after larvae hatched. We used the endogenously tagged DIP-α line and counted Is boutons on m12 and m13. The most difficult dissections were performed by Robert Carrillo and Veera Anand, without whom this work would have been impossible.

For both muscles, there is a slow but steady bouton number increase from 24 hours to 80 hours, at which point growth stops and bouton number stabilizes (Figure C2). This is consistent with early work examining total bouton number on m6 in A4 (Li et al., 2002), suggesting that many NMJs have similar growth dynamics during development.

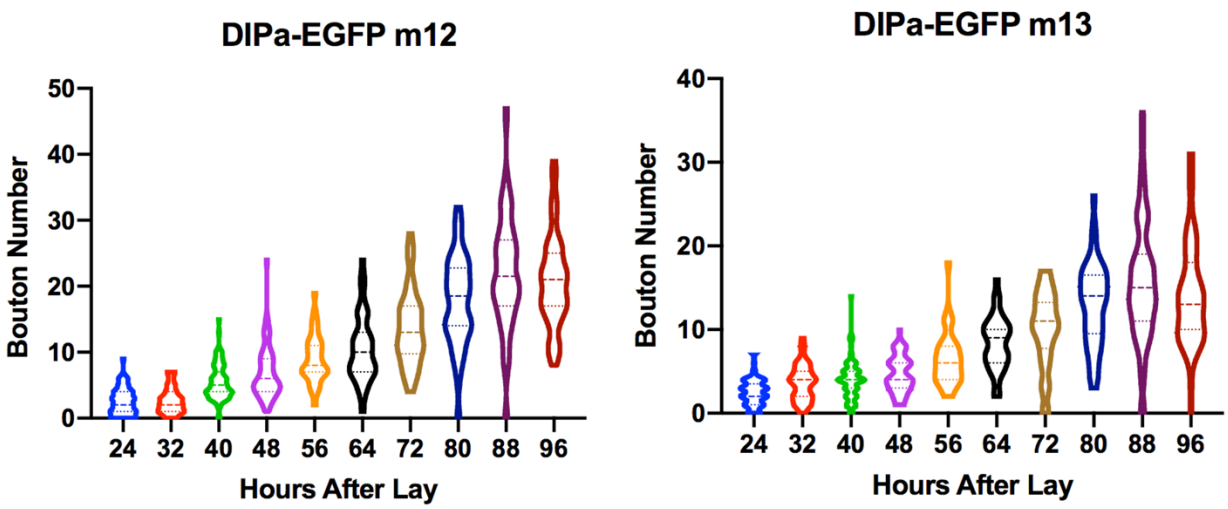

Figure C2. Quantification of Is bouton number on m12 and m13 throughout development.

REFERENCES

Aberle H. 2019. Axon Guidance and Collective Cell Migration by Substrate-Derived Attractants. *Front Mol Neurosci* **12**:148. doi:10.3389/fnmol.2019.00148

Abrell S, Jäckle H. 2001. Axon guidance of Drosophila SNb motoneurons depends on the cooperative action of muscular Krüppel and neuronal capricious activities. *Mech Develop* **109**:3–12. doi:10.1016/s0925-4773(01)00511-1

Akeel M, McNamee CJ, Youssef S, Moss D. 2011. DIgLONs inhibit initiation of neurite outgrowth from forebrain neurons via an IgLON-containing receptor complex. *Brain Res* **1374**:27–35. doi:10.1016/j.brainres.2010.12.028

Anderson M, Halpern M, Keshishian H. 1988. Identification of the neuropeptide transmitter proctolin in Drosophila larvae: characterization of muscle fiber-specific neuromuscular endings. *J Neurosci* **8**:242–255. doi:10.1523/jneurosci.08-01-00242.1988

Aponte-Santiago NA, Ormerod KG, Akbergenova Y, Littleton JT. 2020. Synaptic Plasticity Induced by Differential Manipulation of Tonic and Phasic Motoneurons in Drosophila. *J Neurosci* **40**:6270–6288. doi:10.1523/jneurosci.0925-20.2020

Aradska J, Bulat T, Sialana FJ, Birner-Gruenberger R, Erich B, Lubec G. 2015. Gel-free mass spectrometry analysis of Drosophila melanogaster heads. *Proteomics* **15**:3356–3360. doi:10.1002/pmic.201500092

Artavanis-Tsakonas S, Rand MD, Lake RJ. 1999. Notch Signaling: Cell Fate Control and Signal Integration in Development. *Science* **284**:770–776. doi:10.1126/science.284.5415.770

Arumugam S, Schmieder S, Pezeshkian W, Becken U, Wunder C, Chinnapen D, Ipsen JH, Kenworthy AK, Lencer W, Mayor S, Johannes L. 2021. Ceramide structure dictates glycosphingolipid nanodomain assembly and function. *Nat Commun* **12**:3675. doi:10.1038/s41467-021-23961-9

Ashley J, Sorrentino V, Lobb-Rabe M, Nagarkar-Jaiswal S, Tan L, Xu S, Xiao Q, Zinn K, Carrillo RA. 2019. Transsynaptic interactions between IgSF proteins DIP-α and Dpr10 are required for motor neuron targeting specificity. *Elife* **8**:e42690. doi:10.7554/elife.42690

Astigarraga S, Hofmeyer K, Farajian R, Treisman JE. 2010. Three Drosophila Liprins Interact to Control Synapse Formation. *J Neurosci* **30**:15358–15368. doi:10.1523/jneurosci.1862-10.2010

Bali N, Lee H-K (Peter), Zinn K. 2022. Sticks and Stones, a conserved cell surface ligand for the Type IIa RPTP Lar, regulates neural circuit wiring in Drosophila. *eLife* **11**:e71469. doi:10.7554/elife.71469

Barish S, Nuss S, Strunilin I, Bao S, Mukherjee S, Jones CD, Volkan PC. 2018. Combinations of DIPs and Dprs control organization of olfactory receptor neuron terminals in Drosophila. *Plos Genet* **14**:e1007560. doi:10.1371/journal.pgen.1007560

Bate M. 1990. The embryonic development of larval muscles in Drosophila. *Development* **110**:791–804. doi:10.1242/dev.110.3.791

Baumgartner S, Chiquet-Ehrismann R. 1993. Tena, a Drosophila gene related to tenascin, shows selective transcript localization. *Mech Dev* **40**:165–176. doi:10.1016/0925-4773(93)90074-8

Baumgartner S, Martin D, Hagios C, Chiquet-Ehrismann R. 1994. Tenm, a Drosophila gene related to tenascin, is a new pair-rule gene. *EMBO J* **13**:3728–3740. doi:10.1002/j.1460-2075.1994.tb06682.x

Bellen HJ, Tong C, Tsuda H. 2010. 100 years of Drosophila research and its impact on vertebrate neuroscience: a history lesson for the future. *Nat Rev Neurosci* **11**:514–522. doi:10.1038/nrn2839

Berke B, Wittnam J, McNeill E, Vactor DLV, Keshishian H. 2013. Retrograde BMP signaling at the synapse: A permissive signal for synapse maturation and activity-dependent plasticity. *J Neurosci* **33**:17937–17950. doi:10.1523/jneurosci.6075-11.2013

Blockus H, Chédotal A. 2016. Slit-Robo signaling. *Development* **143**:3037–3044. doi:10.1242/dev.132829

Bornstein B, Meltzer H, Adler R, Alyagor I, Berkun V, Cummings G, Reh F, Keren-Shaul H, David E, Riemensperger T, Schuldiner O. 2021. Transneuronal Dpr12/DIP-δ interactions facilitate compartmentalized dopaminergic innervation of Drosophila mushroom body axons. *Embo J* **40**:e105763. doi:10.15252/embj.2020105763

Boucard AA, Ko J, Südhof TC. 2012. High Affinity Neurexin Binding to Cell Adhesion G-protein-coupled Receptor CIRL1/Latrophilin-1 Produces an Intercellular Adhesion Complex*. *J Biol Chem* **287**:9399–9413. doi:10.1074/jbc.m111.318659

Boyer NP, Gupton SL. 2018. Revisiting Netrin-1: One Who Guides (Axons). *Front Cell Neurosci* **12**:221. doi:10.3389/fncel.2018.00221

Brose K, Bland KS, Wang KH, Arnott D, Henzel W, Goodman CS, Tessier-Lavigne M, Kidd T. 1999. Slit Proteins Bind Robo Receptors and Have an Evolutionarily Conserved Role in Repulsive Axon Guidance. *Cell* **96**:795–806. doi:10.1016/s0092-8674(00)80590-5

Brovero SG, Fortier JC, Hu H, Lovejoy PC, Newell NR, Palmateer CM, Tzeng R-Y, Lee P-T, Zinn K, Arbeitman MN. 2021. Investigation of Drosophila fruitless neurons that express Dpr/DIP cell adhesion molecules. *eLife* **10**:e63101. doi:10.7554/elife.63101

Bumgarner GW, Zampell JC, Nagarajan S, Poloso NJ, Dorn AS, D'Souza MJ, Selvaraj P. 2005. Modified cell ELISA to determine the solubilization of cell surface proteins: Applications in GPI-anchored protein purification. *J Biochem Bioph Meth* **64**:99–109. doi:10.1016/j.jbbm.2005.05.007

Butler SJ, Ray S, Hiromi Y. 1997. klingon, a novel member of the Drosophila immunoglobulin superfamily, is required for the development of the R7 photoreceptor neuron. *Development* **124**:781–792. doi:10.1242/dev.124.4.781

Calderon D, Blecher-Gonen R, Huang X, Secchia S, Kentro J, Daza RM, Martin B, Dulja A, Schaub C, Trapnell C, Larschan E, O'Connor-Giles KM, Furlong EEM, Shendure J. 2022. The continuum of Drosophila embryonic development at single-cell resolution. *Science* **377**:eabn5800–eabn5800. doi:10.1126/science.abn5800

Carrillo RA, Özkan E, Menon KP, Nagarkar-Jaiswal S, Lee PT, Jeon M, Birnbaum ME, Bellen HJ, Garcia KC, Zinn K. 2015. Control of Synaptic Connectivity by a Network of Drosophila IgSF Cell Surface Proteins. *Cell* **163**:1770–1782. doi:10.1016/j.cell.2015.11.022

Cash S, Chiba A, Keshishian H. 1992. Alternate neuromuscular target selection following the loss of single muscle fibers in Drosophila. *J Neurosci* **12**:2051–2064. doi:10.1523/jneurosci.12-06-02051.1992

Chang TN, Keshishian H. 1996. Laser Ablation of Drosophila Embryonic Motoneurons Causes Ectopic Innervation of Target Muscle Fibers. *J Neurosci* **16**:5715–5726. doi:10.1523/jneurosci.16-18-05715.1996

Chen C, Buhl E, Xu M, Croset V, Rees JS, Lilley KS, Benton R, Hodge JJL, Stanewsky R. 2015. Drosophila Ionotropic Receptor 25a mediates circadian clock resetting by temperature. *Nature* **527**:516–520. doi:10.1038/nature16148

Chen C, Xu M, Anantaprakorn Y, Rosing M, Stanewsky R. 2018. nocte Is Required for Integrating Light and Temperature Inputs in Circadian Clock Neurons of Drosophila. *Curr Biol* **28**:1595-1605.e3. doi:10.1016/j.cub.2018.04.001

Cheng S, Ashley J, Kurleto JD, Lobb-Rabe M, Park YJ, Carrillo RA, Özkan E. 2019a. Molecular basis of synaptic specificity by immunoglobulin superfamily receptors in Drosophila. *Elife* **8**:e41028. doi:10.7554/elife.41028

Cheng S, Park Y, Kurleto JD, Jeon M, Zinn K, Thornton JW, Özkan E. 2019b. Family of neural wiring receptors in bilaterians defined by phylogenetic, biochemical, and structural evidence. *Proc National Acad Sci* **116**:9837–9842. doi:10.1073/pnas.1818631116

Chithran AV, Allan DW, O'Connor TP. 2023. Adult expression of Semaphorins and Plexins is essential for motor neuron survival. *Sci Rep* **13**:5894. doi:10.1038/s41598-023-32943-4

Committee EN. 1997. Unified Nomenclature for Eph Family Receptors and Their Ligands, the Ephrins. *Cell* **90**:403–404. doi:10.1016/s0092-8674(00)80500-0

Consortium TU. 2015. UniProt: a hub for protein information. *Nucleic Acids Res* **43**:D204–D212. doi:10.1093/nar/gku989

Corda D, Mosca MG, Ohshima N, Grauso L, Yanaka N, Mariggiò S. 2014. The emerging physiological roles of the glycerophosphodiesterase family. *Febs J* **281**:998–1016. doi:10.1111/febs.12699

Cornejo F, Cortés BI, Findlay GM, Cancino GI. 2021. LAR Receptor Tyrosine Phosphatase Family in Healthy and Diseased Brain. *Front Cell Dev Biol* **9**:659951. doi:10.3389/fcell.2021.659951

Cornell B, Toyo-oka K. 2017. 14-3-3 Proteins in Brain Development: Neurogenesis, Neuronal Migration and Neuromorphogenesis. *Front Mol Neurosci* **10**:318. doi:10.3389/fnmol.2017.00318

Cosmanescu F, Katsamba PS, Sergeeva AP, Ahlsen G, Patel SD, Brewer JJ, Tan L, Xu S, Xiao Q, Nagarkar-Jaiswal S, Nern A, Bellen HJ, Zipursky SL, Honig B, Shapiro L. 2018. Neuron-Subtype-Specific Expression, Interaction Affinities, and Specificity Determinants of DIP/Dpr Cell Recognition Proteins. *Neuron* **100**:1385-1400.e6. doi:10.1016/j.neuron.2018.10.046

Courgeon M, Desplan C. 2019. Coordination between stochastic and deterministic specification in the Drosophila visual system. *Science* **366**:eaay6727. doi:10.1126/science.aay6727

Davis GW, Goodman CS. 1998. Synapse-specific control of synaptic efficacy at the terminals of a single neuron. *Nature* **392**:82–86. doi:10.1038/32176

Davy A, Gale NW, Murray EW, Klinghoffer RA, Soriano P, Feuerstein C, Robbins SM. 1999. Compartmentalized signaling by GPI-anchored ephrin-A5 requires the Fyn tyrosine kinase to regulate cellular adhesion. *Gene Dev* **13**:3125–3135. doi:10.1101/gad.13.23.3125

DePew AT, Aimino MA, Mosca TJ. 2019. The Tenets of Teneurin: Conserved Mechanisms Regulate Diverse Developmental Processes in the Drosophila Nervous System. *Front Neurosci* **13**:27. doi:10.3389/fnins.2019.00027

Dickson BJ, Gilestro GF. 2006. Regulation of Commissural Axon Pathfinding by Slit and its Robo Receptors. *Cell Dev Biology* **22**:651–675. doi:10.1146/annurev.cellbio.21.090704.151234

Droujinine IA, Meyer AS, Wang D, Udeshi ND, Hu Y, Rocco D, McMahon JA, Yang R, Guo J, Mu L, Carey DK, Svinkina T, Zeng R, Branon T, Tabatabai A, Bosch JA, Asara JM, Ting

AY, Carr SA, McMahon AP, Perrimon N. 2021. Proteomics of protein trafficking by in vivo tissue-specific labeling. *Nat Commun* **12**:2382. doi:10.1038/s41467-021-22599-x

Duan X, Krishnaswamy A, Laboulaye MA, Liu J, Peng Y-R, Yamagata M, Toma K, Sanes JR. 2018. Cadherin Combinations Recruit Dendrites of Distinct Retinal Neurons to a Shared Interneuronal Scaffold. *Neuron* **99**:1145-1154.e6. doi:10.1016/j.neuron.2018.08.019

Dudu V, Bittig T, Entchev E, Kicheva A, Jülicher F, González-Gaitán M. 2006. Postsynaptic Mad Signaling at the Drosophila Neuromuscular Junction. *Curr Biol* **16**:625–635. doi:10.1016/j.cub.2006.02.061

Dyczynska E, Sun D, Yi H, Sehara-Fujisawa A, Blobel CP, Zolkiewska A. 2007. Proteolytic Processing of Delta-like 1 by ADAM Proteases*. *J Biol Chem* **282**:436–444. doi:10.1074/jbc.m605451200

Eisenhaber B, Bork P, Eisenhaber F. 1999. Prediction of Potential GPI-modification Sites in Proprotein Sequences. *J Mol Biol* **292**:741–758. doi:10.1006/jmbi.1999.3069

Eisenhaber B, Bork P, Eisenhaber F. 1998. Sequence properties of GPI-anchored proteins near the omega-site: constraints for the polypeptide binding site of the putative transamidase. *Protein Eng, Des Sel* **11**:1155–1161. doi:10.1093/protein/11.12.1155

Enriquez J, Boukhatmi H, Dubois L, Philippakis AA, Bulyk ML, Michelson AM, Crozatier M, Vincent A. 2010. Multi-step control of muscle diversity by Hox proteins in the Drosophila embryo. *Development* **137**:457–466. doi:10.1242/dev.045286

Evans CJ, Olson JM, Ngo KT, Kim E, Lee NE, Kuoy E, Patananan AN, Sitz D, Tran P, Do M-T, Yackle K, Cespedes A, Hartenstein V, Call GB, Banerjee U. 2009. G-TRACE: rapid Gal4-based cell lineage analysis in Drosophila. *Nat Methods* **6**:603–605. doi:10.1038/nmeth.1356

Ferguson MAJ, Williams AF. 1988. Cell-Surface Anchoring of Proteins Via Glycosyl-Phosphatidylinositol Structures. *Annu Rev Biochem* **57**:285–320. doi:10.1146/annurev.bi.57.070188.001441

Fernandes VM, Chen Z, Rossi AM, Zipfel J, Desplan C. 2017. Glia relay differentiation cues to coordinate neuronal development in Drosophila. *Science* **357**:886–891. doi:10.1126/science.aan3174

Figeac N, Jagla T, Aradhya R, Ponte JPD, Jagla K. 2010. Drosophila adult muscle precursors form a network of interconnected cells and are specified by the rhomboid-triggered EGF pathway. *Development* **137**:1965–1973. doi:10.1242/dev.049080

Finean MGL and JB. 1977. Non-lytic release of acetylcholinesterase from erythrocytes by a phosphatidylinositol-specific phospholipase C. *FEBS Letters*.

Foty RA, Steinberg MS. 2005. The differential adhesion hypothesis: a direct evaluation. *Dev Biol* **278**:255–263. doi:10.1016/j.ydbio.2004.11.012

Freeman MR. 2015. Drosophila Central Nervous System Glia. *Cold Spring Harb Perspect Biol* **7**:a020552. doi:10.1101/cshperspect.a020552

Freeman MR, Delrow J, Kim J, Johnson E, Doe CQ. 2003. Unwrapping glial biology: Gcm target genes regulating glial development, diversification, and function. *Neuron* **38**:567–580. doi:10.1016/s0896-6273(03)00289-7

Fuentes-Medel Y, Ashley J, Barria R, Maloney R, Freeman M, Budnik V. 2012. Integration of a retrograde signal during synapse formation by glia-secreted TGF-β ligand. *Curr Biol* **22**:1831–1838. doi:10.1016/j.cub.2012.07.063

Fuentes-Medel Y, Logan MA, Ashley J, Ataman B, Budnik V, Freeman MR. 2009. Glia and muscle sculpt neuromuscular arbors by engulfing destabilized synaptic boutons and shed presynaptic debris. *Plos Biol* **7**:e1000184. doi:10.1371/journal.pbio.1000184

Gale NW, Holland SJ, Valenzuela DM, Flenniken A, Pan L, Ryan TE, Henkemeyer M, Strebhardt K, Hirai H, Wilkinson DG, Pawson T, Davis S, Yancopoulos GD. 1996. Eph Receptors and Ligands Comprise Two Major Specificity Subclasses and Are Reciprocally Compartmentalized during Embryogenesis. *Neuron* **17**:9–19. doi:10.1016/s0896-6273(00)80276-7

George R, Stanewsky R. 2021. Peripheral Sensory Organs Contribute to Temperature Synchronization of the Circadian Clock in Drosophila melanogaster. *Front Physiol* **12**:622545. doi:10.3389/fphys.2021.622545

Gil OD, Zhang L, Chen S, Ren YQ, Pimenta A, Zanazzi G, Hillman D, Levitt P, Salzer JL. 2002. Complementary expression and heterophilic interactions between igLON family members neurotrimin and LAMP. *J Neurobiol* **51**:190–204. doi:10.1002/neu.10050

Gilestro GF. 2008. Redundant Mechanisms for Regulation of Midline Crossing in Drosophila. *PLoS ONE* **3**:e3798. doi:10.1371/journal.pone.0003798

Gíslason MH, Nielsen H, Armenteros JJA, Johansen AR. 2021. Prediction of GPI-anchored proteins with pointer neural networks. *Curr Res Biotechnology* **3**:6–13. doi:10.1016/j.crbiot.2021.01.001

Glaser FT, Stanewsky R. 2005. Temperature Synchronization of the Drosophila Circadian Clock. *Curr Biol* **15**:1352–1363. doi:10.1016/j.cub.2005.06.056

Goel P, Khan M, Howard S, Kim G, Kiragasi B, Kikuma K, Dickman D. 2019. A Screen for Synaptic Growth Mutants Reveals Mechanisms That Stabilize Synaptic Strength. *J Neurosci* **39**:4051–4065. doi:10.1523/jneurosci.2601-18.2019

Goold CP, Davis GW. 2007. The BMP Ligand Gbb Gates the Expression of Synaptic Homeostasis Independent of Synaptic Growth Control. *Neuron* **56**:109–123. doi:10.1016/j.neuron.2007.08.006

Guan B, Hartmann B, Kho Y-H, Gorczyca M, Budnik V. 1996. The Drosophila tumor suppressor gene, dlg, is involved in structural plasticity at a glutamatergic synapse. *Curr Biol* **6**:695–706. doi:10.1016/s0960-9822(09)00451-5

Hachisuka A, Yamazaki T, Sawada J-I, Terao T. 1996. CHARACTERIZATION AND TISSUE DISTRIBUTION OF OPIOID-BINDING CELL ADHESION MOLECULE (OBCAM) USING MONOCLONAL ANTIBODIES. *Neurochem Int* **28**:373–379. doi:10.1016/0197-0186(95)00108-5

Hallgren J, Tsirigos KD, Pedersen MD, Armenteros JJA, Marcatili P, Nielsen H, Krogh A, Winther O. 2022. DeepTMHMM predicts alpha and beta transmembrane proteins using deep neural networks. doi:10.1101/2022.04.08.487609

Harris KP, Littleton JT. 2015. Transmission, development, and plasticity of synapses. *Genetics* **201**:345–375. doi:10.1534/genetics.115.176529

Hartenstein V. 2011. Morphological diversity and development of glia in Drosophila. *Glia* **59**:1237–1252. doi:10.1002/glia.21162

Haussmann IU, Bodi Z, Sanchez-Moran E, Mongan NP, Archer N, Fray RG, Soller M. 2016. m6A potentiates Sxl alternative pre-mRNA splicing for robust Drosophila sex determination. *Nature* **540**:301–304. doi:10.1038/nature20577

Heidbreder A, Philipp K. 2018. Anti-IgLON 5 Disease. *Curr Treat Options Neurol* **20**:29. doi:10.1007/s11940-018-0515-4

Hessinger C, Technau GM, Rogulja-Ortmann A. 2016. The Drosophila Hox gene Ultrabithorax acts in both muscles and motoneurons to orchestrate formation of specific neuromuscular connections. *Development* **144**:139–150. doi:10.1242/dev.143875

Hiramoto M, Hiromi Y, Giniger E, Hotta Y. 2000. The Drosophila Netrin receptor Frazzled guides axons by controlling Netrin distribution. *Nature* **406**:886–889. doi:10.1038/35022571

Hoang B, Chiba A. 2001. Single-cell analysis of Drosophila larval neuromuscular synapses. *Dev Biol* **229**:55–70. doi:10.1006/dbio.2000.9983

Hong W, Mosca TJ, Luo L. 2012. Teneurins instruct synaptic partner matching in an olfactory map. *Nature* **484**:201–207. doi:10.1038/nature10926

Honig B, Shapiro L. 2020. Adhesion Protein Structure, Molecular Affinities, and Principles of Cell-Cell Recognition. *Cell* **181**:520–535. doi:10.1016/j.cell.2020.04.010

Hosoya T, Takizawa K, Nitta K, Hotta Y. 1995. Glial cells missing: A binary switch between neuronal and glial determination in drosophila. *Cell* **82**:1025–1036. doi:10.1016/0092-8674(95)90281-3

Howard LJ, Brown HE, Wadsworth BC, Evans TA. 2019. Midline axon guidance in the Drosophila embryonic central nervous system. *Semin Cell Dev Biol* **85**:13–25. doi:10.1016/j.semcdb.2017.11.029

Hu Y, Flockhart I, Vinayagam A, Bergwitz C, Berger B, Perrimon N, Mohr SE. 2011. An integrative approach to ortholog prediction for disease-focused and other functional studies. *Bmc Bioinformatics* **12**:357–357. doi:10.1186/1471-2105-12-357

Ikezawa Z, Nakajima H. 1976. A STUDY OF MULTICENTRIC RETICULOHISTIOCYTOSIS (LIPOID DERMATOARTHRITIS). *J Dermatology* **3**:289–302. doi:10.1111/j.1346-8138.1976.tb00984.x

Inaki M, Yoshikawa S, Thomas JB, Aburatani H, Nose A. 2007. Wnt4 Is a Local Repulsive Cue that Determines Synaptic Target Specificity. *Curr Biol* **17**:1574–1579. doi:10.1016/j.cub.2007.08.013

Itoh S, Hachisuka A, Kawasaki N, Hashii N, Teshima R, Hayakawa T, Kawanishi T, Yamaguchi T. 2008. Glycosylation Analysis of IgLON Family Proteins in Rat Brain by Liquid Chromatography and Multiple-Stage Mass Spectrometry. *Biochemistry-us* **47**:10132–10154. doi:10.1021/bi8009778

Jan LY, Jan YN. 1976. Properties of the larval neuromuscular junction in Drosophila melanogaster. *J Physiol* **262**:189–214. doi:10.1113/jphysiol.1976.sp011592

Jeong S. 2021. Molecular Mechanisms Underlying Motor Axon Guidance in Drosophila. *Mol Cells* **44**:549–556. doi:10.14348/molcells.2021.0129

Jetti SK, Crane AB, Akbergenova Y, Aponte-Santiago NA, Cunningham KL, Whittaker CA, Littleton JT. 2023. Molecular Logic of Synaptic Diversity Between Drosophila Tonic and Phasic Motoneurons. *bioRxiv* 2023.01.17.524447. doi:10.1101/2023.01.17.524447

Jiang X, Liu B, Nie Z, Duan L, Xiong Q, Jin Z, Yang C, Chen Y. 2021. The role of m6A modification in the biological functions and diseases. *Signal Transduct Target Ther* **6**:74. doi:10.1038/s41392-020-00450-x

Johnson KG, Tenney AP, Ghose A, Duckworth AM, Higashi ME, Parfitt K, Marcu O, Heslip TR, Marsh JL, Schwarz TL, Flanagan JG, Vactor DV. 2006. The HSPGs Syndecan and Dallylike Bind the Receptor Phosphatase LAR and Exert Distinct Effects on Synaptic Development. *Neuron* **49**:517–531. doi:10.1016/j.neuron.2006.01.026

Joo WJ, Sweeney LB, Liang L, Luo L. 2013. Linking Cell Fate, Trajectory Choice, and Target Selection: Genetic Analysis of Sema-2b in Olfactory Axon Targeting. *Neuron* **78**:673–686. doi:10.1016/j.neuron.2013.03.022

Jumper J, Evans R, Pritzel A, Green T, Figurnov M, Ronneberger O, Tunyasuvunakool K, Bates R, Žídek A, Potapenko A, Bridgland A, Meyer C, Kohl SAA, Ballard AJ, Cowie A, Romera-Paredes B, Nikolov S, Jain R, Adler J, Back T, Petersen S, Reiman D, Clancy E, Zielinski M, Steinegger M, Pacholska M, Berghammer T, Bodenstein S, Silver D, Vinyals O, Senior AW, Kavukcuoglu K, Kohli P, Hassabis D. 2021. Highly accurate protein structure prediction with AlphaFold. *Nature* **596**:583–589. doi:10.1038/s41586-021-03819-2

Kafri R, Springer M, Pilpel Y. 2009. Genetic Redundancy: New Tricks for Old Genes. *Cell* **136**:389–392. doi:10.1016/j.cell.2009.01.027

Käll L, Krogh A, Sonnhammer ELL. 2004. A Combined Transmembrane Topology and Signal Peptide Prediction Method. *J Mol Biol* **338**:1027–1036. doi:10.1016/j.jmb.2004.03.016

Karis K, Eskla K-L, Kaare M, Täht K, Tuusov J, Visnapuu T, Innos J, Jayaram M, Timmusk T, Weickert CS, Väli M, Vasar E, Philips M-A. 2018. Altered Expression Profile of IgLON Family of Neural Cell Adhesion Molecules in the Dorsolateral Prefrontal Cortex of Schizophrenic Patients. *Front Mol Neurosci* **11**:8. doi:10.3389/fnmol.2018.00008

Kato K, Losada-Perez M, Hidalgo A. 2018. Gene network underlying the glial regenerative response to central nervous system injury. *Dev Dyn* **247**:85–93. doi:10.1002/dvdy.24565

Kato M, Wang H, Kainulainen V, Fitzgerald ML, Ledbetter S, Ornitz DM, Bernfield M. 1998. Physiological degradation converts the soluble syndecan-1 ectodomain from an inhibitor to a potent activator of FGF-2. *Nat Med* **4**:691–697. doi:10.1038/nm0698-691

Katsamba P, Carroll K, Ahlsen G, Bahna F, Vendome J, Posy S, Rajebhosale M, Price S, Jessell TM, Ben-Shaul A, Shapiro L, Honig BH. 2009. Linking molecular affinity and cellular specificity in cadherin-mediated adhesion. *Proc Natl Acad Sci* **106**:11594–11599. doi:10.1073/pnas.0905349106

Kawakami J, Brooks D, Zalmai R, Hartson SD, Bouyain S, Geisbrecht ER. 2022. Complex protein interactions mediate Drosophila Lar function in muscle tissue. *PLoS ONE* **17**:e0269037. doi:10.1371/journal.pone.0269037

Keleman K, Dickson BJ. 2001. Short- and Long-Range Repulsion by the Drosophila Unc5 Netrin Receptor. *Neuron* **32**:605–617. doi:10.1016/s0896-6273(01)00505-0

Keshishian H, Kim YS. 2004. Orchestrating development and function: Retrograde BMP signaling in the Drosophila nervous system. *Trends Neurosci* **27**:143–147. doi:10.1016/j.tins.2004.01.004

Kidd T, Brose K, Mitchell KJ, Fetter RD, Tessier-Lavigne M, Goodman CS, Tear G. 1998. Roundabout Controls Axon Crossing of the CNS Midline and Defines a Novel Subfamily of Evolutionarily Conserved Guidance Receptors. *Cell* **92**:205–215. doi:10.1016/s0092-8674(00)80915-0

Kinold JC, Pfarr C, Aberle H. 2018. Sidestep-induced neuromuscular miswiring causes severe locomotion defects in *Drosophila* larvae. *Development* **145**:dev163279. doi:10.1242/dev.163279

Kinoshita T. 2020. Biosynthesis and biology of mammalian GPI-anchored proteins. *Open Biol* **10**:190290. doi:10.1098/rsob.190290

Kinoshita T, Fujita M. 2016. Thematic Review Series: Glycosylphosphatidylinositol (GPI) Anchors: Biochemistry and Cell Biology Biosynthesis of GPI-anchored proteins: special emphasis on GPI lipid remodeling. *J Lipid Res* **57**:6–24. doi:10.1194/jlr.r063313

Kohsaka H, Okusawa S, Itakura Y, Fushiki A, Nose A. 2012. Development of larval motor circuits in Drosophila. *Dev, Growth Differ* **54**:408–419. doi:10.1111/j.1440-169x.2012.01347.x

Kolodkin AL, Tessier-Lavigne M. 2011. Mechanisms and Molecules of Neuronal Wiring: A Primer. *Csh Perspect Biol* **3**:a001727. doi:10.1101/cshperspect.a001727

Koon AC, Ashley J, Barria R, Dasgupta S, Brain R, Waddell S, Alkema MJ, Budnik V. 2011. Autoregulatory and paracrine control of synaptic and behavioral plasticity by octopaminergic signalingNature Neuroscience. pp. 190–201. doi:10.1038/nn.2716

Koropouli E, Kolodkin AL. 2014. Semaphorins and the dynamic regulation of synapse assembly, refinement, and function. *Curr Opin Neurobiol* **27**:1–7. doi:10.1016/j.conb.2014.02.005

Kruger RP, Aurandt J, Guan K-L. 2005. Semaphorins command cells to move. *Nat Rev Mol Cell Bio* **6**:789–800. doi:10.1038/nrm1740

Kumari SS, Varadaraj K. 2009. Intact AQP0 performs cell-to-cell adhesion. *Biochem Bioph Res Co* **390**:1034–1039. doi:10.1016/j.bbrc.2009.10.103

Kurmangaliyev YZ, Yoo J, Valdes-Aleman J, Sanfilippo P, Zipursky SL. 2020. Transcriptional Programs of Circuit Assembly in the Drosophila Visual System. *Neuron* **108**:1045-1057.e6. doi:10.1016/j.neuron.2020.10.006

Kurusu M, Cording A, Taniguchi M, Menon K, Suzuki E, Zinn K. 2008. A Screen of Cell-Surface Molecules Identifies Leucine-Rich Repeat Proteins as Key Mediators of Synaptic Target Selection. *Neuron* **59**:972–985. doi:10.1016/j.neuron.2008.07.037

Landgraf M, Bossing T, Technau GM, Bate M. 1997. The Origin, Location, and Projections of the Embryonic Abdominal Motorneurons of Drosophila. *J Neurosci* **17**:9642–9655. doi:10.1523/jneurosci.17-24-09642.1997

Landgraf M, Jeffrey V, Fujioka M, Jaynes JB, Bate M. 2003. Embryonic Origins of a Motor System:Motor Dendrites Form a Myotopic Mapin Drosophila. *PLoS Biol* **1**:e41. doi:10.1371/journal.pbio.0000041

Lavergne G, Zmojdzian M, Ponte JPD, Junion G, Jagla K. 2020. Drosophila adult muscle precursor cells contribute to motor axon pathfinding and proper innervation of embryonic muscles. *Development* **147**:dev183004. doi:10.1242/dev.183004

Lee G-H, Fujita M, Takaoka K, Murakami Y, Fujihara Y, Kanzawa N, Murakami K, Kajikawa E, Takada Y, Saito K, Ikawa M, Hamada H, Maeda Y, Kinoshita T. 2016. A GPI processing phospholipase A2, PGAP6, modulates Nodal signaling in embryos by shedding CRIPTO. *J Cell Biol* **215**:705–718. doi:10.1083/jcb.201605121

Lee H-K (Peter), Wright AP, Zinn K. 2009. Live Dissection of Drosophila Embryos: Streamlined Methods for Screening Mutant Collections by Antibody Staining. *J Vis Exp*. doi:10.3791/1647

Lee P-T, Zirin J, Kanca O, Lin W-W, Schulze KL, Li-Kroeger D, Tao R, Devereaux C, Hu Y, Chung V, Fang Y, He Y, Pan H, Ge M, Zuo Z, Housden BE, Mohr SE, Yamamoto S, Levis RW, Spradling AC, Perrimon N, Bellen HJ. 2018. A gene-specific T2A-GAL4 library for Drosophila. *Elife* **7**:e35574. doi:10.7554/elife.35574

Lence T, Akhtar J, Bayer M, Schmid K, Spindler L, Ho CH, Kreim N, Andrade-Navarro MA, Poeck B, Helm M, Roignant J-Y. 2016. m6A modulates neuronal functions and sex determination in Drosophila. *Nature* **540**:242–247. doi:10.1038/nature20568

Levental I, Levental KR, Heberle FA. 2020. Lipid Rafts: Controversies Resolved, Mysteries Remain. *Trends Cell Biol* **30**:341–353. doi:10.1016/j.tcb.2020.01.009

Li H, Peng X, Cooper RL. 2002. Development of Drosophila larval neuromuscular junctions: Maintaining synaptic strength. *Neuroscience* **115**:505–513. doi:10.1016/s0306-4522(02)00380-9

Li H, Watson A, Olechwier A, Anaya M, Sorooshyari SK, Harnett DP, Lee H-K (Peter), Vielmetter J, Fares MA, Garcia KC, Özkan E, Labrador J-P, Zinn K. 2017. Deconstruction of the beaten Path-Sidestep interaction network provides insights into neuromuscular system development. *eLife* **6**:e28111. doi:10.7554/elife.28111

Liu Y-S, Wang Y, Zhou X, Zhang L, Yang G, Gao X-D, Murakami Y, Fujita M, Kinoshita T. 2023. Accumulated precursors of specific GPI-anchored proteins upregulate GPI biosynthesis with ARV1. *J Cell Biol* **222**:e202208159. doi:10.1083/jcb.202208159

Ljaschenko D, Ehmann N, Kittel RJ. 2013. Hebbian Plasticity Guides Maturation of Glutamate Receptor Fields In Vivo. *Cell Rep* **3**:1407–1413. doi:10.1016/j.celrep.2013.04.003

Lnenicka GA, Keshishian H. 2000. Identified motor terminals in Drosophila larvae show distinct differences in morphology and physiology. *J Neurobiol* **43**:186–97.

Lobb-Rabe M, DeLong K, Salazar RJ, Zhang R, Wang Y, Carrillo RA. 2022. Dpr10 and Nocte are required for Drosophila motor axon pathfinding. *Neural Dev* **17**:10. doi:10.1186/s13064-022-00165-5

Lobb-Rabe M, Nawrocka WI, Carrillo RA, Özkan E. 2023. Neuronal wiring receptors Dprs and DIPs are GPI anchored and this modification contributes to their cell surface organization. *bioRxiv* 2023.03.02.530872. doi:10.1101/2023.03.02.530872

Lopez S, Rodriguez-Gallardo S, Sabido-Bozo S, Muñiz M. 2019. Endoplasmic Reticulum Export of GPI-Anchored Proteins. *Int J Mol Sci* **20**:3506. doi:10.3390/ijms20143506

Lukacs M, Roberts T, Chatuverdi P, Stottmann RW. 2019. Glycosylphosphatidylinositol biosynthesis and remodeling are required for neural tube closure, heart development, and cranial neural crest cell survival. *Elife* **8**:e45248. doi:10.7554/elife.45248

MacDonald JM, Beach MG, Porpiglia E, Sheehan AE, Watts RJ, Freeman MR. 2006. The Drosophila Cell Corpse Engulfment Receptor Draper Mediates Glial Clearance of Severed Axons. *Neuron* **50**:869–881. doi:10.1016/j.neuron.2006.04.028

Maness PF, Schachner M. 2007. Neural recognition molecules of the immunoglobulin superfamily: signaling transducers of axon guidance and neuronal migration. *Nat Neurosci* **10**:19–26. doi:10.1038/nn1827

Mark B, Lai S-L, Zarin AA, Manning L, Pollington HQ, Litwin-Kumar A, Cardona A, Truman JW, Doe CQ. 2021. A developmental framework linking neurogenesis and circuit formation in the Drosophila CNS. *eLife* **10**:e67510. doi:10.7554/elife.67510

Marqués G, Bao H, Haerry TE, Shimell MJ, Duchek P, Zhang B, O'Connor MB. 2002. The Drosophila BMP Type II Receptor Wishful Thinking Regulates Neuromuscular Synapse Morphology and Function. *Neuron* **33**:529–543. doi:10.1016/s0896-6273(02)00595-0

Mayor S, Riezman H. 2004. Sorting GPI-anchored proteins. *Nat Rev Mol Cell Bio* **5**:110–120. doi:10.1038/nrm1309

McCabe BD, Marqués G, Haghighi AP, Fetter RD, Crotty ML, Haerry TE, Goodman CS, O'Connor MB. 2003. The BMP homolog Gbb provides a retrograde signal that regulates synaptic growth at the Drosophila neuromuscular junction. *Neuron* **39**:241–254. doi:10.1016/s0896-6273(03)00426-4

Meng JL, Heckscher ES. 2020. Development of motor circuits: From neuronal stem cells and neuronal diversity to motor circuit assembly. *Curr Top Dev Biol* **142**:409–442. doi:10.1016/bs.ctdb.2020.11.010

Meng JL, Marshall ZD, Lobb-Rabe M, Heckscher ES. 2019. How prolonged expression of Hunchback, a temporal transcription factor, re-wires locomotor circuits. *Elife* **8**:e46089. doi:10.7554/elife.46089

Meng JL, Wang Y, Carrillo RA, Heckscher ES. 2020. Temporal transcription factors determine circuit membership by permanently altering motor neuron-to-muscle synaptic partnerships. *Elife* **9**:e56898. doi:10.7554/elife.56898

Menon KP, Carrillo RA, Zinn K. 2013. Development and plasticity of the *Drosophila* larval neuromuscular junction. *Wiley Interdiscip Rev Dev Biology* **2**:647–670. doi:10.1002/wdev.108

Menon KP, Kulkarni V, Shin-Ya T, Anaya M, Zinn K. 2019. Interactions between dpr11 and dip-y control election of amacrine neurons in drosophila color ision circuits. *Elife* **8**:e48935. doi:10.7554/elife.48935

Meyer F, Aberle H. 2006. At the next stop sign turn right: the metalloprotease Tolloid-related 1 controls defasciculation of motor axons in Drosophila. *Development* **133**:4035–4044. doi:10.1242/dev.02580

Mishra-Gorur K, Rand MD, Perez-Villamil B, Artavanis-Tsakonas S. 2002. Down-regulation of Delta by proteolytic processing. *J Cell Biology* **159**:313–324. doi:10.1083/jcb.200203117

Mitchell KJ, Doyle JL, Serafini T, Kennedy TE, Tessier-Lavigne M, Goodman CS, Dickson BJ. 1996. Genetic Analysis of Netrin Genes in Drosophila: Netrins Guide CNS Commissural Axons and Peripheral Motor Axons. *Neuron* **17**:203–215. doi:10.1016/s0896-6273(00)80153-1

Moran P, Raab H, Kohr WJ, Caras IW. 1991. Glycophospholipid membrane anchor attachment. Molecular analysis of the cleavage/attachment site. *J Biol Chem* **266**:1250–1257. doi:10.1016/s0021-9258(17)35308-5

Morgan TH. 1910. Sex Limited Inheritance in Drosophila. *Science* **32**:120–122. doi:10.1126/science.32.812.120

Mosca TJ, Hong W, Dani VS, Favaloro V, Luo L. 2012. Trans-synaptic Teneurin signalling in neuromuscular synapse organization and target choice. *Nature* **484**:237–241. doi:10.1038/nature10923

Nagarkar-Jaiswal S, Lee P-T, Campbell ME, Chen K, Anguiano-Zarate S, Gutierrez MC, Busby T, Lin W-W, He Y, Schulze KL, Booth BW, Evans-Holm M, Venken KJ, Levis RW, Spradling AC, Hoskins RA, Bellen HJ. 2015. A library of MiMICs allows tagging of genes

and reversible, spatial and temporal knockdown of proteins in Drosophila. *eLife* **4**:e05338. doi:10.7554/elife.05338

Nakamura M, Baldwin D, Hannaford S, Palka J, Montell C. 2002. Defective Proboscis Extension Response (DPR), a Member of the Ig Superfamily Required for the Gustatory Response to Salt. *J Neurosci* **22**:3463–3472. doi:10.1523/jneurosci.22-09-03463.2002

Nose A. 2012. Generation of neuromuscular specificity in Drosophila: Novel mechanisms revealed by new technologies. *Front Mol Neurosci* **5**:62. doi:10.3389/fnmol.2012.00062

Nowak MA, Boerlijst MC, Cooke J, Smith JM. 1997. Evolution of genetic redundancy. *Nature* **388**:167–171. doi:10.1038/40618

Nüsslein-Volhard C, Wieschaus E, Kluding H. 1984. Mutations affecting the pattern of the larval cuticle inDrosophila melanogaster. *Wilhelm Roux's Arch Dev Biol* **193**:267–282. doi:10.1007/bf00848156

O'Connor-Giles KM, Ganetzky B. 2008. Satellite signaling at synapses. *Fly* **2**:259–261. doi:10.4161/fly.7133

O'Connor-Giles KM, Ho LL, Ganetzky B. 2008. Nervous Wreck Interacts with Thickveins and the Endocytic Machinery to Attenuate Retrograde BMP Signaling during Synaptic Growth. *Neuron* **58**:507–518. doi:10.1016/j.neuron.2008.03.007

Ohyama T, Schneider-Mizell CM, Fetter RD, Aleman JV, Franconville R, Rivera-Alba M, Mensh BD, Branson KM, Simpson JH, Truman JW, Cardona A, Zlatic M. 2015. A multilevel multimodal circuit enhances action selection in Drosophila. *Nature* **520**:633–639. doi:10.1038/nature14297

Orlean P, Menon AK. 2007. Thematic review series: Lipid Posttranslational Modifications. GPI anchoring of protein in yeast and mammalian cells, or: how we learned to stop worrying and love glycophospholipids. *J Lipid Res* **48**:993–1011. doi:10.1194/jlr.r700002-jlr200

Otto N, Marelja Z, Schoofs A, Kranenburg H, Bittern J, Yildirim K, Berh D, Bethke M, Thomas S, Rode S, Risse B, Jiang X, Pankratz M, Leimkühler S, Klämbt C. 2018. The sulfite oxidase Shopper controls neuronal activity by regulating glutamate homeostasis in Drosophila ensheathing glia. *Nat Commun* **9**:3514. doi:10.1038/s41467-018-05645-z

Özkan E, Carrillo RA, Eastman CL, Weiszmann R, Waghray D, Johnson KG, Zinn K, Celniker SE, Garcia KC. 2013. An extracellular interactome of immunoglobulin and LRR proteins reveals receptor-ligand networks. *Cell* **154**:228–239. doi:10.1016/j.cell.2013.06.006

Pappu KS, Morey M, Nern A, Spitzweck B, Dickson BJ, Zipursky SL. 2011. Robo-3–mediated repulsive interactions guide R8 axons during Drosophila visual system development. *Proc National Acad Sci* **108**:7571–7576. doi:10.1073/pnas.1103419108

Pasterkamp RJ, Peschon JJ, Spriggs MK, Kolodkin AL. 2003. Semaphorin 7A promotes axon outgrowth through integrins and MAPKs. *Nature* **424**:398–405. doi:10.1038/nature01790

Peixoto RT, Kunz PA, Kwon H, Mabb AM, Sabatini BL, Philpot BD, Ehlers MD. 2012. Transsynaptic Signaling by Activity-Dependent Cleavage of Neuroligin-1. *Neuron* **76**:396–409. doi:10.1016/j.neuron.2012.07.006

Peng J, Santiago IJ, Ahn C, Gur B, Tsui CK, Su Z, Xu C, Karakhanyan A, Silies M, Pecot MY. 2018. Drosophila Fezf coordinates laminar-specific connectivity through cell-intrinsic and cell-extrinsic mechanisms. *eLife* **7**:e33962. doi:10.7554/elife.33962

Pierleoni A, Martelli P, Casadio R. 2008. PredGPI: A GPI-anchor predictor. *Bmc Bioinformatics* **9**:392. doi:10.1186/1471-2105-9-392

Pipes GCT, Lin Q, Riley SE, Goodman CS. 2001. The Beat generation: a multigene family encoding IgSF proteins related to the Beat axon guidance molecule in Drosophila. *Development* **128**:4545–4552. doi:10.1242/dev.128.22.4545

Pischedda F, Piccoli G. 2016. The IgLON Family Member Negr1 Promotes Neuronal Arborization Acting as Soluble Factor via FGFR2. *Front Mol Neurosci* **8**:89. doi:10.3389/fnmol.2015.00089

Ponio JB-D, Wright-Crosnier C, Groyer-Picard M-T, Driancourt C, Beau I, Hadchouel M, Meunier-Rotival M. 2007. Biological function of mutant forms of JAGGED1 proteins in Alagille syndrome: inhibitory effect on Notch signaling. *Hum Mol Genet* **16**:2683–2692. doi:10.1093/hmg/ddm222

Poovathumkadavil P, Jagla K. 2020. Genetic Control of Muscle Diversification and Homeostasis: Insights from Drosophila. *Cells* **9**:1543. doi:10.3390/cells9061543

Purice MD, Ray A, Münzel EJ, Pope BJ, Park DJ, Speese SD, Logan MA. 2017. A novel Drosophila injury model reveals severed axons are cleared through a Draper/MMP-1 signaling cascade. *eLife* **6**:e23611. doi:10.7554/elife.23611

Ramos RG, Igloi GL, Lichte B, Baumann U, Maier D, Schneider T, Brandstätter JH, Fröhlich A, Fischbach KF. 1993. The irregular chiasm C-roughest locus of Drosophila, which affects axonal projections and programmed cell death, encodes a novel immunoglobulin-like protein. *Genes Dev* **7**:2533–2547. doi:10.1101/gad.7.12b.2533

Ranganayakulu G, Elliott DA, Harvey RP, Olson EN. 1998. Divergent roles for NK-2 class homeobox genes in cardiogenesis in flies and mice. *Development* **125**:3037–3048. doi:10.1242/dev.125.16.3037

Reed J, McNamee C, Rackstraw S, Jenkins J, Moss D. 2004. Diglons are heterodimeric proteins composed of IgLON subunits, and Diglon-CO inhibits neurite outgrowth from cerebellar granule cells. *J Cell Sci* **117**:3961–3973. doi:10.1242/jcs.01261

Reiss K, Maretzky T, Ludwig A, Tousseyn T, Strooper B de, Hartmann D, Saftig P. 2005. ADAM10 cleavage of N-cadherin and regulation of cell–cell adhesion and β-catenin nuclear signalling. *Embo J* **24**:742–752. doi:10.1038/sj.emboj.7600548

Ricolo D, Butí E, Araújo SJ. 2015. Drosophila melanogaster Hedgehog cooperates with Frazzled to guide axons through a non-canonical signalling pathway. *Mech Dev* **137**:11–22. doi:10.1016/j.mod.2015.04.003

Rieckhof GE, Yoshihara M, Guan Z, Littleton JT. 2003. Presynaptic N-type Calcium Channels Regulate Synaptic Growth*. *J Biol Chem* **278**:41099–41108. doi:10.1074/jbc.m306417200

Ritzenthaler S, Suzuki E, Chiba A. 2000. Postsynaptic filopodia in muscle cells interact with innervating motoneuron axons. *Nat Neurosci* **3**:1012–1017. doi:10.1038/79833

Rodríguez-Manzaneque JC, Carpizo D, Plaza-Calonge M del C, Torres-Collado AX, Thai SN-M, Simons M, Horowitz A, Iruela-Arispe ML. 2009. Cleavage of syndecan-4 by ADAMTS1 provokes defects in adhesion. *Int J Biochem Cell Biology* **41**:800–810. doi:10.1016/j.biocel.2008.08.014

Rougon G, Hobert O. 2003. NEW INSIGHTS INTO THE DIVERSITY AND FUNCTION OF NEURONAL IMMUNOGLOBULIN SUPERFAMILY MOLECULES. *Annu Rev Neurosci* **26**:207–238. doi:10.1146/annurev.neuro.26.041002.131014

Rozbesky D, Robinson RA, Jain V, Renner M, Malinauskas T, Harlos K, Siebold C, Jones EY. 2019. Diversity of oligomerization in Drosophila semaphorins suggests a mechanism of functional fine-tuning. *Nat Commun* **10**:3691. doi:10.1038/s41467-019-11683-y

Ruiz-Gómez M, Coutts N, Price A, Taylor MV, Bate M. 2000. Drosophila Dumbfounded A Myoblast Attractant Essential for Fusion. *Cell* **102**:189–198. doi:10.1016/s0092-8674(00)00024-6

Rushton E, Drysdale R, Abmayr SM, Michelson AM, Bate M. 1995. Mutations in a novel gene, myoblast city , provide evidence in support of the founder cell hypothesis for Drosophila muscle development. *Development* **121**:1979–1988. doi:10.1242/dev.121.7.1979

Sanz R, Ferraro GB, Fournier AE. 2015. IgLON cell adhesion molecules are shed from the cell surface of cortical neurons to promote neuronal growth. *J Biol Chem* **290**:4330–4342. doi:10.1074/jbc.m114.628438

Schindelin J, Arganda-Carreras I, Frise E, Kaynig V, Longair M, Pietzsch T, Preibisch S, Rueden C, Saalfeld S, Schmid B, Tinevez J-Y, White DJ, Hartenstein V, Eliceiri K, Tomancak P, Cardona A. 2012. Fiji: an open-source platform for biological-image analysis. *Nat Methods* **9**:676–682. doi:10.1038/nmeth.2019

Sehadova H, Glaser FT, Gentile C, Simoni A, Giesecke A, Albert JT, Stanewsky R. 2009. Temperature Entrainment of Drosophila's Circadian Clock Involves the Gene nocte and

Signaling from Peripheral Sensory Tissues to the Brain. *Neuron* **64**:251–266. doi:10.1016/j.neuron.2009.08.026

Sen A, Yokokura T, Kankel MW, Dimlich DN, Manent J, Sanyal S, Artavanis-Tsakonas S. 2011. Modeling spinal muscular atrophy in Drosophila links Smn to FGF signaling. *J Cell Biol* **192**:481–495. doi:10.1083/jcb.201004016

Sepp KJ, Schulte J, Auld VJ. 2000. Developmental dynamics of peripheral glia in Drosophila melanogaster. *Glia* **30**:122–133. doi:10.1002/(sici)1098-1136(200004)30:2<122::aid-glia2>3.0.co;2-b

Serafini T, Colamarino SA, Leonardo ED, Wang H, Beddington R, Skarnes WC, Tessier-Lavigne M. 1996. Netrin-1 is required for commissural axon guidance in the developing vertebrate nervous system. *Cell* **87**:1001–1014. doi:10.1016/s0092-8674(00)81795-x

Sergeeva AP, Katsamba PS, Cosmanescu F, Brewer JJ, Ahlsen G, Mannepalli S, Shapiro L, Honig B. 2020. DIP/Dpr interactions and the evolutionary design of specificity in protein families. *Nat Commun* **11**:2125. doi:10.1038/s41467-020-15981-8

Seroka A, Lai S-L, Doe CQ. 2022. Transcriptional profiling from whole embryos to single neuroblast lineages in Drosophila. *Dev Biol* **489**:21–33. doi:10.1016/j.ydbio.2022.05.018

Sharma P, Varma R, Sarasij RC, Ira, Gousset K, Krishnamoorthy G, Rao M, Mayor S. 2004. Nanoscale Organization of Multiple GPI-Anchored Proteins in Living Cell Membranes. *Cell* **116**:577–589. doi:10.1016/s0092-8674(04)00167-9

Shimozono M, Osaka J, Kato Y, Araki T, Kawamura H, Takechi H, Hakeda-Suzuki S, Suzuki T. 2019. Cell surface molecule, Klingon, mediates the refinement of synaptic specificity in the Drosophila visual system. *Genes Cells* **24**:496–510. doi:10.1111/gtc.12703

Siebert M, Banovic D, Goellner B, Aberle H. 2009. Drosophila motor axons recognize and follow a Sidestep-labeled substrate pathway to reach their target fields. *Genes Dev* **23**:1052–1062. doi:10.1101/gad.520509

Sikorska N, Lemus L, Aguilera-Romero A, Manzano-Lopez J, Riezman H, Muñiz M, Goder V. 2016. Limited ER quality control for GPI-anchored proteins. *J Cell Biol* **213**:693–704. doi:10.1083/jcb.201602010

Simpson JH, Kidd T, Bland KS, Goodman CS. 2000. Short-Range and Long-Range Guidance by Slit and Its Robo Receptors Robo and Robo2 Play Distinct Roles in Midline Guidance. *Neuron* **28**:753–766. doi:10.1016/s0896-6273(00)00151-3

Singh K, Lilleväli K, Gilbert SF, Bregin A, Narvik J, Jayaram M, Rahi M, Innos J, Kaasik A, Vasar E, Philips MA. 2018. The combined impact of IgLON family proteins Lsamp and Neurotrimin on developing neurons and behavioral profiles in mouse. *Brain Res Bull* **140**:5–18. doi:10.1016/j.brainresbull.2018.03.013

Skeath JB. 1999. At the nexus between pattern formation and cell-type specification: the generation of individual neuroblast fates in the Drosophila embryonic central nervous system. *BioEssays* **21**:922–931. doi:10.1002/(sici)1521-1878(199911)21:11<922::aid-bies4>3.0.co;2-t

Sperry RW. 1963. CHEMOAFFINITY IN THE ORDERLY GROWTH OF NERVE FIBER PATTERNS AND CONNECTIONS*.

Stahl R, Schilling S, Soba P, Rupp C, Hartmann T, Wagner K, Merdes G, Eggert S, Kins S. 2014. Shedding of APP limits its synaptogenic activity and cell adhesion properties. *Front Cell Neurosci* **8**:410. doi:10.3389/fncel.2014.00410

Steinbuck MP, Winandy S. 2018. A Review of Notch Processing With New Insights Into Ligand-Independent Notch Signaling in T-Cells. *Front Immunol* **9**:1230. doi:10.3389/fimmu.2018.01230

Stocker B, Bochow C, Damrau C, Mathejczyk T, Wolfenberg H, Colomb J, Weber C, Ramesh N, Duch C, Biserova NM, Sigrist S, Pflüger H-J. 2018. Structural and Molecular Properties of Insect Type II Motor Axon Terminals. *Front Syst Neurosci* **12**:5. doi:10.3389/fnsys.2018.00005

Stoeckli ET. 2018. Understanding axon guidance: are we nearly there yet? *Development* **145**:dev151415. doi:10.1242/dev.151415

Struyk A, Canoll P, Wolfgang M, Rosen C, D'Eustachio P, Salzer J. 1995. Cloning of neurotrimin defines a new subfamily of differentially expressed neural cell adhesion molecules. *J Neurosci* **15**:2141–2156. doi:10.1523/jneurosci.15-03-02141.1995

Suzuki K, Kumanogoh A, Kikutani H. 2008. Semaphorins and their receptors in immune cell interactions. *Nat Immunol* **9**:17–23. doi:10.1038/ni1553

Suzuki M, Morita H, Ueno N. 2012. Molecular mechanisms of cell shape changes that contribute to vertebrate neural tube closure. *Dev Growth Differ* **54**:266–276. doi:10.1111/j.1440-169x.2012.01346.x

Tan L, Zhang KX, Pecot MY, Nagarkar-Jaiswal S, Lee PT, Takemura SY, McEwen JM, Nern A, Xu S, Tadros W, Chen Z, Zinn K, Bellen HJ, Morey M, Zipursky SL. 2015. Ig Superfamily Ligand and Receptor Pairs Expressed in Synaptic Partners in Drosophila. *Cell* **163**:1756–1769. doi:10.1016/j.cell.2015.11.021

Teufel F, Armenteros JJA, Johansen AR, Gíslason MH, Pihl SI, Tsirigos KD, Winther O, Brunak S, Heijne G von, Nielsen H. 2022. SignalP 6.0 predicts all five types of signal peptides using protein language models. *Nat Biotechnol* **40**:1023–1025. doi:10.1038/s41587-021-01156-3

Torre JR de la, Höpker VH, Ming G, Poo M, Tessier-Lavigne M, Hemmati-Brivanlou A, Holt CE. 1997. Turning of Retinal Growth Cones in a Netrin-1 Gradient Mediated by the Netrin Receptor DCC. *Neuron* **19**:1211–1224. doi:10.1016/s0896-6273(00)80413-4

Toth AB, Terauchi A, Zhang LY, Johnson-Venkatesh EM, Larsen DJ, Sutton MA, Umemori H. 2013. Synapse maturation by activity-dependent ectodomain shedding of SIRPα. *Nat Neurosci* **16**:1417–1425. doi:10.1038/nn.3516

Truman JW. 1990. Metamorphosis of the central nervous system of Drosophila. *J Neurobiol* **21**:1072–1084. doi:10.1002/neu.480210711

Truman JW, Bate M. 1988. Spatial and temporal patterns of neurogenesis in the central nervous system of Drosophila melanogaster. *Dev Biol* **125**:145–157. doi:10.1016/0012-1606(88)90067-x

Tucker RP. 2018. Teneurins: Domain Architecture, Evolutionary Origins, and Patterns of Expression. *Front Neurosci* **12**:938. doi:10.3389/fnins.2018.00938

Uesaka N, Uchigashima M, Mikuni T, Nakazawa T, Nakao H, Hirai H, Aiba A, Watanabe M, Kano M. 2014. Retrograde semaphorin signaling regulates synapse elimination in the developing mouse brain. *Science* **344**:1020–1023. doi:10.1126/science.1252514

Um JW, Ko J. 2017. Neural Glycosylphosphatidylinositol-Anchored Proteins in Synaptic Specification. *Trends Cell Biol* **27**:931–945. doi:10.1016/j.tcb.2017.06.007

Varadarajan SG, Kong JH, Phan KD, Kao TJ, Panaitof SC, Cardin J, Eltzschig H, Kania A, Novitch BG, Butler SJ. 2017. Netrin1 Produced by Neural Progenitors, Not Floor Plate Cells, Is Required for Axon Guidance in the Spinal Cord. *Neuron* **94**:790-799.e3. doi:10.1016/j.neuron.2017.03.007

Venkatasubramanian L, Guo Z, Xu S, Tan L, Xiao Q, Nagarkar-Jaiswal S, Mann RS. 2019. Stereotyped terminal axon branching of leg motor neurons mediated by igsf proteins dip-α and dpr10. *Elife* **8**:e42692. doi:10.7554/elife.42692

Venken KJT, Schulze KL, Haelterman NA, Pan H, He Y, Evans-Holm M, Carlson JW, Levis RW, Spradling AC, Hoskins RA, Bellen HJ. 2011. MiMIC: A highly versatile transposon insertion resource for engineering Drosophila melanogaster genes. *Nat Methods* **8**:737–743. doi:10.1038/nmeth.1662

Wang L, Liang P-J, Zhang P-M, Qiu Y-H. 2014. Ionic mechanisms underlying tonic and phasic firing behaviors in retinal ganglion cells. *Channels* **8**:298–307. doi:10.4161/chan.28012

Wang Y, Lobb-Rabe M, Ashley J, Anand V, Carrillo RA. 2021. Structural and Functional Synaptic Plasticity Induced by Convergent Synapse Loss in the Drosophila Neuromuscular Circuit. *J Neurosci* **41**:1401–1417. doi:10.1523/jneurosci.1492-20.2020

Wang Y, Lobb-Rabe M, Ashley J, Chatterjee P, Anand V, Bellen HJ, Kanca O, Carrillo RA. 2022. Systematic expression profiling of dprs and DIPs reveals cell surface codes in Drosophila larval motor and sensory neurons. *Development* **149**. doi:10.1242/dev.200355

Wang Y, Zhang R, Huang S, Valverde PT-T, Lobb-Rabe M, Ashley J, Venkatasubramanian L, Carrillo RA. 2023. Glial Draper signaling triggers cross-neuron plasticity in bystander neurons after neuronal cell death. *bioRxiv* 2023.04.09.536190. doi:10.1101/2023.04.09.536190

Wernet MF, Mazzoni EO, Çelik A, Duncan DM, Duncan I, Desplan C. 2006. Stochastic spineless expression creates the retinal mosaic for colour vision. *Nature* **440**:174–180. doi:10.1038/nature04615

Winberg ML, Noordermeer JN, Tamagnone L, Comoglio PM, Spriggs MK, Tessier-Lavigne M, Goodman CS. 1998. Plexin A Is a Neuronal Semaphorin Receptor that Controls Axon Guidance. *Cell* **95**:903–916. doi:10.1016/s0092-8674(00)81715-8

Winding M, Pedigo BD, Barnes CL, Patsolic HG, Park Y, Kazimiers T, Fushiki A, Andrade IV, Khandelwal A, Valdes-Aleman J, Li F, Randel N, Barsotti E, Correia A, Fetter RD, Hartenstein V, Priebe CE, Vogelstein JT, Cardona A, Zlatic M. 2023. The connectome of an insect brain. *Science* **379**:eadd9330–eadd9330. doi:10.1126/science.add9330

Wu H, Xiong WC, Mei L. 2010. To build a synapse: Signaling pathways in neuromuscular junction assembly. *Development* **137**:1017–1033. doi:10.1242/dev.038711

Wu R, Li A, Sun B, Sun J-G, Zhang J, Zhang T, Chen Y, Xiao Y, Gao Y, Zhang Q, Ma J, Yang X, Liao Y, Lai W-Y, Qi X, Wang S, Shu Y, Wang H-L, Wang F, Yang Y-G, Yuan Z. 2019. A novel m6A reader Prrc2a controls oligodendroglial specification and myelination. *Cell Res* **29**:23–41. doi:10.1038/s41422-018-0113-8

Xu C, Theisen E, Maloney R, Peng J, Santiago I, Yapp C, Werkhoven Z, Rumbaut E, Shum B, Tarnogorska D, Borycz J, Tan L, Courgeon M, Meinertzhagen IA, Bivort B de, Drugowitsch J, Pecot MY. 2019. Control of Synaptic Specificity by Establishing a Relative Preference for Synaptic Partners. *Neuron* **103**:865-877.e7. doi:10.1016/j.neuron.2019.06.006

Xu S, Sergeeva AP, Katsamba PS, Mannepalli S, Bahna F, Bimela J, Zipursky SL, Shapiro L, Honig B, Zinn K. 2022. Affinity requirements for control of synaptic targeting and neuronal cell survival by heterophilic IgSF cell adhesion molecules. *Cell Reports* **39**:110618–110618. doi:10.1016/j.celrep.2022.110618

Xu S, Xiao Q, Cosmanescu F, Sergeeva AP, Yoo J, Lin Y, Katsamba PS, Ahlsen G, Kaufman J, Linaval NT, Lee P-T, Bellen HJ, Shapiro L, Honig B, Tan L, Zipursky SL. 2018a. Interactions between the Ig-Superfamily Proteins DIP-α and Dpr6/10 Regulate Assembly of Neural Circuits. *Neuron* **100**:1369-1384.e6. doi:10.1016/j.neuron.2018.11.001

Xu S, Xiao Q, Cosmanescu F, Sergeeva AP, Yoo J, Lin Y, Katsamba PS, Ahlsen G, Kaufman J, Linaval NT, Lee P-T, Bellen HJ, Shapiro L, Honig B, Tan L, Zipursky SL. 2018b. Interactions between the Ig-Superfamily Proteins DIP-α and Dpr6/10 Regulate Assembly of Neural Circuits. *Neuron* **100**:1369-1384.e6. doi:10.1016/j.neuron.2018.11.001

Yildirim K, Petri J, Kottmeier R, Klämbt C. 2019. Drosophila glia: Few cell types and many conserved functions. *Glia* **67**:5–26. doi:10.1002/glia.23459

Yoshihara M, Rheuben MB, Kidokoro Y. 1997. Transition from growth cone to functional motor nerve terminal in Drosophila embryos. *J Neurosci* **17**:8408–8426. doi:10.1523/jneurosci.17-21-08408.1997

Young TR, Leamey CA. 2009. Teneurins: Important regulators of neural circuitry. *Int J Biochem Cell Biol* **41**:990–993. doi:10.1016/j.biocel.2008.06.014

Yu H-H, Araj HH, Ralls SA, Kolodkin AL. 1998. The Transmembrane Semaphorin Sema I Is Required in Drosophila for Embryonic Motor and CNS Axon Guidance. *Neuron* **20**:207–220. doi:10.1016/s0896-6273(00)80450-x

Zavodszky E, Hegde RS. 2019. Misfolded GPI-anchored proteins are escorted through the secretory pathway by ER-derived factors. *Elife* **8**:e46740. doi:10.7554/elife.46740

Zheng L, Michelson Y, Freger V, Avraham Z, Venken KJT, Bellen HJ, Justice MJ, Wides R. 2011. Drosophila Ten-m and filamin affect motor neuron growth cone guidance. *Plos One* **6**:e22956. doi:10.1371/journal.pone.0022956

Zinn K, Özkan E. 2017. Neural immunoglobulin superfamily interaction networks. *Curr Opin Neurobiol* **45**:99–105. doi:10.1016/j.conb.2017.05.010

Zlatic M, Li F, Strigini M, Grueber W, Bate M. 2009. Positional Cues in the Drosophila Nerve Cord: Semaphorins Pattern the Dorso-Ventral Axis. *PLoS Biol* **7**:e1000135. doi:10.1371/journal.pbio.1000135